Lehrstuhl für Hochfrequenztechnik
der Technischen Universität München

Hybrid Space Discretizing Method - Method of Moments for Numerical Modeling of Transient Interference.

Rachid Khlifi

Vollständiger Abdruck der von der Fakultät für Elektrotechnik und Informationstechnik der Technischen Universität München zur Erlangung des akademischen Grades eines

Doktor–Ingenieurs

genehmigten Dissertation.

Vorsitzender:	Univ.-Prof. Paolo Lugli, Ph. D.
Prüfer der Dissertation:	1. Univ.-Prof. Dr. techn. Peter Russer 2. Prof. W. J. R. Hoefer, Univ. of Victoria, Victoria/Kanada

Die Dissertation wurde am 04. Dezember 2006 bei der Technischen Universität München eingereicht und durch die Fakultät für Elektrotechnik und Informationstechnik am 27. März 2007 angenommen.

1 Abstract

This work deals with the development of a novel efficient hybrid method combining the Transmission Line Matrix (TLM) method and the Time-Domain Method of Moments (TDMOM), for the analysis of transient electromagnetic interference of a complex object exhibiting compound dielectric and lossy materials in interaction with a thin curved structure, separated by large free space regions. The separation of the configuration into a complex object treated by TLM and thin scatterer treated by TDMOM is a crucial detail in the proposed hybrid method. The separation is necessary to reduce the complexity of the problem, two small problems being less expensive than one large. Both problems, i.e. the complex object and the thin scatterer, are tackled with the most appropriate method.

The TLM method is widely used due to its capability of dealing with complex geometries with arbitrary electrical properties. The time-domain electric field integral equation (EFIE) solution using the marching on in time (MOT) procedure is well suited for the analysis of arbitrarily shaped conducting thin wires/surfaces embedded in a homogenous environment, because they need only consider portions of the structure where the currents flow. The application of the equivalence principle with a proper set of ficticious currents (accounting for the coupling) permits us to divide the three-dimensional space into subregions, and to apply each method in its best domain of application. The electromagnetic interaction between the subregions is provided by the dyadic free-space Green's functions in time domain, because they do not need to apply resources to the modeling of homogeneous propagating space.

The present work treats the scattering problem solved through discretization of the EFIE and its direct time-domain solution by means of a marching-on-in-time procedure. An explicit equation that relates the current at a certain time instant to the currents of previous instants and the incident field is obtained. These currents can then be used in radiation integrals to calculate the fields scattered by the objects.

The contributions in this thesis address the theoretical concept of the hybrid TLM-IE/TDMOM method, illustrate the capability of this hybrid method and establish guidelines for its selection in preference to the pure conventional TLM method with a particular focus on the analysis of transient electromagnetic interference between a complex object and a curved conducting structure. The attributes of such methods, both in terms of computational efficiency, solution accuracy and stability, are examined through their application to the analysis of several electromagnetic compatibility prob-

lems. For this purpose the hybridization of the implicit time evolution TLM-scheme with the explicit integral-Equation/Method of Moments is presented and utilized.

The goal of this hybridization is to achieve sufficient accuracy with minimum effort, where effort usually is interpreted as computational cost in terms of computational times and memory requirements. In this work, resource predictions for this hybrid method in comparison with TLM method are determined based on the number of computational elements, as this number takes both the physical problem size and the solution frequency into account.

To validate this new approach, we have compared the results with those obtained using the pure transmission line matrix (TLM) method.

2 Acknowledgments

First of all, I would like to express my gratitude and thanks to Professor Peter Russer for the opportunity to prepare my dissertation in the Institute for High-Frequency Engineering at Munich University and for his guidance on the scientific work presented here. He has offered me certain freedom in choosing my research field, and he always had an open ear for any kinds of problems. I am also very grateful for the financial support and for the possibility to travel to several conferences for presenting parts of this work.

I am also grateful to a lot of people and the fact that I could get the chance to work with the people at the institute of high frequency engineering, TU Munich. My thanks go to all my colleagues at institute for their support, collaboration, encouragement, and friendship during these years.
My deep gratitude goes moreover to a number of persons who have shared with me these past years in the good as well as in the not so good times enriching my professional and private life with their opinion and view of the world. Among them my partner, for her patience and moral support, my many friends and colleagues, and last but, off course not least, my parents without whom all this would not exist at all.

Rachid Khlifi

Munich, Germany
in November 10^{th} 2006

Contents

1 Abstract **iii**

2 Acknowledgments **v**

3 Motivation and Introduction **1**
3.1 State of the Art . . . 3
3.2 The Scope of the Thesis . . . 6
3.3 Structure of the Manuscript . . . 7

4 The Transmission Line Matrix Method **11**
4.1 Introduction . . . 11
4.2 Basics of the TLM Method . . . 11
4.3 The TLM Scheme in Hilbert Space . . . 12
4.4 The Scattering Process . . . 15
4.5 The Connection Process . . . 20
4.6 Field-Mappings for the Symmetrical Condensed Node . . . 21
4.6.1 Centered Field Mapping (CFM) . . . 22
4.6.2 Cell Boundary Mapping (CBM) . . . 25
4.7 Boundary Conditions . . . 27
4.7.1 One-Sided Reflection Wall . . . 28
4.7.2 Two-Sided Reflection-Transmission Wall . . . 29
4.7.3 Matched Layer Absorbers . . . 29
4.8 Excitation . . . 30

5 Time-Domain Method of Moments **33**
5.1 Introduction . . . 33
5.1.1 Derivation of Electric and Magnetic Field Integral Equation . . . 34
5.1.2 Perfectly Conducting Scatterers . . . 36
5.2 Thin-Wire Antennas and Scatterers . . . 37
5.2.1 Current distribution on the wire . . . 40
5.3 Thin-Surface Antennas and Scatterers . . . 45
5.3.1 Current distribution on the surface . . . 46
5.4 Surface Equivalence Principle . . . 49

6 Hybrid TLM-IE method **51**
6.1 Introduction . . . 51
6.2 TLM-IE Concept for Radiation Analysis . . . 51
6.3 TLM-IE Concept for Transient Interferences . . . 56

7 Hybrid TLM-TDMOM **65**
7.1 Introduction . . . 65
7.2 TLM-TDMOM Concept . . . 67
7.3 Calculation of the scattered fields . . . 69
7.3.1 Thin wire scatterer . . . 69
7.3.2 Thin conducting surface scatterer . . . 73
7.4 Radiated field from the TLM-subregion . . . 77
7.5 Total tangential field at TLM-interface . . . 80

8 Numerical Applications **85**
8.1 Introduction . . . 85
8.2 Apertured metallic box and thin wire . . . 85
8.3 Mictrostrip patch antenna and thin wire . . . 89
8.4 Microstrip loop and circular cylinder configuration . . . 97
8.5 Stability analysis . . . 100
8.6 Computational Efficiency . . . 102
8.6.1 Computation time . . . 104
8.6.2 Memory requirement . . . 107

9 Discussion and Conclusions **113**
9.1 Conclusions and outline . . . 113

A Appendix **117**
A.1 Wires with arbitrary orientation and length . . . 117
A.1.1 Overview . . . 117
A.1.2 Coordinate transformations . . . 117
A.1.3 Transformation of the incident field term . . . 121

3 Motivation and Introduction

The impact on modern ultra-wideband (UWB) communication systems of complex radiated interference environments requires fullwave simulation of highly complex three-dimensional electromagnetic structures. To solve the electromagnetic design problems in these fields will require electromagnetic design systems with computing power and capabilities far beyond present systems.

A simulation method intended for solving electromagnetic problems must be capable of dealing with highly non-uniform and non-linear systems, over a wide frequency range including transients in equipment configurations which are electrically large and contain fine features. No single method can be expected to meet fully and in the most efficient manner all these requirements. In some situations, one method is competitive for a part of the problem while another algorithm is better suited for the remaining parts. It is then attractive to combine the different algorithms to form a so-called hybrid method. Hybrid methods, which combine the desirable features of two or more different techniques, offer possibilities to treat significantly larger classes of problems that cannot be resolved conveniently and/or accurately, by using them individually.

Several numerical modeling methods for solving electromagnetic problems have been developed, each possessing particular features advantageous to particular types of problems. Methods can be classified in generic groups based on the domain of the variable (time- or frequency-domain) and the domain of the operator (differential or integral). In dealing with the most general material and conductor configurations at high frequencies, differential time-domain techniques offer the most versatile simulation tool. The foremost methods in this area are the finite-difference time-domain (FDTD) method [42] and the transmission line Matrix (TLM) method [1]. The three-dimensional discretization of the objects leads to a simple description of the field behavior even in complex structures of dielectric and lossy material. However, the space discretizing methods have difficulties when open geometries are analyzed, such as radiating structures and unshielded microwave and millimeter-wave circuits components. Since these techniques require discretization of the whole volume of interest, the difficulties arise from the discretization of an infinite region in cases of open structures. In other words, the TLM and FDTD methods require finite domain to set up a mesh (i.e. the computational space must be of limited size or must be approximated by a limited region by introducing some artificial boundaries, of course without altering the electromagnetic characteristics of the geometry). An other drawback of these methods

is that they work well only on uniform Cartesian (structured) grids, and typically use the so-called staircase approximation of boundaries not aligned with the grid.

Integral equation [3] approaches can be efficiently used to characterize arbitrarily curved thin structure. The MOM [3] discretizes Maxwell's equations in integral form, and the unknowns are sources such as currents or charges on the surfaces of conductors and dielectrics. This method is advantageous for problems involving open regions, and when the current-carrying surfaces are small. MOM model e.m. currents and need only consider portions of the problem where the currents flow. Arbitrarily field values can then be efficiently derived from the current solution at any point in space as a secondary computational step. This means that integral techniques do not need to apply resources to the modeling of homogeneous propagating space. The MOM is often applied to scattering problems. Tab. 3.1 summarizes the comparison between differential (i.e. space discretizing) and integral methods.

	integral	**differential**
inhomogeneous materials	difficult	easy
non-linearities time variations	difficult	easy
open boundaries	easy	difficult
number of nodes	required only on certain surfaces	whole workspace has to be filled
maths.	complex (invert large matrices)	simple

Table 3.1: Comparison between integral and differential methods.

Space discretizing methods such as FDTD or TLM do have a role to play, particularly when dealing with localized inhomogeneous dielectric regions. Integral methods can be applied to analyze multiple and nested dielectric bodies, but are generally less effective than localized space discretizing techniques. MOM used for efficient free-space and curved metallic struture field calculations combined with a TLM formulation method for direct electromagnetic field computations in localized inhomogeneous dielectric regions therefore delivers a most efficient and versatile algorithm for the analysis of transient electromagnetic interferences between objects separated by large free-space regions.

3.1 State of the Art

The Transmission Line Matrix (TLM) method, developed and first published in 1971 by JOHNS [1] has emerged as a powerful method for computer modeling of electromagnetic fields [50] [48] [86]. The TLM method exhibits excellent numerical stability and is also suitable for the modeling of lossy, dispersive, active and nonlinear media [60] [76] [62]. However the state-space representation of TLM is usually very large, requiring significant computational resources and long computation times. It is the objective of the proposed hybrid method TLM-IE/MOM to address these computational difficulties of standard TLM through dividing the original model into subregions, where the best suited method is applied for the field modeling.

In many problems in electromagnetics it is necessary to simulate coupling between electromagnetic fields and thin curved metallic structures (wires/surfaces). Examples are in electromagnetic compatibility (EMC), in antennas and in microwave design. Focusing in particular on the electromagnetic compatibility problems, the main difficulty as far as numerical modeling is concerned is that it is normally inefficient to describe in detail the geometrical features of curved thin metallic structure in a mesh which is normally configured to model propagation in a large space, e.g. free-space, room or equipment cabinet. This problem is particularly acute when space discretizing methods such as TLM and FDTD methods are used in modeling. With integral methods this problem does not arise but other difficulties such as the treatment of non-uniformities and interconnected regions makes modeling again difficult.

Two basic approaches for treating thin wires in TLM have evolved, the so-called separated and integrated solutions. In the separated solutions, the wires are treated separately from the rest of the problem, allowing for field coupling to the wire by introducing equivalent sources derived from knowledge of the incident fields in the vicinity of the wire. Separated solutions for TLM are simple and can deal easily with both single and multi-wire problems [63] [64]. The simplest integrated solutions for TLM are those where wires are modeled by using short-circuits nodes or shorted link-lines adjacent to the wire surface. Here, all the energy incident on the boundary is returned along the link-lines by simply inverting incident voltage pulses for the following time period. In these methods, the wires are explicitly included in the model, hence the model is consistent and two-way coupling is simulated. Taking into consideration the computational resource problems the wire is usually modeled by no more than a single node cross-section on a rectangular Cartesian mesh [50]. More sophisticated integrated solution methods which can allow for accurate modeling of wires with a considerably smaller diameter than the node size have been introduced in [66] [69] [68]. They use special wire networks embedded between or within nodes to model signal propagation along the wires, while allowing for interactions with the electromagnetic field.

The generalization of the TLM for a non-orthogonal mesh and for dispersive anisotropic materials is presented in [74] [75] [60]. Dispersive, active and nonlinear media

[76] can be well modeled by the SCN. Almost radiating boundary conditions, e.g. reflection free walls, matched [70] and perfectly matched layers [77] [78] are already used in the TLM, which yields approximate solutions of a radiating problem and require some distance between the structure to be modeled and boundaries of the computational domain. A novel TLM Multipole Expansion (TLM-ME) method for a potentially exact modeling of the radiating boundary condition is proposed in [57], where an electromagnetic structure is embedded in a spherical region and modeled with the TLM method. Then outside the spherical region the field is expanded into analytically known spherical waves. The problems of the local subgridding in the TLM scheme are investigated in [79] and [80]. The state-space representation of TLM is usually very large, requiring significant computational resources and long computation times. In order to address these computational complexity difficulties of standard TLM, the TLM Model Order Reduction (TLM-MOR) is proposed in [58] to reduce the original model into one of significantly smaller dimension. The dimension of the reduced model, also called model order, is associated with a subset of the eigenmodes of the system that influence its response over the desirable frequency bandwidth of interest. Hybridizations of the TLM method with other numerical methods such as the TLM-Integral Equation (TLM-IE) method [5]- [12] for the solving of radiation problems and the TLM-Mode Matching (TLM-MM) approach [58] for a full-wave analysis of transmission structures in multilayered MMICs occurred to be very efficient. The improved skin effect [81] and thin wire [10] models allowed to spread the usage of the TLM additionally.

TLM is a space-discretizing method that allows the numerical full-wave modeling of 3D structures with nearly arbitrary geometry. Like other full-wave numerical methods (e.g., Finite Element, Finite Difference in Frequency/Time Domain) TLM has typical drawbacks in:

- modeling of exact boundary conditions (e.g. antenna problems),
- dealing with extremely wide "aspect ratio" values, the relative ratio among the maxima and minima geometrical dimensions (e.g. photonic devices),
- dealing with interacting objects embedded in large (respect to the operating wavelength) homogeneous regions; (typical of electromagnetic interference and compatibility problems).
- dealing with arbitrarily curved thin wire and surface structures.

In order to treat large free-space region between electromagnetically coupled objects a hybrid TLM-IE has been developed. The Transmission Line Matrix-Integral Equation (TLM-IE) method is a 3D full-wave time-domain hybrid technique which combines the advantages of the numerical Transmission Line Matrix (TLM) method in dense, finite regions and those of the Integral Equation method in homogeneous regions where

analytical and/or numerical Green's functions are available for representing the electromagnetic field. The hybrid TLM-IE method has been developed in order to treat efficiently transient interferences between complex objects separated by large free-space region. In such a method the 3D-space is segmented in different sub-regions containing the physical objects (structures, devices, circuits). Inside the subregions the electromagnetic field is modeled by the TLM method, whereas outside the subregions it is represented by equivalent sources located on the surfaces which bound the subregions. These equivalent current/charges distributions are coupled via the dyadic Green's function (be it analytical and/or numerical) of the homogeneous region. At the boundary between the discretized TLM regions and the continuous region the two representations are then interfaced by applying the continuity of the EM tangential field, thus providing appropriate sets of Electric Field Integral Equations (EFIE) and Magnetic Field Integral Equations (MFIE). The latter integral equations are then transformed in matrix systems by applying the Moment Method in the time-domain (TDMOM) and solved explicitly, at each time step, for the unknown tangential field. The tangential field components represent, in turns, the exact boundary condition for the TLM subregions.

The method of moments (MOM) plays a crucial role in numerical electromagnetics [3] [4] [34]. In the MOM the field functions are expanded into series of basis functions. The problem of solving partial differential equations or integral equations for the field functions is converted into the problem of solving linear systems of equations for determining the coefficients of the series expansions of the field functions. Within the methods for field computation the MOM holds a special position since most of the methods of field computation - for example the integral equation method, the spectral domain method, the partial wave synthesis, the transmission line matrix method and the finite difference method - may be considered in connection with the MOM. The MOM is a very general scheme for the discretization of the field problem, whereas the other methods specify in detail how to the discretization is performed. The integral equation (IE) method introduces the far-field interaction via Green's functions and may reduce the dimension of the field problem [4] [29]. Since the interaction with infinite space is included in the Green's function integral equation methods are especially powerful in the case of radiating structures. In the spectral domain method the integral equations are transformed into algebraic equations by Fourier transformation with respect to the space coordinates [36]. Integral equation methods as well as spectral domain methods are computationally efficient but require considerable analytic preprocessing for the specific class of structures to be modeled.

The well-known marching-on-in-time (MOT) method is usually adopted to solve the time domain integral equations (TDIE) for transient scattering problems [23]. An explicit equation that relates the current at a certain time instant to the currents of previous instants and the incident field is obtained. An important disadvantage of this procedure is the possible occurrence of rapidly growing spurious oscillations at later instant which is apparently due to the accumulation of errors during the calculations.

Many researchers have extensively analyzed the stability of time marching numerical schemes. Although the instability can often be reduced or eliminated on a particular mesh by averaging the current in time [21] [22] [23] or space [82], the schemes typically become more unstable as more mesh points are used. This means that even if a method appears to be stable on one particular mesh it cannot be assumed that it will be stable on another finer mesh and, hence, cannot be used for general surfaces with any degree of confidence. Many works have been done for suppressing the late time instability, such as conjugate degree method [25], weighted Laguerre polynomials [26], smoothing procedures [84] and others. But these methods need more additional computation time. The schemes in [27] pushes the late-time instability further down in time but could not eliminate it completely unless an implicit scheme, such as the one proposed in [28], which requires solving a large matrix equation, is employed. The solution of the system matrix can become an excessive burden on CPU time. This characteristic is especially burdensome in the time-domain version, where a matrix equation has to be solved at each time step of the marching-on-in-time algorithm, so without matrix inversion, the speed of MOT method is very fast. In the present work, we have used the averaging scheme proposed in [21], because the scheme is simple, accurate, and involves a negligible amount of extra computation.

3.2 The Scope of the Thesis

The analysis of the electromagnetic interaction between objects separated by wide free space regions with a full-wave method such as the TLM or the FDTD method, based on a full discretization of the environment, represents a challenging task with regard to computational resources and modeling effort. A suitable hybrid method which drastically reduces computation time and effort is to combine the TLM method and the Integral-Equation (IE) method in a hybrid method that permits to incorporate the treatment of large free space regions with high efficiency. However, there still exist some drawbacks to this hybrid technique since, for objects with thin curved boundaries, the staircasing approach employed in the conventional TLM method can introduce significant errors into the solution unless very dense grids are used to accurately resolve the variations in the geometric features, with a consequent increase in the computational demands. Although an alternative might be to use a nonuniform mesh or a local subcell approach, these are still susceptible to the errors introduced by staircasing. Furthermore, they may, in fact, be less accurate than their uniform counterpart. Staircase errors can be mitigated by using the method of moment solution of the EFIE, which has the advantage over TLM that it employs surface discretization that are well suited for modeling of thin curved structure. The considered problem space is separated into subregions. The segmentation of the problem space can be applied very easily on the TLM method. In the TLM scheme the field dynamics are expressed as incident and reflected wave pulses which are propagating in a mesh of

transmission lines. Hence spatial regions can be described as multiports. This enables us to separate the considered problem space into subregions which are connected with each other via interface surfaces. Since in the TLM method the segmentation of the space can be handled very easily the TLM method is also very suitable to be combined with other methods. The TLM-TDMOM approach takes advantage of the capability of the TLM to analyze inhomogeneous bodies with arbitrary material properties and that of the IE/MOM to deal with thin wire/surface structures located in free space, in a numerically efficient manner to calculate the electromagnetic interaction between a complex inhomogeneous objects and arbitrarily oriented thin wire/surface structures, separated by large free-space regions.

The present work focuses on the theoretical concept of the hybrid TLM-IE/TDMOM method combining the flexibility of Transmission line Matrix method (TLM) with the efficiency of the Integral-Equation/Method of Moments for the efficient numerical modeling of transient electromagnetic interferences. The attributes of such methods, both in terms of computational efficiency, solution accuracy and stability, are examined through their application to the analysis of several electromagnetic problems. For this purpose the hybridization of the explicit time evolution TLM-scheme with the explicit integral-Equation/Method of Moments algorithm is presented and utilized. Also, a comparison is provided between the pure conventional TLM and the hybrid method (TLM-IE/MOM) with regards to the computational efficiency.

The main goals to be set and achieved by the hybrid TLM-IE/MOM are:

- Acceleration of TLM simulations and enhancement of computational efficiency (Simulation time and memory)
- Accurate and efficient treatment of free-space regions, arbitrarily curved thin wire and surface structures.

The purpose of this thesis is to address the different steps of the hybrid TLM-IE/MOM method implementation, to illustrate the capability of this hybrid method and to establish guidelines for its selection in preference to the pure conventional TLM method with a particular focus on the analysis of transient electromagnetic interference between a complex object and a curved conducting structure.

3.3 Structure of the Manuscript

This section outlines the organization of the work contained in this thesis. In cases where a novel technique has been introduced comparisons with results gained from existing methods are drawn upon as appropriate and discussed in context with the work described. The present work can be divided into two main areas: development and application of the hybrid TLM-IE/MOM method to the numerical modeling of transient interference.

In **Chapter 3**, after a brief introduction, the motivation for this work is expanded in the context of the present state-of-the-art of the Transmission Line Matrix (TLM) method, its hybrid algorithms and of the time domain integral equation in combination with the method of moments.

In **Chapter 4**, the principles of the TLM method with symmetrical condensed node are explained. The discretization of the computational domain using TLM cells and nodes is illustrated. The TLM scattering algorithm is presented and the symmetrical condensed node both with and without stubs is recalled. Various mappings between the TLM wave pulses and the discretized electromagnetic field components are given. The Hilbert space formulation of the TLM is introduced using the DIRAC notation; the TLM method is expressed by operator equations. The Hilbert space formulation of the TLM method will be used.

In **Chapter 5,** after a short introduction with some background theory of electromagnetic fields, special emphasis is placed on the time domain integral equation methods. Consideration is given to the application of the electric field integral equation in combination with the method of moments for the investigation of the scattering of arbitrarily oriented thin wire and surface structures. The goal of this chapter is to find current distribution on the structure surface excited by a incident electromagnetic signal using the marching on in time technique. Using the MOT procedure an explicit equation that relates the current at a certain time instant to the currents of previous instants and the incident field is obtained. The resulting current distribution is the major parameter of interest. Wire structures are traditionally studied in terms of a one-dimensional segment model. The method of moments (MOM) used for conducting surfaces relies on RWG (Rao-Wilton-Glisson) edge elements. Conducting surfaces are divided into separate triangles. Each pair of triangles, having a common edge, constitutes the corresponding RWG edge element.

At this point, we are well equipped for the introduction of the hybrid TLM-IE method in **Chapter 6**. This chapter illustrates the hybridization of the Transmission Line Matrix method with the integral equation method to investigate the transient electromagnetic coupling between two complex objects separated by large free space region. The near field region of the complex objects is modeled by the full-wave TLM method, while the electromagnetic interaction between the subregions is modeled by the integral equation.

In **Chapter 7**, the novel efficient hybrid Transmission Line Matrix - Method of Moments (TLM-TDMOM) approach is proposed for a full-wave analysis of the electromagnetic interaction between a complex structure and thin curved wire or surface structures. Using the hybrid TLM-TDMOM approach, time and memory requirements for structure response generation can be reduced in comparison to pure TLM simulations, while improving solution accuracy.

The application of the hybrid TLM-TDMOM method to different electromagnetic problems is presented in **Chapter 8**. A comparison between the results obtained from the novel hybrid method and those obtained from the pure conventional TLM

method is presented. A direct comparison of the two methods is discussed, focusing on accuracy, computation time and memory requirements. The objective of this chapter is to illustrate the validation and capability of the hybrid method and to establish guidelines for its selection in preference to TLM with a particular focus on the analysis of electromagnetic transient interferences.

Finally, **Chapter 9** draws together the main conclusions of this work by summarizing and discussing its main results.

4 The Transmission Line Matrix Method

4.1 Introduction

The three-dimensional Transmission Line Matrix (TLM) method with symmetrical condensed node (SCN) introduced by Johns [1] has proven to be a very powerful method of electromagnetic field computation [50] [48] [86]. The technique was originally based on Huygens model of wave propagation and inspired by earlier network simulation techniques. According to Huygens principle, a wave front consists of a number of secondary radiators that give rise to spherical wavelets. The envelope of these wavelets forms a new wavefront which in turns give rise to spherical wavelets and so forth.

The Transmission Line Matrix, TLM, method employs a network of discrete transmission lines connected at scattering junctions in order to simulate the behavior of a distributed system [48]. It is based on the analogy between the field quantities and lumped circuit equivalents. The space is discretised using a mesh of transmission lines connected at nodes. The field, which is represented by wave pulses scattered in the nodes and propagating in the transmission lines, is calculated at each node at every time step. The theoretical foundation, generalization are presented in the next sections.

4.2 Basics of the TLM Method

The TLM method is a powerful and versatile time-domain algorithm for the numerical full-wave analysis of electromagnetic field problems. The TLM is founded on the propagation of electromagnetic waves according to the Huygens principle and based on the analogy between the propagation of discretized electromagnetic fields and a mesh of transmission lines and nodes. The TLM method involves dividing the solution region into a rectangular cells and the tangential components of the electromagnetic field are sampled at the center of each boundary surface of a cell (or at the cell center according to Johns), at so-called ports according to Fig. 4.1. The transmission line connect the center of a cell (the node) with its ports at the boundary surfaces. The continuous

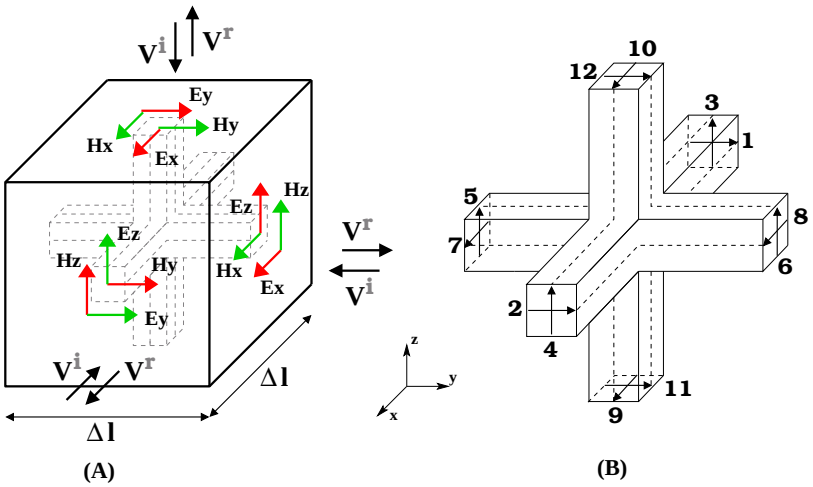

Figure 4.1: Symmetrical condensed node; (A) TLM cell, (B) three-dimensional SCN.

space is approximated by a mesh of TLM nodes interconnected by transmission lines (or by a mesh of transmission lines interconnecting TLM nodes). The time evolution of the electromagnetic field is modeled by wave pulses propagating between adjacent cells and scattered within the cells, i.e. the wave pulses are scattered at the nodes and these scattered pulses are propagated through the transmission lines to the adjacent nodes, where these pulses are scattered again. In general, the TLM cell, as indicated in Fig. 4.1(A), is represented by a respective abstract network model containing a scattering center with six stubs which is connected via twelve transmission lines with ports of adjacent cells. When all transmission lines have the same length and the node is located in the cell center this model is called as the symmetrical Condensed Node (SCN). The lossless three-dimensional SCN shown in Fig. 4.1(B) was introduced by Johns in 1987 [1] first. As a basis for the present thesis the Johns original form of the TLM method with SCN is preferred.

4.3 The TLM Scheme in Hilbert Space

The field state of each cell is given by the 12 or 18-dimensional vectors of incident and reflected TLM pulses. The whole set of these vectors comprises an approximate solution of the electromagnetic field problem. As one has not only in space but also in time an enumerable infinite number of intervals, it is possible to define an Hilbert space for describing the discrete field problem [2] [85]. In this abstract Hilbert space, it is possible to investigate the TLM algorithm algebraically, which facilates the calculation

of the dispersion characteristics of TLM meshes.

Now we introduce the Hilbert space spanned by the sequence of the grid points with normalized space coordinates l, m and n. The indices l, m and n are linked to the space coordinates with unitary spatial steps Δl_x, Δl_y and Δl_z through $x = l\Delta l_x$, $y = m\Delta l_y$ and $z = n\Delta l_z$. A base vector, characterized by the number triple (l, m, n), is assigned to each TLM cell.

If the Hilbert space is chosen appropriately, the base vectors fulfill the orthogonality relation

$$\langle l_i, m_i, n_i | l_j, m_j, n_j \rangle = \delta_{l_i,l_j} \delta_{m_i m_j} \delta_{n_i n_j}. \tag{4.1}$$

The Hermitian conjugate is denoted by $\langle l, m, n|$. The Cartesian product of the space of base vectors with the space of TLM pulse vectors defines a space for describing the complete field state at time k. We now introduce the wave amplitude vectors

$${}_k\mathbf{a}_{l,m,n} = {}_k \left[a_1, a_2, a_3, ...a_{10}, a_{11}, a_{12}\right]^T_{l,m,n}, \tag{4.2}$$

$${}_k\mathbf{b}_{l,m,n} = {}_k \left[b_1, b_2, b_3, ...b_{10}, b_{11}, b_{12}\right]^T_{l,m,n}, \tag{4.3}$$

where the state vectors ${}_k\mathbf{a}_{l,m,n}$ and ${}_k\mathbf{b}_{l,m,n}$ summarize the incident and the scattered wave pulses at the single SCN (l, m, n) at the discrete time k corresponding to the unit time interval Δt. The instant scattering of the wave pulses at the single SCN is represented by

$${}_{k+1}\mathbf{b}_{l,m,n} = {}_k\mathbf{S}_{l,m,n} \; {}_k\mathbf{a}_{l,m,n}, \tag{4.4}$$

where the operator ${}_k\mathbf{S}_{l,m,n}$is related to the scattering rules of wave amplitudes at the single SCN (l, m, n). The Cartesian product of the space of base vectors with the space of TLM pulse vectors defines a space for describing the complete field state at time k. The state vector of all incident $|{}_k\mathbf{a}\rangle$ and scattered $|{}_k\mathbf{b}\rangle$ wave amplitudes of the complete TLM mesh at time k are given by

$$|{}_k\mathbf{a}\rangle = \sum_{l,m,n=-\infty}^{+\infty} {}_k\mathbf{a}_{l,m,n} \, |l, m, n\rangle \, , \tag{4.5}$$

$$|{}_k\mathbf{b}\rangle = \sum_{l,m,n=-\infty}^{+\infty} {}_k\mathbf{b}_{l,m,n} \, |l, m, n\rangle \, . \tag{4.6}$$

Applying the projection operator $|l, m, n\rangle \langle l, m, n|$ yields the vector of the incident and scattered wave pulses of TLM cell (l, m, n),

$$|l, m, n\rangle \langle l, m, n| \; {}_k\mathbf{a}\rangle =_k \mathbf{a}_{l,m,n} \, |l, m, n\rangle \, , \tag{4.7}$$

$$|l, m, n\rangle \langle l, m, n| \; {}_k\mathbf{b}\rangle =_k \mathbf{b}_{l,m,n} \, |l, m, n\rangle \, . \tag{4.8}$$

The simultaneous scattering at all TLM mesh nodes can be described by the operator equation

$$|_{k+1}\mathbf{b}\rangle = {}_k\mathbf{S}\,|_k\mathbf{a}\rangle\,, \tag{4.9}$$

where the scattering matrix ${}_k\mathbf{S}$ is given by

$${}_k\mathbf{S} = \sum_{l,m,n=-\infty}^{+\infty} |l,m,n\rangle\, {}_k\mathbf{S}_{l,m,n}\, \langle l,m,n|\,. \tag{4.10}$$

The operator ${}_k\mathbf{S}$ represents the scattering operations at the time k for the complete TLM mesh. Introducing the connection operator ${}_k\mathbf{\Gamma}$ to specify the interaction between adjacent cells (or nodes) we obtain the TLM time evolution scheme for a lossless case

$$|_{k+1}\mathbf{a}\rangle = {}_k\mathbf{\Gamma}_k\mathbf{S}\,|_k\mathbf{a}\rangle\,. \tag{4.11}$$

In order to describe the time evolution of electromagnetic fields in the TLM scheme we define an unitary time shift operator as

$$\mathbf{T}\,|k,l,m,n\rangle = |k+1,l,m,n\rangle\,, \tag{4.12}$$

which does not describe the time evolution of the vector $|l,m,n\rangle$, it just shifts the vector $|l,m,n\rangle$ for a time step Δt, i.e.

$$\mathbf{T}\,(\mathbf{T}\,|k,l,m,n\rangle) = |k+2,l,m,n\rangle\,. \tag{4.13}$$

Its inverse shift operator

$$\mathbf{T}^\dagger\,|k,l,m,n\rangle = |k-1,l,m,n\rangle\,, \tag{4.14}$$

satisfies

$$\mathbf{T}\mathbf{T}^\dagger = \mathbf{T}^\dagger\mathbf{T} = \sum_{l,m,n=-\infty}^{+\infty} |k,l,m,n\rangle\,\langle k,l,m,n| = 1. \tag{4.15}$$

Therfore the TLM algorithm can be summarized as

$$|\mathbf{b}\rangle = \mathbf{\Gamma}\mathbf{S}\,|\mathbf{a}\rangle\,, \tag{4.16}$$

$$|\mathbf{a}\rangle = \mathbf{\Gamma}\,|\mathbf{b}\rangle\,, \tag{4.17}$$

where the global scattering $\mathbf{S}$ and $\mathbf{\Gamma}$ connection operators are defined as

$$\mathbf{S} = \sum_{l,m,n=-\infty}^{+\infty} |k,l,m,n\rangle\, {}_k\mathbf{S}_{k,l,m,n}\, \langle k,l,m,n|\,, \tag{4.18}$$

and

$$\mathbf{\Gamma} = \sum_{k=-\infty}^{+\infty} |k\rangle \, {}_k\mathbf{\Gamma} \, \langle k| \, . \tag{4.19}$$

The eqs. (4.16) with (4.18) describes the scattering process of all incident wave amplitudes at every time step k. The eqs. (4.17) with (4.19) describes the connection between all cells at every time step k. The system of these equations gives the complete description of the TLM algorithm. Using the time shift operator $\mathbf{T}$ the complete time-spatial state of the TLM scheme can be written as,

$$|\mathbf{a}\rangle = \mathbf{T\Gamma S} \, |\mathbf{a}\rangle \, , \tag{4.20}$$

$$|\mathbf{b}\rangle = \mathbf{T\Gamma S} \, |\mathbf{b}\rangle \, . \tag{4.21}$$

The TLM scheme can be fully characterized by using only one of the state vector (incident or scattered) amplitudes, as shown in the eqs. (4.20) and (4.21). It means also that only one (incident or scattered) wave vector has to be stored to calculate the electromagnetic field state vector.

4.4 The Scattering Process

The scattering Matrix $\mathbf{S}_{l,m,n}$ of Johns original node [1] for homogeneous media is defined as follows

$$\mathbf{S}_{l,m,n} = \begin{pmatrix}
a & c & 0 & 0 & 0 & 0 & d & -d & 0 & 0 & b & b \\
c & a & 0 & 0 & 0 & 0 & -d & d & 0 & 0 & b & b \\
0 & 0 & a & c & b & b & 0 & 0 & d & -d & 0 & 0 \\
0 & 0 & c & a & b & b & 0 & 0 & -d & d & 0 & 0 \\
0 & 0 & b & b & a & c & 0 & 0 & 0 & 0 & d & -d \\
0 & 0 & b & b & c & a & 0 & 0 & 0 & 0 & -d & d \\
d & -d & 0 & 0 & 0 & 0 & a & c & b & b & 0 & 0 \\
-d & d & 0 & 0 & 0 & 0 & c & a & b & b & 0 & 0 \\
0 & 0 & d & -d & 0 & 0 & b & b & a & c & 0 & 0 \\
0 & 0 & -d & d & 0 & 0 & b & b & c & a & 0 & 0 \\
b & b & 0 & 0 & d & -d & 0 & 0 & 0 & 0 & a & c \\
b & b & 0 & 0 & -d & d & 0 & 0 & 0 & 0 & c & a
\end{pmatrix} . \tag{4.22}$$

The scattering matrix $\mathbf{S}_{l,m,n}$ has the following properties:

- Each incident pulse is according to the field component assigned to it, only connected with some of the other ports. For example the pulse a_7 having an E_x and a H_z field component assigned to it, can according to

$$\frac{dH_z}{dy} - \frac{dH_y}{dz} = \varepsilon \frac{dE_x}{dt}, \qquad \frac{dE_y}{dx} - \frac{dE_x}{dy} = -\mu \frac{dH_z}{dt}, \tag{4.23}$$

only be scattered into ports 7, 8, 9, and 10, as E_x and H_z are also associated with port 8 on a y-directed line. whereas E_x and H_y are associated with ports 7 and 9 on z-directed lines.

- Due to the symmetry of the node, there are only four unknown parameters, and

$$\mathbf{S}_{l,m,n} = \mathbf{S}_{l,m,n}^T. \tag{4.24}$$

- The scattering process must preserve charge.
- The scattering process is supposed to be lossless, so energy must be conserved. It means that the energy must be conserved meaning that the scattering matrix must be unitary, i.e.

$$\mathbf{S}_{l,m,n}^T \mathbf{S}_{l,m,n} = 1. \tag{4.25}$$

With the last two properties, the one of four possible solutions for the unknown parameters a, b, c and d can be determined as

$$a = 0, \quad b = \frac{1}{2}, \quad c = 0, \quad d = \frac{1}{2}. \tag{4.26}$$

The scattering Matrix from the eq. (4.22) can be written in compact form as

$$\mathbf{S}_{l,m,n} = \begin{pmatrix} 0 & \mathbf{S}_0 & \mathbf{S}_0^T \\ \mathbf{S}_0^T & 0 & \mathbf{S}_0 \\ \mathbf{S}_0 & \mathbf{S}_0^T & 0 \end{pmatrix}, \text{ with } \mathbf{S}_0 = \begin{pmatrix} 0 & 0 & \frac{1}{2} & -\frac{1}{2} \\ 0 & 0 & -\frac{1}{2} & \frac{1}{2} \\ \frac{1}{2} & \frac{1}{2} & 0 & 0 \\ \frac{1}{2} & \frac{1}{2} & 0 & 0 \end{pmatrix}. \tag{4.27}$$

The scattering matrix $\mathbf{S}_{l,m,n}$ has the property $\mathbf{S} = \mathbf{S}^T = \mathbf{S}^\dagger = \mathbf{S}^{-1}$, i.e. it is real, symmetric, hermitian and unitary. Consequently the TLM scheme fulfills energy conservation, reciprocity and invariance with respect to time reversal exactly.

We consider the TLM mesh to be composed of condensed symmetric TLM nodes as shown in Fig. 4.1(B), where each of the six arms is of length $\Delta l/2$, with the same characteristic impedance

$$Z_0 = \sqrt{\frac{\mu_0}{\varepsilon_0}} = \sqrt{\frac{L_0}{C_0}}, \tag{4.28}$$

and propagation velocity

$$c_0 = \frac{1}{\sqrt{\mu_0 \varepsilon_0}} = \frac{1}{\sqrt{L_0 C_0}}. \tag{4.29}$$

The characteristic impedance and the propagation velocity in each arm can be modeled by network with one capacitance C_0 and the inductance L_0 [50] with

$$C_0 = Y_0 \frac{\Delta t}{2} = \varepsilon_0 \frac{\Delta l}{h} \quad \text{and} \quad L_0 = Z_0 \frac{\Delta t}{2} = \mu_0 \frac{\Delta l}{h}, \tag{4.30}$$

where h is a stability factor introduced as

$$h \geq \frac{2\Delta l}{c_0 \Delta t}. \tag{4.31}$$

To account for inhomogeneous media and non-cubic TLM cells with dimensions

$$(\Delta l_x,\, \Delta l_y,\, \Delta l_z) \equiv (u\Delta l,\, v\Delta l,\, w\Delta l)\,,$$

Johns added open and short circuited stubs to the node. Each stub has a length according to a propagation time of $\Delta t/2$. The port numbers 13-18 are assigned to the six stubs. The first three stubs couple to E_x, E_y and E_z. They are open, as to add additional capacitance to the node. The other three stubs are shorted and couple to H_x, H_y and H_z and add further inductance to the node. As each stub only couples to one of the field components, it is possible to account for anisotropic material properties, namely permittivity ϵ_x, ϵ_y and ϵ_z, and permeability μ_x, μ_y and μ_z. For more details see [1] and [50]. The variation of the node arm length causes the changing of the propagation time through the node. The equal time variation can be achieved through the corresponding scaling of capacitances and inductances as well. The required total capacitances at a SCN of dimension $(u\Delta l,\, v\Delta l,\, w\Delta l)$ introduced by Johns in [1] are

$$C_x = \varepsilon_x \frac{vw}{u}\Delta l,\; C_y = \varepsilon_y \frac{uw}{v}\Delta l,\; C_z = \varepsilon_z \frac{uv}{w}\Delta l, \tag{4.32}$$

and inductances are

$$L_x = \mu_x \frac{vw}{u}\Delta l,\; L_y = \mu_y \frac{uw}{v}\Delta l,\; L_z = \mu_z \frac{uv}{w}\Delta l. \tag{4.33}$$

For example, the modeled capacitance C_x is associated with lines 7, 8, 9 and 10, and as following, is equivalent to $4C_0$ for a cubic TLM cell in free space. The modeled inductance L_x is linked to the lines 5, 6, 11 and 12, and is equivalent to $4L_0$. Therefore, in order to model non-uniform cells the capacitance and inductance have to be added to the symmetric node, e.g. for the x-components we have

$$C_x^{stub} = \varepsilon_x \frac{vw}{u} - 4C_0,\;\; and \;\; L_x^{stub} = \mu_x \frac{vw}{u} - 4\Delta L_0 \tag{4.34}$$

From eqs. (4.30-4.34) and from the relations normalized with respect to Y_0 and/or Z_0 we get,

$$C^{stub} = Y_0 Y^{stub} \frac{\Delta t}{2},\;\; and \;\; L^{stub} = Z_o Z^{stub} \frac{\Delta t}{2}, \tag{4.35}$$

where the admittances $Y^{stub}$of the stubs $13 - 15$ are calculated by

$$Y_x = 2(\frac{vw}{u} h\varepsilon_{rx} - 2),\;\; Y_y = 2(\frac{uw}{v} h\varepsilon_{ry} - 2),\;\; Y_z = 2(\frac{uv}{w} h\varepsilon_{rz} - 2), \tag{4.36}$$

where ε_{rx}, ε_{ry} and ε_{rz} denote the relative permittivities. The impedances of stubs $16-18$ are calculated in a similar manner, which results in

$$Z_x = 2(\frac{vw}{u}h\mu_{rx} - 2),\ \ Z_y = 2(\frac{uw}{v}h\mu_{ry} - 2),\ \ Z_z = 2(\frac{uv}{w}h\mu_{rz} - 2), \tag{4.37}$$

where μ_{rx}, μ_{ry} and μ_{rz} represent the permeabilities. If ohmic and magnetic losses have to be included, six additional stubs are connected to the center of the SCN, so the 18×18 scattering matrix gets six additional lines. The scattering in these stubs needs not explicitly be considered as the energy dissipated in these lines is lost. The values of the loss stubs for the simulating ohmic losses are given by

$$G_x = \frac{vw}{u}\sigma_{ex}\Delta l Z_0,\ C_y = \frac{uw}{v}\sigma_{ey}\Delta l Z_0,\ C_z = \frac{uv}{w}\sigma_{ez}\Delta l Z_0, \tag{4.38}$$

where σ_{ex}, σ_{ey} and σ_{ex} represent the electric conductivities in x-, y- and z-direction. The magnetic loss stubs are analogously calculated as

$$R_x = \frac{vw}{u}\sigma_{mx}\Delta l Y_0,\ R_y = \frac{uw}{v}\sigma_{my}\Delta l Y_0,\ R_z = \frac{uv}{w}\sigma_{mz}\Delta l Y_0, \tag{4.39}$$

where σ_{mx} , σ_{my} and σ_{mz} stand for the anisotropic magnetic conductivities. Considering the loss stubs, the general scattering 18×18 matrix of any deformed SCN has been introduced by Johns [1] as following

$$\mathbf{S}^{stubs}_{l,m,n} = \begin{pmatrix}
a & c & 0 & 0 & 0 & 0 & d & \bar{d} & 0 & 0 & b & b & 0 & g & 0 & 0 & 0 & \bar{d} \\
c & a & 0 & 0 & 0 & 0 & \bar{d} & d & 0 & 0 & b & b & 0 & g & 0 & 0 & 0 & d \\
0 & 0 & a & c & b & b & 0 & 0 & d & \bar{d} & 0 & 0 & 0 & 0 & g & 0 & d & 0 \\
0 & 0 & c & a & b & b & 0 & 0 & \bar{d} & d & 0 & 0 & 0 & 0 & g & 0 & \bar{d} & 0 \\
0 & 0 & b & b & a & c & 0 & 0 & 0 & 0 & d & \bar{d} & 0 & 0 & g & \bar{d} & 0 & 0 \\
0 & 0 & b & b & c & a & 0 & 0 & 0 & 0 & \bar{d} & d & 0 & 0 & g & d & 0 & 0 \\
d & \bar{d} & 0 & 0 & 0 & 0 & a & c & b & b & 0 & 0 & g & 0 & 0 & 0 & 0 & d \\
\bar{d} & d & 0 & 0 & 0 & 0 & c & a & b & b & 0 & 0 & g & 0 & 0 & 0 & 0 & \bar{d} \\
0 & 0 & d & \bar{d} & 0 & 0 & b & b & a & c & 0 & 0 & g & 0 & 0 & 0 & \bar{d} & 0 \\
0 & 0 & \bar{d} & d & 0 & 0 & b & b & c & a & 0 & 0 & g & 0 & 0 & 0 & d & 0 \\
b & b & 0 & 0 & d & \bar{d} & 0 & 0 & 0 & 0 & a & c & 0 & g & 0 & d & 0 & 0 \\
b & b & 0 & 0 & \bar{d} & d & 0 & 0 & 0 & 0 & c & a & 0 & g & 0 & \bar{d} & 0 & 0 \\
0 & 0 & 0 & 0 & 0 & 0 & b & b & b & b & 0 & 0 & h & 0 & 0 & 0 & 0 & 0 \\
b & b & 0 & 0 & 0 & 0 & 0 & 0 & 0 & 0 & b & b & 0 & h & 0 & 0 & 0 & 0 \\
0 & 0 & b & b & b & b & 0 & 0 & 0 & 0 & 0 & 0 & 0 & 0 & h & 0 & 0 & 0 \\
0 & 0 & 0 & 0 & \bar{f} & f & 0 & 0 & 0 & 0 & f & \bar{f} & 0 & 0 & 0 & j & 0 & 0 \\
0 & 0 & f & \bar{f} & 0 & 0 & 0 & 0 & \bar{f} & f & 0 & 0 & 0 & 0 & 0 & 0 & j & 0 \\
\bar{f} & f & 0 & 0 & 0 & 0 & f & \bar{f} & 0 & 0 & 0 & 0 & 0 & 0 & 0 & 0 & 0 & j
\end{pmatrix}, \tag{4.40}$$

with coefficients

$$a = -\frac{G+Y}{2(G+Y+4)} + \frac{R+Z}{2(R+Z+4)},\ b = \frac{2}{G+Y+4},$$

$$c = -\frac{G+Y}{2(G+Y+4)} - \frac{R+Z}{2(R+Z+4)},\ d = \frac{2}{Z+R+4},\ \bar{d} = -d$$
$$f = \frac{2Z}{R+Z+4},\ \bar{f} = -f, \qquad g = \frac{2Y}{G+Y+4}, \tag{4.41}$$
$$h = -\frac{G-Y+4}{G+Y+4}, \qquad j = -\frac{-R+Z-4}{R+Z+4}.$$

For the general scattering matrix eq. (4.40) with losses we have that

$$\mathbf{S}^{stub}_{l,m,n} \neq \left[\mathbf{S}^{stub}_{l,m,n}\right]^{\dagger} \neq \left[\mathbf{S}^{stub}_{l,m,n}\right]^{-1}. \tag{4.42}$$

The symmetry of $\mathbf{S}^{stub}_{l,m,n}$ is not preserved due to the stub parameter normalization proposed by Johns. The unitarity of the scattering matrix is not only lost due to the losses in an analyzed structure. Indeed, even though the scattering matrix in eq. (4.40) comprises no losses, it is also non-unitary. In other words, the unitarity and symmetry are lost due to the normalization in accord with eq. (4.40). However, the symmetry of the general scattering operator in eq. (4.40) can be reconstructed by a new normalization without its energy conservation property being changed by following

$$\hat{\mathbf{S}}^{stub}_{l,m,n} = \mathbf{N}^{-1}\mathbf{S}^{stub}_{l,m,n}\mathbf{N}, \tag{4.43}$$

here the diagonal matrix $\mathbf{N}$ is given as

$$N = diag\left[1,1,1,1,1,1,1,1,1,1,1,1,1,1,1,1,(\sqrt{Y})^{-1},\sqrt{Z}\right]. \tag{4.44}$$

Now the modified general scattering operator for the lossy SCN in eq. (4.43) satisfies next relations

$$\hat{\mathbf{S}}^{stub}_{l,m,n} = \left[\hat{\mathbf{S}}^{stub}_{l,m,n}\right]^{\dagger} \neq \left[\hat{\mathbf{S}}^{stub}_{l,m,n}\right]^{-1}. \tag{4.45}$$

The general scattering operator ${}_k\mathbf{S}$ describing the scattering at all nodes of the TLM mesh at the time k, has the block-diagonal matrix structure, i.e.

$${}_k\mathbf{S} = diag\left[\hat{\mathbf{S}}^{stub}_{l,m,n}\right]. \tag{4.46}$$

Then we obtain the following properties of the operator $\mathbf{S}$,

$${}_k\mathbf{S} = {}_k\mathbf{S}^{\dagger} \neq {}_k\mathbf{S}^{-1}. \tag{4.47}$$

Further, we will deal with the modified scattering operators in accord with eq. (4.43) and eq. (4.46), which are self-adjoint (or Hermitian) and non-unitary. The modifications of the $\mathbf{S}_{l,m,n}$ in eq. (4.43) does not infringe mapping between the electromagnetic field and the wave amplitudes.

4.5 The Connection Process

In order to describe the connection process with the operator $\mathbf{\Gamma}$ representing the interaction between all adjacent nodes, we define first the unitary shift operators $\mathbf{X}$, $\mathbf{Y}$, $\mathbf{Z}$ and their Hermitian conjugate $\mathbf{X}^\dagger$, $\mathbf{Y}^\dagger$, $\mathbf{Z}^\dagger$ as

$$\begin{aligned}
\mathbf{X}\,|l,m,n\rangle &= |l+1,m,n\rangle\,,\\
\mathbf{X}^\dagger\,|l,m,n\rangle &= |l-1,m,n\rangle\,,\\
\mathbf{Y}\,|l,m,n\rangle &= |l,m+1,n\rangle\,,\\
\mathbf{Y}^\dagger\,|l,m,n\rangle &= |l,m-1,n\rangle\,,\\
\mathbf{Z}\,|l,m,n\rangle &= |l,m,n+1\rangle\,,\\
\mathbf{Z}^\dagger\,|l,m,n\rangle &= |l,m,n-1\rangle\,.
\end{aligned} \tag{4.48}$$

The spatial operators $\mathbf{X}$, $\mathbf{Y}$ and $\mathbf{Z}$ shift the position of the node (l,m,n) by Δl in positive $x-$, $y-$ or $z-$direction respectively. The operators $\mathbf{X}^\dagger$, $\mathbf{Y}^\dagger$ and $\mathbf{Z}^\dagger$ make the opposite moving by one step. The shift operators (4.48) can be written as proposed in [2] in the next form

$$\begin{aligned}
\mathbf{X} &= \sum_{l,m,n=-\infty}^{+\infty} |l+1,m,n\rangle\,\langle l,m,n|\,,\\
\mathbf{X}^\dagger &= \sum_{l,m,n=-\infty}^{+\infty} |l-1,m,n\rangle\,\langle l,m,n|\,,\\
\mathbf{Y} &= \sum_{l,m,n=-\infty}^{+\infty} |l,m+1,n\rangle\,\langle l,m,n|\,,\\
\mathbf{Y}^\dagger &\sum_{l,m,n=-\infty}^{+\infty} |l,m-1,n\rangle\,\langle l,m,n|\,,\\
\mathbf{Z} &= \sum_{l,m,n=-\infty}^{+\infty} |l,m,n+1\rangle\,\langle l,m,n|\,,\\
\mathbf{Z}^\dagger &= \sum_{l,m,n=-\infty}^{+\infty} |l,m,n-1\rangle\,\langle l,m,n|\,.
\end{aligned} \tag{4.49}$$

The shift operators have the properties to be self-adjoint, unitary and commutative with itself [2]. Using these operators, the connection between all nodes in the infinite

space can be summarized in the following matrix form

$$
{}_k\mathbf{\Gamma} = \begin{pmatrix}
0 & X & 0 & 0 & 0 & 0 & 0 & 0 & 0 & 0 & 0 & 0 \\
\mathbf{X}^\dagger & 0 & 0 & 0 & 0 & 0 & 0 & 0 & 0 & 0 & 0 & 0 \\
0 & 0 & 0 & X & 0 & 0 & 0 & 0 & 0 & 0 & 0 & 0 \\
0 & 0 & \mathbf{X}^\dagger & 0 & 0 & 0 & 0 & 0 & 0 & 0 & 0 & 0 \\
0 & 0 & 0 & 0 & 0 & \mathbf{Y} & 0 & 0 & 0 & 0 & 0 & 0 \\
0 & 0 & 0 & 0 & \mathbf{Y}^\dagger & 0 & 0 & 0 & 0 & 0 & 0 & 0 \\
0 & 0 & 0 & 0 & 0 & 0 & \mathbf{Y} & 0 & 0 & 0 & 0 & 0 \\
0 & 0 & 0 & 0 & 0 & \mathbf{Y}^\dagger & 0 & 0 & 0 & 0 & 0 & 0 \\
0 & 0 & 0 & 0 & 0 & 0 & 0 & 0 & 0 & \mathbf{Z} & 0 & 0 \\
0 & 0 & 0 & 0 & 0 & 0 & 0 & 0 & \mathbf{Z}^\dagger & 0 & 0 & \mathbf{Z} \\
0 & 0 & 0 & 0 & 0 & 0 & 0 & 0 & 0 & 0 & 0 & \mathbf{Z} \\
0 & 0 & 0 & 0 & 0 & 0 & 0 & 0 & 0 & 0 & \mathbf{Z}^\dagger & 0
\end{pmatrix} \tag{4.50}
$$

The connection operator ${}_k\mathbf{\Gamma}$ according to eq. (4.50) has the properties

$$
{}_k\mathbf{\Gamma} = {}_k\mathbf{\Gamma}^\dagger = {}_k\mathbf{\Gamma}^{-1}, \tag{4.51}
$$

and

$$
{}_k\mathbf{\Gamma}\,{}_k\mathbf{\Gamma}^\dagger = {}_k\mathbf{\Gamma}^\dagger\,{}_k\mathbf{\Gamma} = 1. \tag{4.52}
$$

Therfore the connection operator ${}_k\mathbf{\Gamma}$ is unitary and Hermitian. As the reflected pulses from one TLM cell are the incident TLM pulses of the neighboring cells, the field state is completely defined by the incident $|{}_k\mathbf{a}\rangle$ and scattered $|{}_k\mathbf{b}\rangle$ pulse amplitudes,

$$
|{}_k\mathbf{a}\rangle = {}_k\mathbf{\Gamma}\,|{}_k\mathbf{b}\rangle \quad \text{and} \quad |{}_k\mathbf{b}\rangle = {}_k\mathbf{\Gamma}^\dagger\,|{}_k\mathbf{a}\rangle\,. \tag{4.53}
$$

Actually, it is self-evident that the matrix ${}_k\mathbf{\Gamma}$ for the infinite space filled with ones, since no losses come into play during the linking operations.

4.6 Field-Mappings for the Symmetrical Condensed Node

Considering a TLM cell as depicted in Fig. 4.1(B), it is possible to define the mapping between the 18 incident and/or scattered TLM pulse variables and the six electromagnetic field components either at the centre of the cell located at (l, m, n), or at the centre of the tangential planes as shown in Fig. 4.1(A). The mapping in the centre shall be reflected to by *centered field-mapping* (CFM) and the mapping at the boundaries of the TLM cell by *cell boundary mapping* (CBM).

4.6.1 Centered Field Mapping (CFM)

The mapping in the SCN TLM node was originally defined at the centre. Consequently, this mapping is not bijective, as in the TLM algorithm one has twelve or more variables and in MAXWELL's equations, there are only six electromagnetic field components in one point of space. In order to describe the centered Field Mapping in the Hilbert space, we introduce the field state vector

$$|\mathbf{F}\rangle = \sum_{l,m,n=-\infty}^{+\infty} \begin{bmatrix} {}_kE^x_{l,m,n} \\ {}_kE^y_{l,m,n} \\ {}_kE^z_{l,m,n} \\ Z_k H^x_{l,m,n} \\ Z_k H^y_{l,m,n} \\ Z_k H^z_{l,m,n} \end{bmatrix} |l,m,n\rangle\,, \tag{4.54}$$

where Z is the impedance of one of the six equivalent arms of the TLM cell. In order to describe the projection of the wave amplitude state vector onto the field state vector we introduce the projection operator $\mathbf{P}$ as in [1]

$$|\mathbf{F}\rangle = \frac{1}{\Delta l}\mathbf{P}\,|\mathbf{a}\rangle\,, \tag{4.55}$$

with

$$\mathbf{P} = \frac{1}{2}\begin{pmatrix} 0 & 0 & 0 & 0 & 0 & 0 & 1 & 1 & 1 & 1 & 0 & 0 \\ 1 & 1 & 0 & 0 & 0 & 0 & 0 & 0 & 0 & 0 & 1 & 1 \\ 0 & 0 & 1 & 1 & 1 & 1 & 0 & 0 & 0 & 0 & 0 & 0 \\ 0 & 0 & 0 & 0 & 1 & -1 & 0 & 0 & 0 & 0 & -1 & 1 \\ 0 & 0 & -1 & 1 & 0 & 0 & 0 & 0 & 1 & -1 & 0 & 0 \\ 1 & -1 & 0 & 0 & 0 & 0 & -1 & 1 & 0 & 0 & 0 & 0 \end{pmatrix}, \tag{4.56}$$

where The vector $|\mathbf{F}\rangle$ comprises the six electromagnetic field components, sampled in the centre of a TLM cell. Whereas $|\mathbf{a}\rangle$ is the vector of the incident TLM pulses. Then the inverse mapping $\mathbf{P}^T$ is given as

$$|\mathbf{a}\rangle = \Delta l \mathbf{P}^T\,|\mathbf{F}\rangle\,. \tag{4.57}$$

From eqs. (4.55) and (4.57) it follows that

$$|\mathbf{F}'\rangle = \mathbf{P}\mathbf{P}^T\,|\mathbf{F}\rangle \tag{4.58}$$

and

$$|\mathbf{a}'\rangle = \mathbf{P}^T\mathbf{P}\,|\mathbf{a}\rangle\,. \tag{4.59}$$

Since the operator $\mathbf{P}\mathbf{P}^T$ has ones at its diagonal, i.e.

$$\mathbf{P}\mathbf{P}^T = diag\,[1,1,1,1,1,1]\,, \tag{4.60}$$

the application of the operator $\mathbf{P}\mathbf{P}^T$ onto the field state vector does not change it, or $|\mathbf{F}'\rangle = |\mathbf{F}\rangle$. A different situation occurs for $\mathbf{P}^T\mathbf{P}$, due to the relation

$$\mathbf{P}^T\mathbf{P} = \mathbf{U}\, diag[0,0,0,0,0,0,1,1,1,1,1,1]\mathbf{U}^{-1}, \tag{4.61}$$

where $\mathbf{U}$ is an unitary matrix. The operator $\mathbf{P}^T\mathbf{P}$ transfers the vector $|\mathbf{a}\rangle$ and leads to $|\mathbf{a}'\rangle \neq |\mathbf{a}\rangle$. An important property, which has to be noticed, is that the whole energy in the wave amplitudes is conserved during a TLM simulation. According to [1] and taking into account the losses in the media with eqs. (4.38) and (4.39), the deformations of the TLM mesh in eqs. (4.36) and (4.37) and the normalization of the scattering matrix given by eq. (4.43), we obtain all six components of the electromagnetic field as

$$E_x = \frac{2}{u\Delta l}\left(\frac{a_7 + a_8 + a_9 + a_{10} + \sqrt{Y_x}a_{13}}{4 + Y_x + G_x}\right), \tag{4.62}$$

$$E_y = \frac{2}{v\Delta l}\left(\frac{a_1 + a_2 + a_{11} + a_{12} + \sqrt{Y_y}a_{14}}{4 + Y_y + G_y}\right), \tag{4.63}$$

$$E_z = \frac{2}{w\Delta l}\left(\frac{a_3 + a_4 + a_5 + a_6 + \sqrt{Y_z}a_{15}}{4 + Y_z + G_z}\right), \tag{4.64}$$

$$H_x = \frac{2}{u\Delta l Z_0}\left(\frac{a_5 - a_6 - a_{11} + a_{12} + \sqrt{Z_x}a_{16}}{4 + Z_x + R_x}\right), \tag{4.65}$$

$$H_y = \frac{2}{v\Delta l Z_0}\left(\frac{-a_3 + a_4 + a_9 - a_{10} + \sqrt{Z_y}a_{17}}{4 + Z_y + R_y}\right), \tag{4.66}$$

$$H_z = \frac{2}{w\Delta l Z_0}\left(\frac{a_1 - a_2 - a_7 + a_8 + \sqrt{Z_x}a_{18}}{4 + Z_z + R_z}\right). \tag{4.67}$$

The mapping from field components to TLM pulses to excite the TLM mesh is given as

$$a_1 = \frac{1}{2}\Delta l\,(vE_y + wZ_0H_z), \qquad a_7 = \frac{1}{2}\Delta l\,(uE_x - wZ_0H_z), \tag{4.68}$$

$$a_2 = \frac{1}{2}\Delta l\,(vE_y - wZ_0H_z), \qquad a_8 = \frac{1}{2}\Delta l\,(uE_x + wZ_0H_z), \tag{4.69}$$

$$a_3 = \frac{1}{2}\Delta l\,(wE_z - vZ_0H_y), \qquad a_9 = \frac{1}{2}\Delta l\,(uE_x + vZ_0H_y), \tag{4.70}$$

$$a_4 = \frac{1}{2}\Delta l\,(wE_z + vZ_0H_y), \qquad a_{10} = \frac{1}{2}\Delta l\,(uE_x - vZ_0H_y), \tag{4.71}$$

$$a_5 = \frac{1}{2}\Delta l\,(wE_z + uZ_0H_x), \qquad a_{11} = \frac{1}{2}\Delta l\,(vE_y - uZ_0H_x), \tag{4.72}$$

$$a_6 = \frac{1}{2}\Delta l\left(wE_z - uZ_0H_x\right), \qquad a_{12} = \frac{1}{2}\Delta l\left(vE_y + uZ_0H_x\right), \tag{4.73}$$

$$a_{13} = \frac{1}{2}u\Delta l\sqrt{Y_x}E_x, \qquad a_{16} = \frac{1}{2}u\Delta lZ_0\sqrt{Z_x}H_x, \tag{4.74}$$

$$a_{14} = \frac{1}{2}v\Delta l\sqrt{Y_y}E_y, \qquad a_{17} = \frac{1}{2}v\Delta lZ_0\sqrt{Z_y}H_y, \tag{4.75}$$

$$a_{15} = \frac{1}{2}w\Delta l\sqrt{Y_z}E_z, \qquad a_{18} = \frac{1}{2}w\Delta lZ_0\sqrt{Z_z}H_z. \tag{4.76}$$

The operator $\mathbf{P}_{stubs}$ can be summarized in the form

$$\mathbf{P}_{stub} = \begin{pmatrix} 0 & a_y^E & 0 & 0 & 0 & a_z^H \\ 0 & a_y^E & 0 & 0 & 0 & -a_z^H \\ 0 & 0 & a_z^E & 0 & -a_y^H & 0 \\ 0 & 0 & a_z^E & 0 & a_y^H & 0 \\ 0 & 0 & a_z^E & a_x^H & 0 & 0 \\ 0 & 0 & a_z^E & -a_x^H & 0 & 0 \\ a_x^E & 0 & 0 & 0 & 0 & -a_z^H \\ a_x^E & 0 & 0 & 0 & 0 & a_z^H \\ a_x^E & 0 & 0 & 0 & a_y^H & 0 \\ a_x^E & 0 & 0 & 0 & -a_y^H & 0 \\ 0 & a_y^E & 0 & -a_x^H & 0 & 0 \\ 0 & a_y^E & 0 & a_x^H & 0 & 0 \\ a_x^E\sqrt{Y_x} & 0 & 0 & 0 & 0 & 0 \\ 0 & a_y^E\sqrt{Y_y} & 0 & 0 & 0 & 0 \\ 0 & 0 & a_z^E\sqrt{Y_z} & 0 & 0 & 0 \\ 0 & 0 & 0 & a_x^H\sqrt{Z_x} & 0 & 0 \\ 0 & 0 & 0 & 0 & a_y^H\sqrt{Z_y} & 0 \\ 0 & 0 & 0 & 0 & 0 & a_z^H\sqrt{Z_z} \end{pmatrix}^T \tag{4.77}$$

where

$$a_x^E = \frac{2}{u\left(4 + Y_x + G_x\right)}, \quad a_y^E = \frac{2}{v\left(4 + Y_y + G_y\right)}, \quad a_z^E = \frac{2}{w\left(4 + Y_z + G_z\right)},$$

$$a_x^H = \frac{2}{u\left(4 + Z_x + R_x\right)}, \quad a_y^H = \frac{2}{v\left(4 + Z_y + R_y\right)}, \quad a_z^H = \frac{2}{w\left(4 + Z_z + R_z\right)}. \tag{4.78}$$

The operator $\mathbf{P}_{stub}$ can be presented as

$$\mathbf{P}_{stub} = \begin{pmatrix} 0 & e_y & 0 & 0 & 0 & h_z \\ 0 & e_y & 0 & 0 & 0 & -h_z \\ 0 & 0 & e_z & 0 & -h_y & 0 \\ 0 & 0 & e_z & 0 & h_y & 0 \\ 0 & 0 & e_z & h_x & 0 & 0 \\ 0 & 0 & e_z & -h_x & 0 & 0 \\ e_x & 0 & 0 & 0 & 0 & -h_z \\ e_x & 0 & 0 & 0 & 0 & h_z \\ e_x & 0 & 0 & 0 & h_y & 0 \\ e_x & 0 & 0 & 0 & -h_y & 0 \\ 0 & e_y & 0 & -h_x & 0 & 0 \\ 0 & e_y & 0 & h_x & 0 & 0 \\ e_x\sqrt{Y_x} & 0 & 0 & 0 & 0 & 0 \\ 0 & e_y\sqrt{Y_y} & 0 & 0 & 0 & 0 \\ 0 & 0 & e_z\sqrt{Y_z} & 0 & 0 & 0 \\ 0 & 0 & 0 & h_x\sqrt{Z_x} & 0 & 0 \\ 0 & 0 & 0 & 0 & h_y\sqrt{Z_y} & 0 \\ 0 & 0 & 0 & 0 & 0 & h_z\sqrt{Z_z} \end{pmatrix}^T, \tag{4.79}$$

with coefficients

$$\begin{aligned} e_x = \frac{u}{2}, \qquad e_y = \frac{v}{2}, \qquad e_z = \frac{w}{2}, \\ h_x = \frac{u}{2}Z_0, \qquad h_y = \frac{v}{2}Z_0, \qquad h_z = \frac{w}{2}Z_0. \end{aligned} \tag{4.80}$$

4.6.2 Cell Boundary Mapping (CBM)

Assuming a correspondence between the TLM state variables and the electromagnetic field components at the centre of the tangential planes (or the ends of the six arms) $(l\pm\frac{1}{2}, m, n)$, $(l, m\pm\frac{1}{2}, n)$ and $(l, m, n\pm\frac{1}{2})$ yields a bijective field-mapping introduced by Krumpholz and Russer [2]. The waves amplitudes at the center of the cell boundaries are defined as

$$|\mathbf{a}\rangle = 1/2\ (-|\mathbf{E}\rangle + Z \cdot \mathbf{n} \times |\mathbf{H}\rangle)\,, \tag{4.81}$$

$$|\mathbf{b}\rangle = -1/2\ (|\mathbf{E}\rangle + Z \cdot \mathbf{n} \times |\mathbf{H}\rangle)\,, \tag{4.82}$$

where $|\mathbf{E}\rangle$ and $|\mathbf{H}\rangle$ are electric and magnetic field vectors sampled at a boundary. The unity vector $\mathbf{n}$ is normal to the cell boundary. For example, we take a look at the mapping operation for the arm $(l \pm \frac{1}{2}, m, n)$ at time k. From eqs. (4.81) and (4.82) we obtain the following relations for

$$\mathbf{n} = [1, 0, 0]^T,$$

$$
\begin{aligned}
{}_k[a_x]_{l+1/2,m,n} &= 0,\\
{}_k[a_y]_{l+1/2,m,n} &=_k [a_2]_{l,m,n} = \frac{\Delta l}{2}\left(v\,{}_kE^y_{l+1/2,m,n} - wZ\,{}_kH^z_{l+1/2,m,n}\right),\\
{}_k[a_z]_{l+1/2,m,n} &=_k [a_4]_{l,m,n} = \frac{\Delta l}{2}\left(w\,{}_kE^z_{l+1/2,m,n} + vZ\,{}_kH^y_{l+1/2,m,n}\right),\\
{}_k[b_x]_{l+1/2,m,n} &= 0,\\
{}_k[b_y]_{l+1/2,m,n} &=_k [b_2]_{l,m,n} = \frac{\Delta l}{2}\left(v\,{}_kE^y_{l+1/2,m,n} + wZ\,{}_kH^z_{l+1/2,m,n}\right),\\
{}_k[b_z]_{l+1/2,m,n} &=_k [b_4]_{l,m,n} = \frac{\Delta l}{2}\left(w\,{}_kE^z_{l+1/2,m,n} - vZ\,{}_kH^y_{l+1/2,m,n}\right),
\end{aligned}
\tag{4.83}
$$

and

$$
\begin{aligned}
{}_kE^y_{l+1/2,m,n} &= \frac{1}{v\Delta l}\left({}_k[a_2]_{l,m,n} +_k [b_2]_{l,m,n}\right),\\
{}_kE^z_{l+1/2,m,n} &= \frac{1}{w\Delta l}\left({}_k[a_4]_{l,m,n} +_k [b_4]_{l,m,n}\right),\\
{}_kH^y_{l+1/2,m,n} &= \frac{1}{v\Delta lZ}\left({}_k[a_4]_{l,m,n} -_k [b_4]_{l,m,n}\right),\\
{}_kH^z_{l+1/2,m,n} &= \frac{1}{w\Delta lZ}\left({}_k[b_2]_{l,m,n} -_k [a_2]_{l,m,n}\right),
\end{aligned}
\tag{4.84}
$$

respectively. In order to obtain the *Cell Boundary Mapping* (CBM) in a matrix form we define the electromagnetic field state vectors in $|{}_k\mathbf{F}_E\rangle$ and $|{}_k\mathbf{F}_M\rangle$ as

$$
|{}_k\mathbf{F}_E\rangle_{\frac{1}{2}} = \sum_{l,m,n=-\infty}^{+\infty}
\begin{pmatrix}
{}_kE^y_{l-1/2,m,n}\\
{}_kE^y_{l+1/2,m,n}\\
{}_kE^z_{l-1/2,m,n}\\
{}_kE^z_{l+1/2,m,n}\\
{}_kE^z_{l,m-1/2,n}\\
{}_kE^z_{l,m+1/2,n}\\
{}_kE^x_{l,m-1/2,n}\\
{}_kE^x_{l,m+1/2,n}\\
{}_kE^x_{l,m,n-1/2}\\
{}_kE^x_{l,m,n+1/2}\\
{}_kE^y_{l,m,n-1/2}\\
{}_kE^y_{l,m,n+1/2}
\end{pmatrix}
|l,m,n\rangle\,,
\tag{4.85}
$$

$$|_k\mathbf{F}_M\rangle_{\frac{1}{2}} = Z \sum_{l,m,n=-\infty}^{+\infty} \begin{pmatrix} {}_kH^z_{l-1/2,m,n} \\ {}_kH^z_{l+1/2,m,n} \\ {}_kH^y_{l-1/2,m,n} \\ {}_kH^y_{l+1/2,m,n} \\ {}_kH^x_{l,m-1/2,n} \\ {}_kH^x_{l,m+1/2,n} \\ {}_kH^z_{l,m-1/2,n} \\ {}_kH^z_{l,m+1/2,n} \\ {}_kH^y_{l,m,n-1/2} \\ {}_kH^y_{l,m,n+1/2} \\ {}_kH^x_{l,m,n-1/2} \\ {}_kH^x_{l,m,n+1/2} \end{pmatrix} |l,m,n\rangle \,. \tag{4.86}$$

From eqs. (4.81) and (4.82) we obtain the mapping operations in the next operator expressions,

$$\begin{aligned} |_k\mathbf{F_E}\rangle_{\frac{1}{2}} &= \frac{1}{\Delta l}\,\mathbf{P}_\mathbf{E}^{-1}\left(|_k\mathbf{a}\rangle + |_k\mathbf{b}\rangle\right), \\ |_k\mathbf{F_H}\rangle_{\frac{1}{2}} &= \frac{1}{\Delta l}\,\mathbf{P}_\mathbf{H}^{-1}\left(|_k\mathbf{a}\rangle - |_k\mathbf{b}\rangle\right), \end{aligned} \tag{4.87}$$

and

$$\begin{aligned} |_k\mathbf{a}\rangle_{\frac{1}{2}} &= \frac{\Delta l}{2}\,\left(\mathbf{P_E}\,|_k\mathbf{F_E}\rangle_{\frac{1}{2}} + \mathbf{P_H}\,|_k\mathbf{F_H}\rangle_{\frac{1}{2}}\right), \\ |_k\mathbf{b}\rangle_{\frac{1}{2}} &= \frac{\Delta l}{2}\,\left(\mathbf{P_E}\,|_k\mathbf{P_E}\rangle_{\frac{1}{2}} - \mathbf{P_H}\,|_k\mathbf{P_H}\rangle_{\frac{1}{2}}\right), \end{aligned} \tag{4.88}$$

where the operators $\mathbf{P}_E$ and $\mathbf{P}_H$ are given as

$$\mathbf{P}_E = diag\,[v, v, w, w, w, w, u, u, u, u, v, v]\,, \tag{4.89}$$

and

$$\mathbf{P}_H = diag\,[w, -w, -v, v, u, -u, -w, w, v, -v, -u, u]\,. \tag{4.90}$$

Since 24 equations are involved in order to establish the relations between the 24 wave amplitudes and the 24 electromagnetic field components, the CBM operation is definite and bijective in contrast to CFM. We note, that we do not need to utilize the wave amplitudes at stubs during the mapping. Thus, the normalizing presented in eq. (4.43) does not have any influence on CBM.

4.7 Boundary Conditions

The simulation of an electromagnetic structure using the SCN-TLM method is truncating the finite computational domain with absorbing boundary conditions. An

improper mesh truncation results in back scattering of electromagnetic waves into the computational domain. These back scattered waves interference with the propagating modes in the simulated structure such that they effect or corrupt the field solution. A number of different methods have been developed to absorb electromagnetic waves that impinge on the boundaries of the open space problem. Examples are the discretization of the analytical conditions [70] and Taylor's expansion of the plane wave solution [87]. The use of discrete Green's functions is also an approach to describe absorbing boundary conditions [85], but implies a large amount of memory requirement when regions with different media have to be truncated. The simplest absorbing boundary condition is a matched load with zero reflection coefficient, truncating the transmission lines of the TLM mesh, which are cut by the boundary of the computatioanl domain. This simple ABC yields good approximations in many cases. One of the best way to truncat media is to use matched layer absorber (ML), where electric and magnetic losses are introduced in layers to absorb the incident electromagnetic energy. However these methods deliver only an approximate solution of the problem and require that a distance must be kept between the strucutre and the boundary of the computational region. The realization of interne boundaries PEC and PMC in the computational domain with simple reflection coefficients do not pose any challenge in the TLM algorithm.

4.7.1 One-Sided Reflection Wall

Absorbing boundary condition may be modelled by terminating the transmission lines on the edge of the computational domain with an appropriate load. Then the incident waves impignes normal on the boundary wall with impedance $Z_{load} = \sqrt{\frac{\mu_r}{\varepsilon_r}} Z_0$ are fully absorbed. The local reflection coefficient is in general dependent on the wall cell properties can be calculated through the effective reflection coefficient as

$$r_{loc}(r_{eff}, \epsilon_r, \mu_r, (l, m, n)) = r_{loc} = \frac{r_0 + r_{eff}}{1 + r_0 r_{eff}}, \tag{4.91}$$

with

$$r_0 = r_0 = \frac{\frac{g_\parallel}{g_\perp}\sqrt{\frac{\mu_r}{\varepsilon_r}} - 1}{\frac{g_\parallel}{g_\perp}\sqrt{\frac{\mu_r}{\varepsilon_r}} + 1}, \quad with \quad \begin{cases} g_\parallel \in \{u, v, w\}, & g_\parallel \parallel a_i, \\ g_\perp \in \{u, v, w\}, & g_\perp \perp a_i. \end{cases} \tag{4.92}$$

For the special case of PEC and PMC, $r_{eff} = \pm 1$ leads to $r_{loc} = \pm 1$. The geometry parameter $g_\parallel$ and $g_\perp$ mean the cell sizes in directions parallel and perpendicular to the incident wave pulses respectively. We note, that even though the effective reflection coefficient is set to zero, the local reflection is not, that, actually, conserves the TLM nature. Boundaries with fixed reflection coefficients present only a first order for the general problem of reflection free boundary conditions, because they do not take into

consideration the falling wave angle, but deliver good results in numerous electromagnetic problems with enough distance betwenn the structure and the boundaries.

4.7.2 Two-Sided Reflection-Transmission Wall

The two-sided reflection-transmission wall is used in the discretized TLM domain, when thin layer with constant surface impedance has to be modelled. The electromagnetic simulation of a thin layer with the smallest space step, defined by the thicknes of the layer leads to a significant increase of computational effort. The two-sided reflection wall is represented via additional boundary conditions, which model the variation of the wave impedance. One part of the incident wave on the boundary wall is transmitted through the wall with the transmission coefficient t_{loc} and the second part is reflected back to the neighboring cells with the reflection coefficient r_{loc}. Using the two-sided reflection wall, the analysis of the electromagnetic structures with discretization of lower order allows to reduce the computational effort. When a thin layer with a thicknes d is discretized, the wave impedance change is considered through material properties in the connection process, the loss are considered in the scattering matrix. In the TLM-mesh the surface impedane $\rho_{\square}$ of the thin layer in the connecting surface between adjacent cells is

$$\rho_{\square} = \frac{\rho}{d}. \tag{4.93}$$

The coefficients r_{loc} and t_{loc} are defined as

$$r_{loc} = -\frac{1}{1 + 2Y_0\rho_{\square}\frac{g_{\parallel}}{g_{\perp}}}, \tag{4.94}$$

$$t_{loc} = \frac{Y_0\rho_{\square}}{Y_0\rho_{\square} + \frac{g_{\parallel}}{g_{\perp}}}. \tag{4.95}$$

This type of wall can be efficiently used to model impedance layers in high frequency planar circuits. If the skin-effect must be taken into consideration, then a more complicated model have to be used as in [81].

4.7.3 Matched Layer Absorbers

In the *matched layer absorber* (ML), the impedance of the absorbing medium matches the impedance of the medium to be truncated. Electric and magnetic losses are introduced to absorb the incident electromagnetic energy. The loss of the absorbing material increases from layer to layer, wheras the wave impedance Z_{ML_1} remains constant as

$$Z_{ML_1} = \sqrt{\frac{\mu}{\varepsilon}} = Z_{ML_i} = \sqrt{\frac{\mu + \frac{\rho_{mi}}{j\omega}}{\varepsilon + \frac{\rho_{ei}}{j\omega}}}. \tag{4.96}$$

This equation (4.96) holds if

$$\frac{\varepsilon}{\mu} = \frac{\rho_{ei}}{\rho_{mi}}, \tag{4.97}$$

this condition is known as "*Matched Layer Condition*". The conductivity profile in the matched layer is given according to

$$\rho = \rho_{max} \left(\frac{i}{N_{ML}} \right)^p, \tag{4.98}$$

where ρ_{max} denotes the maximum matched layer electric conductivity at the outer layer N of the matched layer, $i \in 1, ..., N_{ML}$ denotes the index of the matched layer. The maximum conductivity is calculated according to

$$\rho_{max} = -\frac{\alpha(p+1)\ln(R_o)}{2N_{ML}\Delta l Z_0}, \tag{4.99}$$

with R_o denotes the theoretical reflection coefficient when the matched layer absorber is terminated by an electric wall. Z_o represents the free space impedance. p respresents the profile coefficients. Using a constant $\alpha = 0.1$ results a good performance in reducing the differences in dispersion between neighbouring layers [88]. In layered media, the matched condition is as follows

$$\frac{\sigma_e^1}{\varepsilon^1} = \frac{\sigma_m^1}{\mu^1} = ... = \frac{\sigma_e^j}{\varepsilon^j} = \frac{\sigma_m^j}{\mu^j} = const. \tag{4.100}$$

The optimum conductivity profile depends on the number of matched layers. In the cases of 5 matched layers comprehensive practical investigations have shown that $\alpha = 0.1$, $R_0 = 10^{-4}$ and $p = 1$ delivers the best results in terms of minimum return loss [88]. The thicker the absorbing layer and the flatter the profile are the better absorption will be achieved.

4.8 Excitation

Energy is generally introduced into a simulation by means of an impulse excitation either at nodes or on transmission lines of the TLM cell. For the analysis of electromagnetic problems, the Gaussian pulse represents one of the most useful excitation waveforms. The time and frequency characteristics are given, respectively, by

$$g_g(t) = 2f_g \exp\left(-\pi(2f_g t)^2\right) \quad with \quad \int_{-\infty}^{+\infty} g_n(t) = 1, \tag{4.101}$$

and

$$G_g(f) = \exp\left(-\frac{\pi f^2}{4f_g^2}\right). \tag{4.102}$$

$G_g(f)$ represents the spectrum of the normalized Gaussian pulse given by Fourier-transform. The Gaussian time function must be offset by t_0 so that the negative tail of the pulse is not significantly truncated. Then the shifted Gauss pulse in time-domain is given as

$$g_g(t) = 2f_g \exp\left(-\pi(2f_g(t-t_0))^2\right), \tag{4.103}$$

where f_g is a parameter to control the bandwith and the amplitude of the Gaussian pulse. For the excitation of an electromagnetic structure, a choice has to be made on whether to excite in a completely general way or in a more restrictive way. For example, placing a source at a single point in a cavity will excite many modes but only a limited set of modes will be excited if sources are placed on a plane, or, if a TEM cell is excited by the steady-state field distribution over a plane then only the TEM mode will propagate. For some waveguide structure such as a microstrip line or coplanar waveguide it is very simple to define the input-output voltages and currents corresponding to the fundamental and to several higher modes. These voltages and currents can be transformed to the electromagnetic fields and to the waves amplitude and vice versa. The decision on wheter to excite in general or restrictive way will be based upon the particular aspect of the electromagnetic structure which is to be investigated.

5 Time-Domain Method of Moments

5.1 Introduction

Time Domain Integral Equation, TDIE, based solvers are poised to be increasingly applied throughout the computational electromagnetics community for the analysis of complex, wide-band, electromagnetic scattering and radiation phenomena. Indeed, TDIE based methods promise to deliver a combination of advantages not seen in any other simulation technique in broad use today. As integral equation methods, they only require discretization of the interior or boundary of regions whose material properties differ from an assumed background, e.g. a within scattering object, and automatically impose the correct radiation and causality conditions, which must be imposed artificially in the truncation of finite grids used by space discretizing methods such as TLM or FDTD methods. As time-domain techniques, they analyze wide-band and potentially time-varying phenomena in a single simulation.

In general, the electromagnetic community refers to the integral formulation as the Method of Moments (MOM). The MOM technique has been used since the 1960s as it is a more computationally efficient method compared to the TLM algorithm for homogeneous objects. This is because the MOM method discretizes only the surface of objects as opposed to a volumetric cell discretization of the entire simulation domain as in the TLM method [3] [4]. In the MOM technique, the Electric Field Integral Equation (EFIE) is typically used to mathematically define the problem and is solved for the surface/line currents generated on the objects of interest. These currents can then be used in radiation integrals to calculate the fields scattered by the objects.

In the following sections we will rewrite the full Maxwell equations as an integral equation for currents on the surfaces of conductors, and apply this formulation to a scattering problem. We will develop the EFIE and MFIE and describe the MOM technique used to solve it in determining the line or surface currents generated on an arbitrarily-shaped conducting body by an incident electromagnetic field. The condition that the tangential electric field vanishes on conductor surfaces then gives an integral equation from which we can compute the surface currents. The scattered electromagnetic field can be expressed in terms of surface currents on conductors.

5.1.1 Derivation of Electric and Magnetic Field Integral Equation

The Maxwell equations in the time domain in a linear, non-dispersive, and isotropic medium take the following differential and integral forms [3]:

$$\begin{aligned} &Differential\ form && Integral\ form \\ \nabla \times \mathbf{H} = \mathbf{J} + \frac{\partial \mathbf{D}}{\partial t}, \qquad & \oint_L H \cdot d\mathbf{l} = \mathbf{I} + \int_S \frac{\partial \mathbf{D}}{\partial t} \cdot dS, && (5.1) \\ \nabla \times \mathbf{E} = -\frac{\partial \mathbf{B}}{\partial t}, \qquad & \oint_C \mathbf{E} \cdot d\mathbf{l} = -\frac{\partial \Phi}{\partial t}, && (5.2) \\ \nabla \cdot \mathbf{D} = \rho_v, \qquad & \oint_S \mathbf{D} \cdot dS = Q, && (5.3) \\ \nabla \cdot \mathbf{B} = 0, \qquad & \oint_S \mathbf{B} \cdot dS = 0. && (5.4) \end{aligned}$$

We will first consider the simple case in which a scatterer occupying a volume V enclosed by a surface S is illuminated by a source in an unbounded free space. In this case and using the constitutive relationships $\mathbf{D} = \epsilon_0 \mathbf{E}$ and $\mathbf{B} = \mu_0 \mathbf{H}$ the eqs. (5.1-5.4) become:

$$\nabla \times \mathbf{H}(\mathbf{r}, t) = \mathbf{J}(\mathbf{r}, t) + \epsilon_0 \frac{\partial \mathbf{E}(\mathbf{r}, t)}{\partial t}, \tag{5.5}$$

$$\nabla \times \mathbf{E}(\mathbf{r}, t) = -\mu_0 \frac{\partial H(\mathbf{r}, t)}{\partial t}, \tag{5.6}$$

$$\nabla \cdot \mathbf{E} = \frac{\rho_v(\mathbf{r}, t)}{\epsilon_0}, \tag{5.7}$$

$$\nabla \cdot \mathbf{H}(\mathbf{r}, t) = 0. \tag{5.8}$$

A solution can be constructed in terms of the time domain scalar and vector potentials, Φ_t and $\mathbf{A}$, as

$$\mathbf{H}(\mathbf{r}, t) = \frac{1}{\mu_0} \nabla \times \mathbf{A}(\mathbf{r}, t), \tag{5.9}$$

$$\mathbf{E}(\mathbf{r}, t) = -\nabla \Phi_t(\mathbf{r}, t) - \frac{\partial \mathbf{A}(\mathbf{r}, t)}{\partial t}. \tag{5.10}$$

It can be shown that Φ_t and $\mathbf{A}$ are solutions to the following vector and scalar wave equations [3]:

$$\begin{aligned} \nabla^2 \mathbf{A}(\mathbf{r}, t) - \epsilon_0 \mu_0 \frac{\partial^2}{\partial t^2} \mathbf{A}(\mathbf{r}, t) &= -\mu_0 \mathbf{J}(\mathbf{r}, t) \\ \nabla^2 \Phi_t(\mathbf{r}, t) - \epsilon_0 \mu_0 \frac{\partial^2}{\partial t^2} \Phi_t(\mathbf{r}, t) &= -\frac{\rho_v(\mathbf{r}, t)}{\epsilon_0}. \end{aligned} \tag{5.11}$$

The time-domain scalar and vector potentials are related to each other by the following time-domain Lorentz condition:

$$\nabla \cdot \mathbf{A} + \epsilon_0 \mu_0 \frac{\partial \Phi_t(\mathbf{r}, t)}{\partial t} = 0. \tag{5.12}$$

The solution to eqs. (5.11) can be constructed directly from the following scalar wave equation in the time domain.

$$(\nabla^2 - \frac{1}{c^2}\frac{\partial^2}{\partial t^2})\, g_t(\mathbf{r}, \mathbf{r}', t, t') = -\delta(\mathbf{r} - \mathbf{r}')\delta(t - t'), \tag{5.13}$$

where $c = 1/(\epsilon_0\mu_0)^{1/2}$ is the the speed of light in vacuum. It can be readily shown that the solution to eq. (5.13) subject to the causality and radiation conditions (outgoing wave condition) is

$$g_t(\mathbf{r}, \mathbf{r}', t, t') = \begin{cases} \frac{1}{4\pi R}\,\delta(t - t' - R/c) & \text{for } t > t' \\ 0 & \text{for } t \le t', \end{cases} \tag{5.14}$$

$g_t(\mathbf{r}, \mathbf{r}', t, t')$ is called the free-space scalar Green's function in the time domain. $R = |\mathbf{r} - \mathbf{r}'|$ denotes the distance between the source points $\mathbf{r}'$ and destination points $\mathbf{r}$. By comparing eqs. (5.11) through (5.14), we obtain the following solutions for $\mathbf{A}$ and Φ_t:

$$\begin{aligned} \mathbf{A}(\mathbf{r}, t) &= \mu_0 \int_V dv' \int_{-\infty}^{\infty} dt' \mathbf{J}(\mathbf{r}', t)\; g_t(\mathbf{r}, \mathbf{r}', t, t') \\ &= \mu_0 \int_V \frac{\mathbf{J}(\mathbf{r}', t - R/c)}{4\pi R}\, dV', \end{aligned} \tag{5.15}$$

and

$$\Phi_t(\mathbf{r}, t) = \int_V \frac{\rho_t(\mathbf{r}', t - R/c)}{4\pi\epsilon_0 R}\, dV'. \tag{5.16}$$

Substituting the above equations into eqs. (5.9) and (5.10) yields

$$\mathbf{H}(\mathbf{r}, t) = \frac{1}{4\pi}\int_V \left\{ \left[\frac{1}{c}\frac{\partial}{\partial \tau}\mathbf{J}(\mathbf{r}', \tau) + \frac{1}{R}\mathbf{J}(\mathbf{r}', \tau)\right] \times \frac{\mathbf{R}}{R^2} \right\}_{\tau = t - R/c} dv' \tag{5.17}$$

$$\mathbf{E}(\mathbf{r}, t) = \frac{1}{4\pi}\int_V \left\{ \left[\frac{1}{c}\frac{\partial}{\partial \tau}\rho_t(\mathbf{r}', \tau) + \frac{1}{R}\rho_t(\mathbf{r}', \tau)\right] \frac{\mathbf{R}}{\epsilon_0 R^2} - \frac{\mu_0}{R}\frac{\partial}{\partial \tau}\mathbf{J}(\mathbf{r}', \tau) \right\}_{\tau = t - R/c} dv', \tag{5.18}$$

where $\tau = t - R/c$ denotes the retarded time. In deriving these equations, the following mathematical identities were used:

$$\begin{gathered} \nabla\frac{1}{R} = \frac{-\mathbf{R}}{R^3} \quad \nabla R = \frac{\mathbf{R}}{R} \\ \nabla \times \mathbf{J}(\mathbf{r}', \tau) = \frac{-1}{c}\frac{\mathbf{R}}{R} \times \frac{\partial \mathbf{J}}{\partial \tau} \quad \nabla \rho_t(\mathbf{r}, \tau) = -\frac{\mathbf{R}}{cR}\frac{\partial \rho_t}{\partial \tau} \end{gathered} \tag{5.19}$$

5.1.2 Perfectly Conducting Scatterers

Considering the case in which the surface S enclosing the volume V is perfectly conducting. The object is illuminated by an external source. Under such a condition, eqs. (5.17) and (5.18) take the form :

$$\mathbf{E}^s(\mathbf{r},t) = \frac{1}{4\pi}\int_S \left\{ \left[\frac{1}{c}\frac{\partial}{\partial\tau}\rho_s(\mathbf{r}',\tau) + \frac{1}{R}\rho_s(\mathbf{r}',\tau)\right]\frac{\mathbf{R}}{\epsilon_0 R^2} - \frac{\mu_0}{R}\frac{\partial}{\partial\tau}\mathbf{J}_s(\mathbf{r}',\tau)\right\}_{\tau=t-R/c} ds', \tag{5.20}$$

$$\mathbf{H}^s(\mathbf{r},t) = \frac{1}{4\pi}\int_S \left\{ \left[\frac{1}{c}\frac{\partial}{\partial\tau}\mathbf{J}_s(\mathbf{r}',\tau) + \frac{1}{R}\mathbf{J}_s(\mathbf{r}',\tau)\right]\times\frac{\mathbf{R}}{R^2}\right\}_{\tau=t-R/c} ds', \tag{5.21}$$

where $\mathbf{E}^s$ and $\mathbf{H}^s$ denote the scattered electric and magnetic field, respectively. $\mathbf{J}_s$ and ρ_s are the equivalent surface current and charge, respectively, on S due to an incident field $\mathbf{E}^i$. The Electric Field Integral Equation (EFIE) is derived from the zero total tangential electric field condition on the surface of a perfectly conducting body S. Since the total electric field is composed of the incident and scattered fields ($\mathbf{E}^i$ and $\mathbf{E}^s$), we have

$$\mathbf{n}\times(\mathbf{E}^s+\mathbf{E}^i) = 0 \quad on\ S. \tag{5.22}$$

Substituting eq. (5.20) into eq. (5.22), we obtain the (EFIE):

$$n\times\mathbf{E}^i(\mathbf{r},t) + \frac{1}{4\pi}\mathbf{n}\times\int_S^* \left\{ \left[\frac{1}{c}\frac{\partial}{\partial\tau}\rho_s(\mathbf{r}',\tau) + \frac{1}{R}\rho_s(\mathbf{r}',\tau)\right]\frac{\mathbf{R}}{\epsilon_0 R^2} - \frac{\mu_0}{R}\frac{\partial}{\partial\tau}\mathbf{J}_s(\mathbf{r}',\tau)\right\}_{\tau=t-R/c} ds' = 0, \tag{5.23}$$

where the $\int^*$ sign denotes a principal value integral with the singular point $\mathbf{r}' = \mathbf{r}$ excluded. The magnetic field integral equation (MFIE) can be derived from eq. (5.21) and the following boundary condition:

$$\mathbf{n}\times(\mathbf{H}^s+\mathbf{H}^i) = \mathbf{J}_s \quad on\ S, \tag{5.24}$$

resulting in

$$\mathbf{J}_s(\mathbf{r},t) = 2\mathbf{n}\times\mathbf{H}^i(\mathbf{r},t) + \frac{1}{2\pi}\mathbf{n}\times\int_S^* \left\{ \left[\frac{1}{c}\frac{\partial}{\partial\tau}\mathbf{J}_s(\mathbf{r}',\tau) + \frac{1}{R}\mathbf{J}_s(\mathbf{r}',\tau)\right]\times\frac{\mathbf{R}}{R^2}\right\}_{\tau=t-R/c} ds', \tag{5.25}$$

where $\mathbf{J}_s(\mathbf{r}',\tau)$ is the current distribution on the surface S at a source point $\mathbf{r}'$ and at the retarded time $\tau = t - R/c$; $\mathbf{r}'$ is the integration point, $R = |\mathbf{r}-\mathbf{r}'|$. $\mathbf{n}$ is a unitary vector normal to the surface of the scatterer. As was the case in eq. (5.23), a principal-value integral sign is used here to exclude the singular point at $r' = r$. Note that in the principal value, we essentially exclude the part for which $R = 0$.

Since $\tau = t - R/c$ and $R \neq 0$, we always have that $\tau < t$. The time domain integral equations have a time-retardation feature that allows them to be solved by a generally more straightforward method. The time domain equations therefore state that the current at location $\mathbf{r}$ and time t is equal to a known term $2\mathbf{n} \times \mathbf{H}^i(\mathbf{r}, t)$ plus a term (integral) known from the past history of $\mathbf{J}_s$. This is the basis for solving the time domain integral equation by iterative methods, the most well-known one being the marching-on-in-time technique. An important feature of the MFIE equation is that it presents a kernel with both derivatives and singularities of a lower order that the EFIE. As a consequence, it is possible to employ base and testing functions that are simpler than the ones required for the electric field integral equation.

The electric field integral equation (EFIE) and the magnetic field integral equation (MFIE) can be used to model the electromagnetic response of general structures. Each equation has advantages for particular structure types. The EFIE is well suited for thin-wire structures of small or vanishing conductor volume while the MFIE, which fails for the thin-wire case, is more attractive for voluminous structures, especially those having large smooth surfaces. The EFIE can also be used to model surfaces and is preferred for thin structures where there is little separation between a front and back surface.

Eq. (5.23) is referred to the Electric Field Integral Equation (EFIE) and is expressed in terms of the known incident electric field. In order to determine the unknown surface current density $\mathbf{J}_s$, a technique known as the marching on in time (MOT) will be applied. This is described in the next sections for the first case of a thin wire and the second case of a thin surface.

5.2 Thin-Wire Antennas and Scatterers

An important engineering problem is the electromagnetic behavior of thin wire objects. A general analysis of such objects according to the method of moments is presented in this section. The impressed field is considered arbitrary, and hence both the antenna and scatterer problems are included in the solution. The distinction between antennas and scatterers is primarily that of the location of the source. If the source is at the object it is viewed as an antenna; if the source is distant from the object it is viewed as a scatterer. So that the development of the solution may be easily followed, it is given with few references to the general theory. Basically, it involves

1. an approximation of the exact equation for conducting bodies by an approximate equation valid for thin wires,

2. replacement of the derivatives by finite difference approximations, yielding an approximate operator,

3. use of pulse functions for expansion functions, to give a step approximation to the current and charge, and

4. the use of point-matching for testing.

The scattering problem is solved through discretization of the EFIE and its direct time-domain solution by means of a marching-on-in-time procedure. An explicit equation that relates the current at a certain time instant to the currents of previous instants and the incident field is obtained.

Consider an arbitrary shaped conducting wire with length l, radius a, and surface S, which may be closed or open, illuminated by a transient electromagnetic field. This field induces a surface current on S, $\mathbf{J}(\mathbf{r}, t)$, which then reradiates. According to the electromagnetic theory, the total tangential electrical field on the wire surface equals to zero, therefore we derive an integro-differential vector equation in the unknown induced surface current [3],

$$\left[\frac{\partial \mathbf{A}(\mathbf{r},\, t)}{\partial t} + \nabla\phi(\mathbf{r}, t)\right]_{tan} = \left[\mathbf{E}^{inc}(\mathbf{r}, t)\right]_{tan}, \quad \mathbf{r} \in S \tag{5.26}$$

where $\mathbf{A}$ and ϕ are the magnetic vector and the electric scalar potential, respectively, and $\mathbf{E}^{inc}$ is the incident field. The subscript *tan* denotes the tangential component. Using the thin-wire approximation, the current and charge can be seen as current and charge filaments lying along the axis of the wire. The vector $\mathbf{A}$ and scalar potentials ϕ are given by the retarded integrals involving the electric line current density $\mathbf{I}(\mathbf{r}, t)$ and the line charge density $\rho(\mathbf{r}, t)$, respectively, as

$$\mathbf{A}(\mathbf{r}\ , t) = \frac{\mu_o}{4\pi}\int_l \frac{\mathbf{I}(\mathbf{r}'\, , \tau)}{R}\, dl' \tag{5.27}$$

$$\phi(\mathbf{r}\ , t) = \frac{1}{4\pi\epsilon_o}\int_l \frac{\rho(\mathbf{r}', \tau)}{R}\, dl', \tag{5.28}$$

where $R = |\mathbf{r} - \mathbf{r}'|$ represents the distance between the observation point $\mathbf{r}$ and the source point $\mathbf{r}'$, $\tau = t - R/c$ is the retarded time. The current density and the electric charge are coupled through the conservation of charge equation [3], since

$$\nabla \cdot \mathbf{I}(\mathbf{r}, t) = -\frac{\partial \rho(\mathbf{r}, t)}{\partial t} \tag{5.29}$$

and

$$\rho(\mathbf{r}, t) = -\int_{-\infty}^{t} \nabla \cdot \mathbf{I}(\mathbf{r}, \zeta) d\zeta. \tag{5.30}$$

For excitation with smooth time dependence, the time derivative of the EFIE (5.26) is generally used, because it avoids the time integral due to the charge contribution,

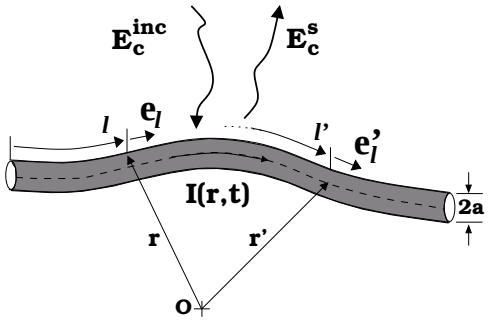

Figure 5.2: A wire scatterer

we derive,

$$\left[\frac{\partial^2 \mathbf{A}(\mathbf{r},\, t)}{\partial t^2} + \nabla\psi(\mathbf{r},t)\right]_{tan} = \left[\frac{\partial \mathbf{E}^{inc}(\mathbf{r},t)}{\partial t}\right]_{tan}, \quad \mathbf{r} \in S \tag{5.31}$$

with

$$\psi(\mathbf{r},t) = \frac{\partial \phi}{\partial t} = \frac{-1}{\epsilon}\int_l \frac{\partial \mathbf{I}(r', t - R/c)/\partial l}{4\pi R} dl'. \tag{5.32}$$

Hence

$$\begin{aligned}\frac{\partial \mathbf{E}^{inc}(\mathbf{r},t)}{\partial t} \cdot \mathbf{e}_l = {} & \frac{\mu}{4\pi}\frac{\partial^2}{\partial t^2}\int_{l(\mathbf{r})} \frac{I(\mathbf{r}',\tau)}{R}\mathbf{e}_l \cdot \mathbf{e}'_l\, dl' \\ & -\frac{1}{4\pi\epsilon}\frac{\partial}{\partial s}\int_{l(\mathbf{r})} \frac{\partial I(\mathbf{r}',\tau)}{\partial l'}\frac{1}{R} dl',\end{aligned} \tag{5.33}$$

where $\mathbf{I}(\mathbf{r},t)$ denotes the unknown current distribution flowing along the wire axis, $l(\mathbf{r})$ is the integration path, $\mathbf{E}_C^{inc}$ is the incident field at the wire surface, l and l' are curvilinear coordinates along the wire axis, as indicated in Fig. 5.2. $\mathbf{e}_l$ and $\mathbf{e}'_l$ are unit vectors tangential to the wire axis in the field and the source points, respectively. R is the distance between the source and the field points. $\tau = t - R/c$ is the retarded time and c the light velocity in free space. The singularity of the integral is overcome choosing the field point on the wire surface, where the boundary condition is applied, and the source point on the wire axis, where the current is assumed to flow, according to the thin wire approximation.

The eq. (5.33) can be numerically solved using the marching on in time version of the MOM; in this way the integro-differential equation is transformed into a linear, iterative relation that provides an explicit evaluation of the current, as reported in the next section.

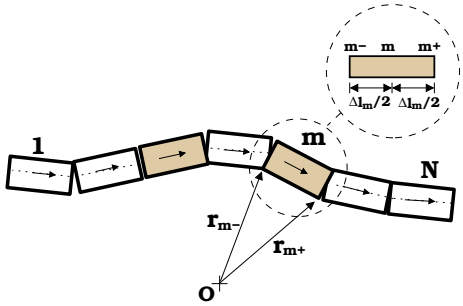

Figure 5.3: Thin wire discretization into straight segments.

5.2.1 Current distribution on the wire

The marching on in time (MOT) procedure allows to transform the integro-differential equation (5.33) into an iterative relation: to simplify the formulation for the curved wire in Fig. 5.2, it is a general practice to approximate it by discretized segments of straight wires of the same radius. Fig. 5.3 illustrates the division of the wire into N segments, which corresponds to the same number of subdomains and defines the notation. The mth segment is identified by its starting point m^-, its midpoint m, and its terminated m^+. An increment Δl_m denotes that between m^+ and m^- , Δl_m^- and Δl_m^+ denote increments shifted 1/2 segment minus or plus along the wire axis. The tangential unit vector $\mathbf{e}_m$ of the m^{th} segment is given by

$$\mathbf{e}_m = \frac{\mathbf{r}_{m+} - \mathbf{r}_{m-}}{|\mathbf{r}_{m+} - \mathbf{r}_{m-}|}. \tag{5.34}$$

Adopting the conventional procedure of MOT to solve equation (5.33), we use pulse basis functions to expand the unknown current distribution $\mathbf{I}(\mathbf{r}, t)$ both in time and space domain as well as delta test functions according to the point matching technique [25]. The set of basic functions, chosen as the standard pulse functions on a linear segment, is given by

$$\mathbf{f}_m(\mathbf{r}) = \begin{cases} 1 & \text{for } \mathbf{r} \in [\mathbf{r}_{m-}, \mathbf{r}_{m+}] \\ 0 & otherwise. \end{cases} \tag{5.35}$$

The set of basis functions is used as a testing function where the inner product is defined as:

$$< a,\, b > = \int_l a \cdot b \, dl'. \tag{5.36}$$

The time is also discretized into time intervals with span of Δt. The relationship between the length of wire segment and time interval is given by $\Delta t \leq \Delta l / c\sqrt{2}$. By

using point-matching method, that is, considering the field at the center point of the mth segment $\mathbf{r}_m$ and at moment $t_n(t_n = n\Delta t)$. Using the test function (5.36) and apply into eq. (5.31) gives

$$< \mathbf{f}_m \mathbf{e}_m, \frac{\partial^2 \mathbf{A}}{\partial t^2} + \nabla\psi > = < \mathbf{f}_m \mathbf{e}_m \,, \frac{\partial \mathbf{E}^{inc}}{\partial t} > . \tag{5.37}$$

Using a central difference to approximate the time derivatives of the vector potential function, we get

$$< \mathbf{f}_m \mathbf{e}_m \,, \frac{\mathbf{A}(\mathbf{r},\, t_{n+1}) - 2\mathbf{A}(\mathbf{r},\, t_n) + \mathbf{A}(\mathbf{r},\, t_{n-1})}{\Delta t^2} + \nabla\psi > = < \mathbf{f}_m \mathbf{e}_m \,, \frac{\partial \mathbf{E}^{inc}}{\partial t} > . \tag{5.38}$$

Using a 1-point integration to test the vector potential, across a segment, we get

$$< \mathbf{f}_m \mathbf{e}_m, \mathbf{A}(\mathbf{r},\, t_n) > \simeq \mathbf{A}(\mathbf{r}_m,\, t_n) \cdot \Delta l_m \mathbf{e}_m. \tag{5.39}$$

This approximation is done by evaluating the vector potential, $\mathbf{A}$, at point $\mathbf{r}_m$, at the present time t_n, and multiply by the length of the segment, Δl_m where $\Delta l_m = |\mathbf{r}_{m+} - \mathbf{r}_{m-}|$. The same testing approximation is applied to the testing of the incident electric field $\mathbf{E}^{inc}$.

$$< \mathbf{f}_m \mathbf{e}_m \,, \frac{\partial \mathbf{E}^{inc}(\mathbf{r}, t_n)}{\partial t} > \simeq \frac{\partial \mathbf{E}^{i}(\mathbf{r}_m, t_n)}{\partial t} \cdot \Delta l_m \mathbf{e}_m. \tag{5.40}$$

Using the fact that the line integral of the gradient of a potential function is the function evaluated at its end points, the testing of the time derivative of the scalar potential can be written as

$$\begin{aligned} < \mathbf{f}_m \mathbf{e}_m \,, \nabla\psi(\mathbf{r}_n, t_n) > &= \int_l \nabla\psi(\mathbf{r}, t_n) \cdot \mathbf{f}_m \mathbf{e}_l dl' \\ &\simeq \psi(\mathbf{r}_{m+}, t_n) - \psi(\mathbf{r}_{m-}, t_n) \end{aligned} \tag{5.41}$$

Using the eqs. (5.39), (5.40) and (5.41), the eq. (5.38) can be rewritten as:

$$\begin{aligned} &\left[\frac{\mathbf{A}(\mathbf{r},\, t_{n+1}) - 2\mathbf{A}(\mathbf{r},\, t_n) + \mathbf{A}(\mathbf{r},\, t_{n-1})}{\Delta t^2}\right] \cdot \Delta l_m \mathbf{e}_m \\ &+\psi(\mathbf{r}_{m+}, t_n) - \psi(\mathbf{r}_{m-}, t_n) = \frac{\partial \mathbf{E}^{inc}(\mathbf{r}_m, t_n)}{\partial t} \cdot \Delta l_m \mathbf{e}_m, \end{aligned} \tag{5.42}$$

where $m = 1,\, 2,\, ...\, N$. Next, the unknown line current, $\mathbf{I}(\mathbf{r}, t)$, over the wire structure, is approximated as

$$\mathbf{I}(\mathbf{r}\ , t) = \sum_{k=1}^{N} \mathbf{I}_k(t)\, \mathbf{f}_k(\mathbf{r}), \tag{5.43}$$

where $\mathbf{I}_k(t)$ is the unknown coefficient in the segment k with $\mathbf{r} = \mathbf{r}_k$ for $k = 1, 2, ..., N$. Substituting eq. (5.43) into eq. (5.27) and assuming the current over a segment to be constant with time, results in

$$\begin{aligned}\mathbf{A}(\mathbf{r},\, t_n) \;&=\; \frac{\mu}{4\pi}\int_l \frac{\mathbf{e}'_l \sum_{k=1}^{N} I_k(t_n - \frac{R_{mk}}{c})\,\mathbf{f}_k(\mathbf{r}')}{R}dl' \\ &\simeq\; \frac{\mu}{4\pi}\sum_{k=1}^{N} \mathbf{I}_k(t_n - \frac{R_{mk}}{c})\,\mathbf{k}_{m,k}\,\mathbf{e}_k, \end{aligned} \tag{5.44}$$

where

$$\mathbf{k}_{m,k} = \int_l \frac{\mathbf{f}_k(\mathbf{r}')}{R_m}dl', \tag{5.45}$$

$$R_{mk} = |\mathbf{r}_m - \mathbf{r}_k|\,,$$

and

$$R_m = \sqrt{|\mathbf{r}_m - \mathbf{r}'|^2 + a^2},$$

where a denotes the wire radius. The integral $\mathbf{k}_{m,k}$ term can be further expressed as

$$\mathbf{k}_{m,k} = \begin{cases} \frac{\Delta l_k}{\sqrt{|\mathbf{r}_m - \mathbf{r}_k|^2 + a^2}} & k \neq m \\ \mathbf{k}_{m,m} & k = m, \end{cases} \tag{5.46}$$

where

$$\mathbf{k}_{m,m} = 2\,ln\left[\frac{\frac{\Delta l_m}{2} + \sqrt{\left(\frac{\Delta l_m}{2}\right)^2 + a^2}}{a^2}\right], \tag{5.47}$$

represents the self-term integral. $\Delta l_m = |\mathbf{r}_{m+} - \mathbf{r}_{m-}|$ denotes the length of the mth wire segment.

Removing the self term, $k = m$, the vector potential can be rewritten as:

$$\mathbf{A}(\mathbf{r}, t_n) = \underbrace{\frac{\mu}{4\pi}\mathbf{k}_{m,m} I_m(t_n)\mathbf{e}_m}_{self-term} + \underbrace{\frac{\mu}{4\pi}\sum_{k=1,k\neq m}^{N} \mathbf{I}_k(t_n - \frac{R_{mk}}{c})\,\mathbf{k}_{m,k}\,\mathbf{e}_k}_{\breve{\mathbf{A}}(\mathbf{r},t_n)}, \tag{5.48}$$

where $\breve{\mathbf{A}}$ indicates that the self-term is excluded from the summation. $\breve{\mathbf{A}}$ is computing at earlier time instant since the distance R_{mk} can never be zero. Fig. 5.4(b) represents the case for $k \neq m$, in which the source and field segments are different. When $k = m$, Fig. 5.4(a), the field point can be chosen to be any point on the circumference without affecting the computation. Note also that by approximating the source current as an axial line current, we have circumvented the singularity problem occurring at $k = m$.

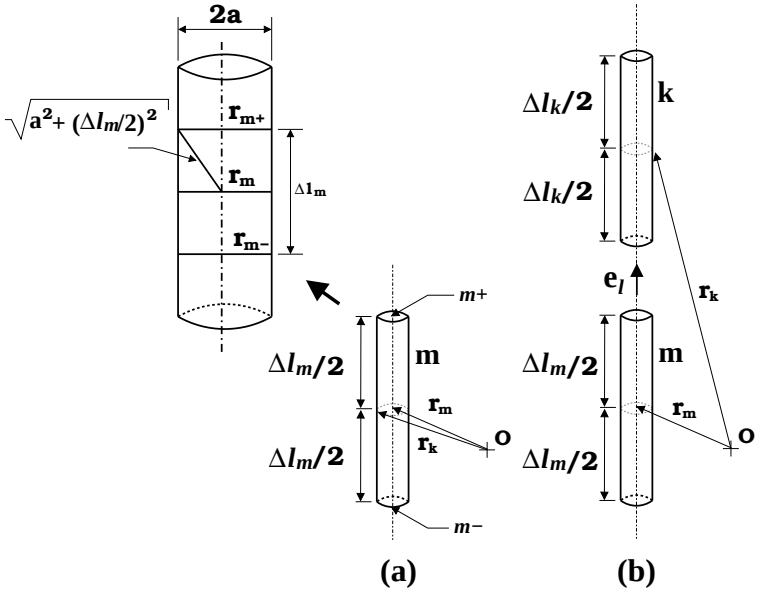

Figure 5.4: Field and source points when $m = k$ (a) and when $m \neq k$ (b).

That is, since the field point is on the surface S of the wire, and the source point is on the center axis of the wire, $\mathbf{r}$ never equals $\mathbf{r}'$, even for the self-element in which $k = m$.

Next the time derivative of the scalar potential is evaluated. Using the current approximation (5.43), the time derivative of scalar potential (5.32) is expressed as:

$$\psi(\mathbf{r}_m, t_n) = \frac{\partial \phi}{\partial t} = \frac{-1}{\epsilon} \sum_{k=1}^{N} \int_l \frac{\partial \left[\mathbf{I}_k (t_n - \frac{R_{mk}}{c}) \mathbf{f}_k \right] / \partial l}{4\pi R_m} \, dl', \tag{5.49}$$

where $R_m = |\mathbf{r}_m - \mathbf{r}'|$. Using the basic pulse functions, the derivative of the function $\mathbf{f}_k$ results in two delta functions at $\mathbf{r}_{k+}$and $\mathbf{r}_{k-}$. The effect of these delta functions can be spread across the region $\mathbf{r}_{k-1}$ to $\mathbf{r}_{k+1}$. Fig. 5.5 illustrates the procedure.

The used of the basic function essentially approximate the derivative by a finite difference. Using this approximation, eq. (5.49) can be rewritten as

$$\psi(\mathbf{r}_m, t_n) = \sum_{k=1}^{N} \psi^+(\mathbf{r}_m, t_n) - \psi^-(\mathbf{r}_m, t_n), \tag{5.50}$$

where

$$\psi^+(\mathbf{r}_m, t_n) = \frac{-1}{4\pi\epsilon} \frac{\mathbf{I}_k (t_n - \frac{\mathbf{R}^+_{mk}}{c})}{\Delta l^+_k} \int_{\mathbf{r}_k}^{\mathbf{r}_{k+1}} \frac{1}{\sqrt{|\mathbf{r} - \mathbf{r}'|^2 + a^2}} dl', \tag{5.51}$$

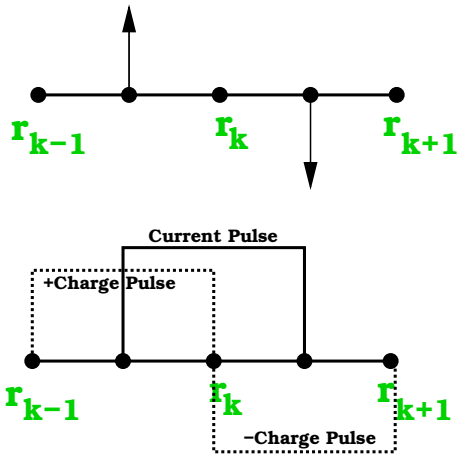

Figure 5.5: Approximation of Delta Functions by Pulse Function

$$\psi^{-}(\mathbf{r}_m, t_n) = \frac{-1}{4\pi\epsilon} \frac{\mathbf{I}_k(t_n - \frac{\mathbf{R}^{-}_{mk}}{c})}{\Delta l^{-}_k} \int_{\mathbf{r}_{k-1}}^{\mathbf{r}_k} \frac{1}{\sqrt{|\mathbf{r} - \mathbf{r}'|^2 + a^2}} dl', \tag{5.52}$$

and

$$\mathbf{R}^{\pm}_{mk} = \sqrt{|\mathbf{r}_m - \mathbf{r}_{k\pm}|^2 + a^2}, \quad \Delta l^{+}_k = |\mathbf{r}_{k+1} - \mathbf{r}_k|, \quad \Delta l^{-}_k = |\mathbf{r}_k - \mathbf{r}_{k-1}|. \tag{5.53}$$

Using Equation (5.48) and replacing the n-terms with $n-1$, eq. (5.42) can be rewritten as

$$\begin{aligned} \frac{\mu \mathbf{k}_{m,m} I_m(t_n) \Delta l_m \mathbf{e}_m}{\Delta t^2} &= \frac{\partial \mathbf{E}^i(\mathbf{r}_m, t_{n-1})}{\partial t} \cdot \Delta l_m \mathbf{e}_m \\ - \left[\frac{\breve{\mathbf{A}}(\mathbf{r}_m, t_n) - 2\breve{\mathbf{A}}(\mathbf{r}_m, t_{n-1}) + \breve{\mathbf{A}}(\mathbf{r}_m, t_{n-2})}{\Delta t^2} \right] &\cdot \Delta l_m \mathbf{e}_m \\ + [\psi(\mathbf{r}_{m+}, t_{n-1}) - \psi(\mathbf{r}_{m-}, t_{n-1})] \quad for \quad m = 1, 2, ..., N. \end{aligned} \tag{5.54}$$

It is clear from eq. (5.54) that the present time unknown current $\mathbf{I}_m(t_n)$ is calculated by utilizing the retarded known currents at the earlier instants. The right side involves only currents and incident field up to the time $t = t_{n-1}$. An important advantage of this method, is the fact that no matrix inversion is needed to solve the integral equation. As stated earlier, the explicit approach is applied, therfore, the time interval, Δt, must be less than the minimum distances between observation and the source points on the wire, $c\Delta t \leq R_{min}$. The equation of current continuity dictates that any current flowing

toward the end of a thin wire must decrease to zero as it approaches the end, otherwise there will be an infinite amount of accumulation of charge, which is not possible unless the end is a source or a sink. If a wire-end is free, we assume that there is no current flow though the end point and therefore we enforce the current to be zero at the wire-end (for the segments $m = 1$ and $m = N$). On the other hand, if a wire ends on a large perfectly conducting surface the charge per unit length is zero and therefore we enforce the voltage to be zero at that wire-end. This enforcement is valid only for wires ending on large PECs.

5.3 Thin-Surface Antennas and Scatterers

The problem of obtaining transient response of an arbitrary shaped conducting body excited either as an antenna or as a scatterer is of much interest in electromagnetic community. This is partly due to the recent developments in the area of high resolution radar technology, target identification techniques, and electromagnetic compatibility related problems where the transient response plays a major role.

Earlier models in frequency domain as well as integral-equation in time-domain adopted wires in the geometry representation. The structure is modeled as a net of wires, but as noted in [4], the wire grid model is not well suited for calculating quantities such as current distribution. Recently in TDIE, surface-patch models have shown advantage of better representing the true circumstances, particularly with regard to the near-field quantities [17]. The most widely used surface discretization method is based on Rao-Wilton-Glisson (RWG) elements, which are simple, flat, triangular facets. It can be used both in PEC and dielectric surfaces. In the RWG discretization methods, the singular integrands vanish, whilst the methods still can give good results on simple shapes [17]. In this approach, a singularity is subtracted, leaving the kernel only weakly singular.

In this thesis, we use planar triangular patch modeling and apply the marching on in time technique to develop a simple numerical procedure to solve the EFIE directly in the time-domain. The solution technique is capable of handling either open or closed arbitrarily curved structures of finite extent. In the following, the time domain EFIE formulation and the numerical solution is presented.

Consider the case where we have a conducting structure which we subject to an incident electromagnetic field, Fig. 5.6(a). Due to the incident field a current will be induced on the surface of the structure and this current will in turn produce a field which we call the scattered field. We denote the incident field as $\mathbf{E}^{inc}$ and the scattered field $\mathbf{E}^{scat}$. If the structure is assumed to be a perfect conductor, we know that the tangential component of the electric field at the surface of the structure must vanish. Thus, the following equation follows:

$$(\mathbf{E}^{inc} + \mathbf{E}^{scat})_{tan} = 0, \ on\, S. \tag{5.55}$$

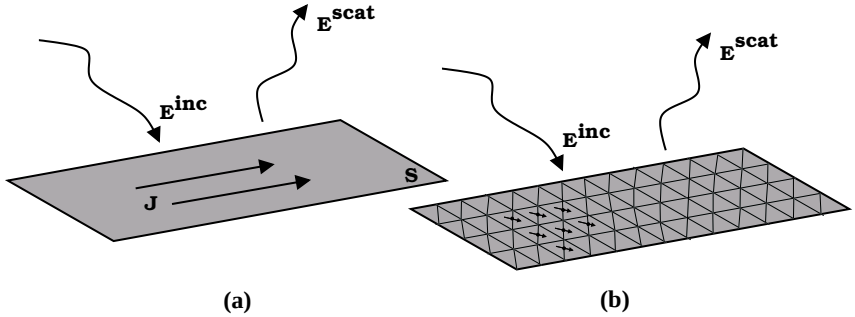

Figure 5.6: Planar conducting structure subject to an incident electromagnetic field; (a) thin surface (b) RWG discretization.

$\mathbf{E}^{scat}$ can be constructed in terms of the time domain scalar and vector potentials, ϕ and $\mathbf{A}$, respectively. Therefore we derive an integro-differential vector equation in the unknown induced surface current [3] as

$$\left[\frac{\partial \mathbf{A}(\mathbf{r},\, t)}{\partial t} + \nabla\phi(\mathbf{r}, t)\right]_{tan} = \left[\mathbf{E}^{inc}(\mathbf{r}, t)\right]_{tan}, \quad \mathbf{r} \in S. \tag{5.56}$$

The forcing term of this equation is given by the tangential component of the incident electric field $\mathbf{E}^{inc}$. For the case of thin planar conducting structures, we can assume the conducting sheet to be infinitesimal thin and that the current only can flow in the orthogonal directions. The solution of the EFIE (5.56) for the unknown surface current using the marching on in time technique is performed in the next section.

5.3.1 Current distribution on the surface

In order to obtain a numerical solution of eq. (5.56), we use the MOT procedure and the same type of basis and test functions as were introduced by Glisson & Wilton [17]. In particular, the spatial variation of the surface currents induced on the body can be accurately approximated by discretizing its exterior surface in sub-domain patches , over which a suitable set of basis functions can be defined, Fig. 5.6(b). The choice here is to use the triangular current expansion and approximating the conducting surface S by triangular patches. Thus the surface current distribution $\mathbf{J}_s(\mathbf{r}, t)$ can be numerically approximated as:

$$\mathbf{J}(\mathbf{r}\ , t) = \sum_{k=1}^{Ne} \mathbf{I}_k(t)\, \mathbf{f}_k(\mathbf{r}), \tag{5.57}$$

where Ne is the number of the edges of the triangles which models the scatterer, excluding the boundary edges if S is open. Each unknown coefficient $\mathbf{I}_k(t_n)$ denotes

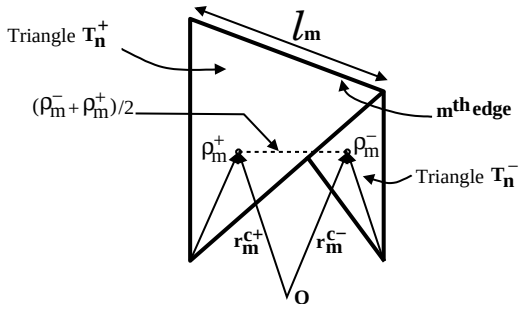

Figure 5.7: Geometry of triangular patches.

the value of the component of the current, normal to the kth edge at the instant $t_n = n\Delta t$. The adopted basis functions $\mathbf{f}_k(\mathbf{r})$ are defined over each triangle pair discretizing the body surface. Let T_m^+ and T_m^- be two triangular patches associated with the mth edge of length l_m as shown in Fig. 5.7. The same procedure as applied in [17]; then

$$\mathbf{f}_m(\mathbf{r}) = \begin{cases} \frac{l_m}{2A_m^\pm}\,\rho_m^\pm & \text{for } \mathbf{r} \in T_m^\pm \\ 0 & \text{for } \mathbf{r} \notin T_m^\pm, \end{cases} \tag{5.58}$$

where l_m and $A_m^\pm$ are the length of the edge and the area of triangle $T_m^\pm$. $\rho_m^\pm$ is the position vectors referenced at the free vertex to the centroid of $T_m^\pm$. Next the testing functions are the same as the expansion function $\mathbf{f}_m$, presented above, the inner product is chosen as

$$< A,\, B > = \int_S A \cdot B^*\, dS, \tag{5.59}$$

where the asterisk represents the conjugate. We begin by applying the testing procedure to (5.56), which results in

$$< \mathbf{f}_m, \frac{\partial \mathbf{A}(\mathbf{r},\, t)}{\partial t} + \nabla\phi(\mathbf{r}, t) > = < \mathbf{f}_m\,, \mathbf{E}_C^{inc} > . \tag{5.60}$$

By considering (5.56) at a time instant t_n, and assuming that the current does not vary appreciably with time within the pair of triangles, so that

$$\mathbf{I}_k(t_n - R/c) \Rightarrow \mathbf{I}_k(t_n - R_{mk}/c)$$

$$< \mathbf{f}_m\,, \mathbf{E}_C^{inc} > \simeq \frac{l_m}{2}\,(\rho_m^+ + \rho_m^-)\,\cdot\,\mathbf{E}_C^{inc}(\mathbf{r}_m,\, t_n) \tag{5.61}$$

$$\mathbf{A}(\mathbf{r}_m,\, t_n) \;\simeq\; \frac{\mu}{4\pi}\sum_{k=1}^{Ne} \mathbf{I}_k(t_n - \frac{R_{mk}}{c})\,\mathbf{e}_{mk} \tag{5.62}$$

$$\mathbf{e}_{mk} = \int_{T_k^+ + T_k^-} \frac{\mathbf{f}_k}{R_m}\, dS \tag{5.63}$$

$$R_m = |\mathbf{r}_m - \mathbf{r}'| \qquad R_{mk} = |\mathbf{r}_m - \mathbf{r}_k|\,, \tag{5.64}$$

where $\mathbf{r}_m$ and $\mathbf{r}_k$ are the positions vectors to the center of the mth and kth edges, respectively. Separating the self term ($k = m$) from (5.62) and applying the inner product ,

$$\begin{aligned} < \mathbf{f}_m\,, \frac{\partial \mathbf{A}(\mathbf{r},\, t)}{\partial t} > &= < \frac{\mathbf{f}_m,\, (\mathbf{A}(\mathbf{r},\, t_{n+1}) - \mathbf{A}(\mathbf{r},\, t_n))}{\Delta t} > \\ &= \frac{l_m}{2}(\rho_m^+ + \rho_m^-) \cdot \frac{\mu_o}{4\pi} \frac{\mathbf{e}_{mm}}{\Delta t}\, \mathbf{I}_m(t_{n+1}) \\ &+ \frac{l_m}{2}(\rho_m^+ + \rho_m^-) \left[\frac{(\breve{\mathbf{A}}(\mathbf{r}_m,\, t_{n+1}) - \breve{\mathbf{A}}(\mathbf{r}_m,\, t_n))}{\Delta t} \right], \end{aligned} \tag{5.65}$$

where $\breve{\mathbf{A}}(\mathbf{r}_m,\, t_n)$ represents $\mathbf{A}(\mathbf{r}_m,\, t_n)$ with the self term deleted. $\Delta t = t_{n+1} - t_n$. $\mathbf{e}_{mm}$ denotes the self term integral ($m = k$).

The scalar potential term becomes

$$\begin{aligned} < \mathbf{f}_m\,, \nabla\phi(\mathbf{r}, t) > &= -\int_S \phi\, \nabla \cdot \mathbf{f}_m\, dS \\ &\simeq -l_m\, [\phi(\mathbf{r}_m^{c+}, t_n) - \phi(\mathbf{r}_m^{c-}, t_n)], \end{aligned} \tag{5.66}$$

with

$$\begin{aligned} \phi(\mathbf{r}\,,\, t_n) &= -\frac{1}{4\pi\epsilon_o} \int_S \frac{dS}{R} \Big[\int_0^{t_n - R/c} \sum_{k=1}^{Ne} I_k(\tau) \nabla \cdot \mathbf{f}_k\, d\tau \Big] \\ &\simeq -\frac{1}{4\pi\epsilon_o} \int_S \frac{dS}{R} \sum_{k=1}^{Ne} \Big[\int_0^{t_n - R_{mk}^+/c} I_k(\tau)\, \phi_{mk}^+\, d\tau \\ &\qquad + \int_0^{t_n - R_{mk}^-/c} I_k(\tau)\, \phi_{mk}^-\, d\tau \Big], \end{aligned} \tag{5.67}$$

where

$$\phi_{mk}^{\pm} = \frac{l_k}{A_k^{\pm}} \int_{T_k^{\pm}} \frac{dS}{R_m^{\pm}} \tag{5.68}$$

$$R_{mk}^{\pm} = \left|\mathbf{r} - \mathbf{r}_k^{c\pm}\right| \qquad R_m^{\pm} = |\mathbf{r} - \mathbf{r}'|\,. \tag{5.69}$$

Moreover, vector potentials $\mathbf{A}(\mathbf{r}, t)$ are evaluated at the center of each edge, while scalar potentials $\phi_{mk}^{\pm}$ are evaluated at the centroids of the triangles by replacing $\mathbf{r}$ with $\mathbf{r}_m^{c+}$ or $\mathbf{r}_m^{c-}$, Fig. 5.7.

By combining all the relationships presented above, we obtain:

$$\begin{aligned}
\frac{l_m}{2}(\rho_m^+ + \rho_m^-) \cdot \mathbf{e}_{mm} \frac{\mu_o}{4\pi\Delta t} \mathbf{I}_m(t_{n+1}) \\
= \frac{l_m}{2}(\rho_m^+ + \rho_m^-) \cdot \mathbf{E}^{inc}(\mathbf{r}_m, t_n) \\
-\frac{l_m}{2}(\rho_m^+ + \rho_m^-) \cdot \left[\frac{(\breve{\mathbf{A}}(\mathbf{r}_m, t_{n+1}) - \breve{\mathbf{A}}(\mathbf{r}_m, t_n))}{\Delta t}\right] \\
+l_m[\phi(\mathbf{r}_m^{c+}, t_n) - \phi(\mathbf{r}_m^{c-}, t_n)].
\end{aligned} \tag{5.70}$$

On close examination of (5.70), it is clear that the right-hand side involves only currents and incident fields up to the time $t = t_n$. Hence the currents $\mathbf{I}_m(t_{n+1})$ can be determined if the currents up to the previous time step t_n are available, this allowing us to treat (5.70) as a recursion formula by which the current is computed by marching-on-in-time and without solving simultaneous equations. This is well-known feature of the numerical solution of the time domain formulations of scattering problems [19]. An important parameter to be noted in (5.70) is the choice of the time step Δt, which should satisfy the condition $\Delta t \leq R_{min}/c$, where R_{min} represents the minimum distance between the edge centers. In order to generate a stable numerical results, the Courant's stability condition [22] forces the choice of the time step to be less than $R_{min}/c\sqrt{2}$ and in the present work we chose $\Delta t = R_{min}/2c$.

The electric field integral equation EFIE is used with the Method of Moments (MOM) to develop a simple and efficient numerical procedure for treating problems of transient scattering by arbitrarily shaped conducting objects. For numerical purposes the objects are modeled by triangular surface patch models. Because the EFIE formulation is used, the procedure is applicable to both open and closed objects. The solution technique of the scattering problem will be implemented in the hybrid method TLM-TDMOM combining the Transmission Line Matrix and the Method of Moments presented in Chapter 7. This hybrid method is very efficient to analyze the transient electromagnetic interaction between a complex object, modeled by TLM, and a conducting scatterer, modeled by the time domain Method of Moments (TDMOM).

5.4 Surface Equivalence Principle

It is generally impractical to simulate a large domain that includes the far field of a radiating object or scatterer. Using a Green's function and radiation integral, far fields can be computed from near fields. One way to do this is to surround all material objects and sources in the simulation domain with an imaginary closed contour (2D) or surface (3D), which is sometimes called a Huygens surface. For convenience with rectangular grids used in TLM, this is often chosen to be a box, as shown in Fig. 5.8. Once the TLM-simulation has reached steady state, electric and magnetic fields are

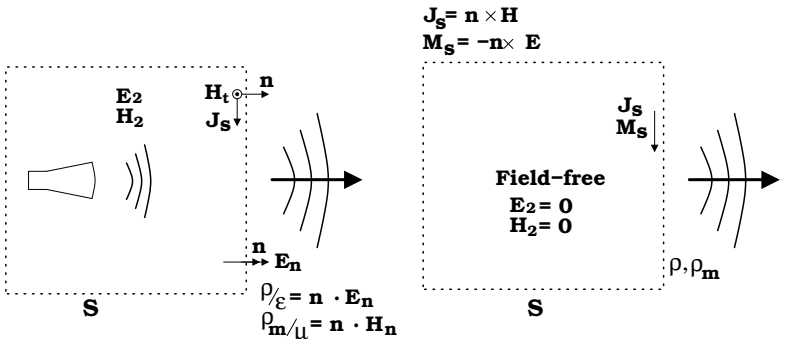

Figure 5.8: The equivalence principle

stored along the surface. If the contour lies exactly on electric field grid points, then for a maximum accuracy the magnetic field values must be obtained by interpolation of two values on either side of the surface. The equivalence principle can be used to relate the fields on the surface to equivalent sources which if impressed in free-space would radiate the same fields outside the surface [4]. In the equivalent problem, suppose that the fields inside the surface are arbitrary fields $\mathbf{E}_2$ and $\mathbf{H}_2$. By the boundary condition, the sources

$$\mathbf{J}_S = \mathbf{n} \times (\mathbf{H} - \mathbf{H}_2) \tag{5.71}$$

$$\mathbf{M}_S = -\mathbf{n} \times (\mathbf{E} - \mathbf{E}_2), \tag{5.72}$$

must lie on the surface S. If we choose $\mathbf{E}_2$ and $\mathbf{H}_2$ to be zero, then

$$\mathbf{J}_S = \mathbf{n} \times \mathbf{H} \tag{5.73}$$

$$\mathbf{M}_S = -\mathbf{n} \times \mathbf{E} \tag{5.74}$$

Since these sources lie in free space, we can use the free-space radiation integral to compute the fields radiated by these sources. $\mathbf{n}$ is the unit vector normal to S. $\mathbf{J}_s$ and $\mathbf{M}_s$ denote the equivalent electric and magnetic surface current densities on S, respectively.

6 Hybrid TLM-IE method

6.1 Introduction

A simulation method for solving EMC problems must be capable of dealing with highly non-uniform and non-linear systems, over a wide frequency range including transients in equipment configurations which are electrically large and contain fine features. The space discretizing TLM or FDTD methods are very flexible for the field modeling of general structures with arbitrary shapes [1] [72], their disadvantages occur in modeling of problems involving wide free-space regions. The analysis of the electromagnetic interaction between objects separated by large free-space regions with a full-wave method such as the TLM method, based on a full discretization of the environment, represents a challenging task with regard to computational resources and modeling effort. On the other hand, field propagation in large free-space environments can be efficiently studied by using the time domain integral equation (TDIE). Since in the TLM method the segmentation of the space can be handled very easily the TLM method is also very suitable to be combined with other methods. Therefore, a suitable hybrid method which drastically reduces computation time and effort is to combine the TLM method and the Integral-Equation (IE) method in a hybrid TLM-IE method that permits to analyze complex objects and to incorporate the treatment of large free-space regions with high efficiency [6] [7] [12]. In the TLM-IE method, the application of the equivalence principle allows to divide the three-dimensional space into subregions. Each object is enclosed by a discretized subregion where the TLM method is applied. The electromagnetic interaction between the subregions is performed by the dyadic free-space Green's functions in time domain.

6.2 TLM-IE Concept for Radiation Analysis

In the framework of the Electromagnetic Compatibility (EMC), it is often necessary to investigate spurious radiation phenomena of complex structures. The electromagnetic analysis is particularly important in the time domain, because with one single time simulation we get the information for all frequencies after a FFT transformation. An accurate analysis of radiating structure with the TLM method requires a great

computational effort, due the necessity of dealing with large metallic structures, including radiating elements and feeding lines. The computational effort increases if we have to deal with radiation problems in large free-space regions. The hybrid method TLM-IE method provide a procedure which allows to treat radiation problems with a high efficiency regarding to the computation time and memory requirements.

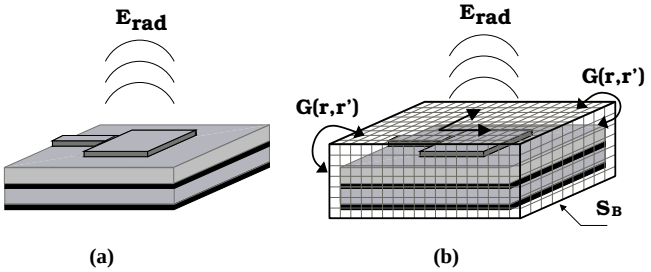

Figure 6.9: Hybrid TLM-Integral Equation concept; (a) radiating structure, (b) the structure is embedded into a TLM-box, the surface elements of the subregion are coupled via Green's functions in time domain $\mathbf{G}(\mathbf{r}, \mathbf{r}')$.

We consider an radiating object with complex geometry, as shown in Fig. 6.9(a). The near field region is discretized by the TLM scheme and surrounded by a surface S_B which represents the interface to the far field region as shown in Fig. 6.9(b) . In the further derivation we apply the TLM algorithm for the calculation of the near field. The boundary of the discretized region is the surface S_B. The tangential field on the surface S_B represents a distribution of equivalent currents and charges, according to the Huygens-Schelkunoff's representation of the equivalence theorem. These sources are mutually coupled via the free space region by the Green's function in time domain. Inside the discretized region there are sources. The field which is excited by the given sources produces an incident tangential field ${}^{TLM}\mathbf{E}_B^{inc}(\mathbf{r}, t)$ and ${}^{TLM}\mathbf{H}_B^{inc}(\mathbf{r}, t)$ on the interface S_B as indicated in Fig. 6.10. This field is calculated by the TLM algorithm. By applying the continuity of the total tangential fields at the interface S_B, we derive the following integral equations as in [55]:

$$\mathbf{E}_{Btot} = {}^{TLM}\ \mathbf{E}_B^{inc} + \mathbf{E}_B^r, \qquad (\mathbf{EFIE}) \tag{6.1}$$

$$\mathbf{H}_{Btot} = {}^{TLM}\ \mathbf{H}_B^{inc} + \mathbf{H}_B^r, \qquad (\mathbf{MFIE}) \tag{6.2}$$

where $\mathbf{E}_{Btot}$, $\mathbf{H}_{Btot}$ represent the unknown total tangential fields at the interface S_B as shown in Fig. 6.10. $\mathbf{E}_B^r$ and $\mathbf{H}_B^r$ are the tangential radiated field at the interface and represent the self interaction between the surface elements belonging to the boundary S_B. These field quantities are derived from the total tangential fields via the dyadic

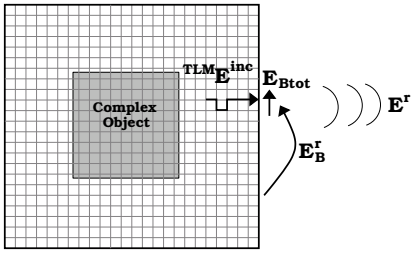

Figure 6.10: Interface between the TLM-box and the free-space region.

free-space Green's function in time domain as [4]

$$\begin{aligned}\mathbf{E}^r(\mathbf{r},\mathrm{t}) = \frac{T}{4\pi}\iint_S dS'\Big\{ &\frac{-\mu}{R}\frac{\partial}{\partial t}\big(\mathbf{n}(\mathbf{r}')\times\mathbf{H}_{Btot}(\mathbf{r}',\tau)\big)\\ +(\mathbf{n}(\mathbf{r}')\times\mathbf{E}_{Btot}(\mathbf{r}',\tau))\times\frac{\mathbf{R}}{4\pi R^3} &+ \frac{\partial}{\partial t}(\mathbf{n}(\mathbf{r}')\times\mathbf{E}_{Btot}(\mathbf{r}',\tau))\times\frac{\mathbf{R}}{4\pi R^2 c}\\ +\big(\mathbf{n}(\mathbf{r}')\cdot\mathbf{E}_{Btot}(\mathbf{r}',\tau)\big)\cdot\frac{\mathbf{R}}{4\pi R^3} &+ \frac{\partial}{\partial t}\big(\mathbf{n}(\mathbf{r}')\cdot\mathbf{E}_{Btot}(\mathbf{r}',\tau)\big)\frac{\mathbf{R}}{4\pi R^2 c}\Big\}_{\tau=t-R/c}\end{aligned} \tag{6.3}$$

$$\begin{aligned}\mathbf{H}^r(\mathbf{r},\mathrm{t}) = \frac{T}{4\pi}\iint_S dS'\Big\{ &\frac{\varepsilon}{R}\frac{\partial}{\partial t}\big(\mathbf{n}(\mathbf{r}')\times\mathbf{E}_{Btot}(\mathbf{r}',\tau)\big)\\ +(\mathbf{n}(\mathbf{r}')\times\mathbf{H}_{Btot}(\mathbf{r}',\tau))\times\frac{\mathbf{R}}{4\pi R^3} &+ \frac{\partial}{\partial t}(\mathbf{n}(\mathbf{r}')\times\mathbf{H}_{Btot}(\mathbf{r}',\tau))\times\frac{\mathbf{R}}{4\pi R^2 c}\\ +(\mathbf{n}(\mathbf{r}')\cdot\mathbf{H}_{Btot}(\mathbf{r}',\tau)\cdot\frac{\mathbf{R}}{4\pi R^3} &+ \frac{\partial}{\partial t}(\mathbf{n}(\mathbf{r}')\cdot\mathbf{H}_{Btot}(\mathbf{r}',\tau))\cdot\frac{\mathbf{R}}{4\pi R^2 c}\Big\}_{\tau=t-R/c},\end{aligned} \tag{6.4}$$

where $\mathbf{r}$ and $\mathbf{r}'$ are the destination and source positions vectors, respectively, R is the distance between these vectors. This equation can be applied to all the space: when $\mathbf{r}$ and $\mathbf{r}'$ belong to the same interface S_B, then with $T = 2$, the calculated radiated field represents the self coupling between the surface elements, $\mathbf{E}^r_B$ and $\mathbf{H}^r_B$ in eqs. (6.1) (6.2), for destination $\mathbf{r}$ outside the TLM-subregion, the radiated electromagnetic field can be calculated using the eqs. (6.3) (6.4) with $T = 1$. The points $\mathbf{r}'$ are defined on the radiating interface while $\mathbf{n}$ are the normal vectors on the interface at these points.

With that, the EFIE (6.1) and MFIE (6.2) can be written in a compact dyadic form:

$$\mathbf{E}_{Btot}(r,t) = {}^{TLM}\ \mathbf{E}^{inc}_B(r,t) + \widetilde{\mathbf{C}}_{EH}(r,r',t-\tau)(\mathbf{E}_{Btot}(r',\tau) + Z\mathbf{H}_{Btot}(r',\tau)) \tag{6.5}$$

$$\mathbf{H}_{Btot}(r,t) = {}^{TLM}\ \mathbf{H}^{inc}_B(r,t) + \widetilde{\mathbf{D}}_{EH}(r,r',t-\tau)(Z^{-1}\mathbf{E}_{Btot}(r',\tau) + \mathbf{H}_{Btot}(r',\tau)), \tag{6.6}$$

where the dyadic forms $\widetilde{\mathbf{C}}_{EH}$ and $\widetilde{\mathbf{D}}_{EH}$ represent matrix operators involving integro-differential operations. Z represent the wave impedance in free space. An important

observation is that the integral eqs. (6.5) (6.6) have a time retardation feature that allows to solve them in an iterative way. In the kernel of the operators on the right side of these equations, the time variable is retarded with respect to the same variable in the left side. Since the point $R = 0$ is excluded in the evaluation of the integrals, R/c is never zero (we consider principal-value integrals). Therefore the variable τ is always less than t and with that the unknown electromagnetic field $\mathbf{E}_{Btot}$, $\mathbf{H}_{Btot}$ is the sum of a known term, the incident field term and an integral that is also known from the past history of the same field. With that we derive the basis for solving integral equations by iterative methods such as the marching on in time (MOT) technique.

Now we discretize the EFIE (6.5) and MFIE (6.6) by expanding the total tangential fields with an appropriate set of functions, in time and in space; the subdomains of such functions are due to the TLM mesh.

$$\mathbf{E}_{Btot}(\mathbf{r},\mathrm{t}) = \sum_{v=1}^{V}\sum_{i=0}^{N} \mathbf{E}_{\varphi}(\mathbf{r}_v\ , t_i)\, \Phi(\mathbf{r}-\mathbf{r}_v)\, P(t-t_i), \tag{6.7}$$

$$\mathbf{H}_{Btot}(\mathbf{r},\mathrm{t}) = \sum_{v=1}^{V}\sum_{i=0}^{N} \mathbf{H}_{\psi}(\mathbf{r}_v\ , t_i)\, \Psi(\mathbf{r}-\mathbf{r}_v)\, Q(t-t_i), \tag{6.8}$$

where Φ and Ψ denote surface pulse functions, being equal to unity for $\mathbf{r}$ on the elementary surface centered at $\mathbf{r}_v$; P and Q are time-pulse functions, being equal to unity for t in the time interval centered at t_i.

We consider V surface element at the boundary S_B and N time steps. $\mathbf{E}_{\varphi}$ and $\mathbf{H}_{\psi}$ are the unknown expanding coefficients. Following the direct Method of Moments approach, as in [4], we choose the following weighting functions:

$$W_{vi}(\mathbf{r}_v, t_i) = \delta(t-t_i)\delta(\mathbf{r}-\mathbf{r}_v),\ with\ t_i = i\Delta t, \tag{6.9}$$

and

$$\langle W_{vi}(\mathbf{r}_v, t_i),\ \Phi(\mathbf{r}-\mathbf{r}_v)\, P(t-t_i)\rangle =$$

$$\int_{-\infty}^{+\infty} dt \int\int_{S} \Phi(\mathbf{r}-\mathbf{r}_v)\, P(t-t_i)\delta(t-t_i)\delta(\mathbf{r}-\mathbf{r}_v)dS = \delta_v\delta_i, \tag{6.10}$$

where the time step is chosen as in the TLM algorithm $\Delta t = \Delta l/2$. We assume a smooth field distribution on the surface S_B, a distance has to be kept between the objects and the surface S_B in order to ensure this. For obtaining a matrix system we give numbers to the coordinates of the fields: v, v', v" are the numbers of the discrete co-ordinates $\mathbf{r}_v$, $\mathbf{r}_{v'}$, $\mathbf{r}_{v''}$ and i, i', i'' are the numbers of the discrete time steps t, $t_{n'}$, $t_{n''}$. Now, by inserting the eqs (6.7,6.8) in (6.5,6.6) and taking the symmetric product with equations (6.9) and (6.10), we get

$$\mathbf{E}_{\varphi}(u,j) = {}^{TLM}\ \mathbf{E}_B^{inc}(u,\ j) + \sum_{v=1}^{V}\sum_{i=0}^{N}\left[\widetilde{\mathbf{C}}_{EH}(u,v,j-i)(\mathbf{E}_{\varphi}(v,i) + Z\mathbf{H}_{\psi}(v,i))\right] \tag{6.11}$$

$$\mathbf{H}_{\psi}(u,j) = {}^{TLM}\,\mathbf{H}_{B}^{inc}(u,\,j) + \sum_{v=1}^{V}\sum_{i=0}^{N}\left[\widetilde{\mathbf{D}}_{EH}(u,v,j-i)(Z^{-1}\mathbf{E}_{\varphi}(v,i) + \mathbf{H}_{\psi}(v,i))\right]. \tag{6.12}$$

In order to solve the above equations for the unknown field coefficients $\mathbf{E}_{\varphi}(u,j)$ and $\mathbf{H}_{\psi}(u,j)$, we introduce two weighting matrices with elements given by:

$$\widetilde{\mathbf{W}}_{E}(u,v) = \delta_{v}^{u}\,\widetilde{\mathbf{I}} - \widetilde{\mathbf{C}}_{EH}(u,v,0) \tag{6.13}$$

$$\widetilde{\mathbf{W}}_{H}(u,v) = \delta_{v}^{u}\,\widetilde{\mathbf{I}} - \widetilde{\mathbf{D}}_{EH}(u,v,0), \tag{6.14}$$

where $\widetilde{\mathbf{I}}$ is a identity dyad and δ_{v}^{u} is a Kronecker delta function. By applying the eqs. (6.13, 6.14) to (6.11, 6.12) and after some manipulations, we derive the following form for the unknown coefficients:

$$\mathbf{E}_{\varphi}(u,j) = \sum_{v=1}^{V}\tilde{W}_{E}^{-1}(u,v)\cdot\left({}^{TLM}\mathbf{E}_{B}^{inc}(v,\,j)\right)$$
$$+\widetilde{\mathbf{W}}_{E}^{-1}(u,v)\cdot\left\{\sum_{v'=1}^{V}\sum_{i=0}^{j-1}\left[\widetilde{\mathbf{C}}_{EH}(v,v',j-i)(\mathbf{E}_{\varphi}(v',i) + Z\mathbf{H}_{\psi}(v',i))\right]\right\} \tag{6.15}$$

$$\mathbf{H}_{\psi}(u,j) = \sum_{v=1}^{V}\tilde{W}_{H}^{-1}(u,v)\cdot\left({}^{TLM}\mathbf{H}_{B}^{inc}(v,\,j)\right)$$
$$+\widetilde{\mathbf{W}}_{H}^{-1}(u,v)\cdot\left\{\sum_{v'=1}^{V}\sum_{i=0}^{j-1}\left[\widetilde{\mathbf{D}}_{EH}(v,v',j-i)(Z^{-1}\mathbf{E}_{\varphi}(v',i) + \mathbf{H}_{\psi}(v',i))\right]\right\}. \tag{6.16}$$

The eqs. (6.15, 6.16) constitute an equation system whose solution permits us to recover iteratively the expanding coefficients of the tangential e.m. field. For every surface element of number u, the expanding coefficients at time j can be directly computed from the incident field at the same time j and the past history of the tangential field in all the surface-elements from the time $i = 0$ up to the time $(j-1)$.

After the computation of the corrected total tangential field values at S_B, the radiated e.m. field at any destination point outside the TLM subregion can be performed using the eqs. (6.3, 6.4) and setting $T = 1$.

We summarize the different steps of the hybrid TLM-IE algorithm for the analysis of radiating structures:

- The TLM algorithm starts with the absorbing boundary condition at the interface S_B.
- For every time step j and for every surface-element u at the interface S_B, the incident tangential field ${}^{TLM}\mathbf{E}_{B}^{inc}(u,\,j)$ is known.

- The known incident tangential field values are now inserted in the equations (6.15, 6.16). Considering now a particular destination surface-element u and all other source elements v on the boundary surface S_B, defined by the TLM grid. The effect of every source element with respect to the destination surface-element depends on the contribution of the discretized integral in (6.15, 6.16), which depends on the case if $t_j \leq R_{uv}/c$, where R_{uv} represents the distance between the destination u and source surface-element v.
- The same procedure is repeated for every destination element at the interface S_B. When the condition $t_j > R_{uv}/c$ is fulfilled, we have contribution providing the correct total tangential field at the interface S_B, calculated from the known values at earlier time steps.
- The calculated total tangential field at the interface on every surface element and at every time step describe exactly the radiation boundary condition at the interface S_B for the TLM scheme.

The hybrid (TLM-IE) method consists of a TLM procedure applied for the field modeling inside the subregion S_B in which, for every time step, the corrected total tangential field values at the interface is evaluated by means of a proper set of integral equations and providing the radiating boundary condition for the TLM algorithm at S_B.

6.3 TLM-IE Concept for Transient Interferences

In Electromagnetic Compatibility we often have to deal with transient interference among objects of arbitrary shape which are separated by wide free space regions. For the electromagnetic field analysis of such problems, an efficient numerical time domain method is required. The field simulation of very general structures exhibiting complex geometry and lossy materials may be performed by space discretizing method like the Transmission Line Matrix (TLM) method. However , using the space discretizing TLM method, the numerical modeling of electromagnetic interference problems involving wide free space regions requires a high computational effort. In order to overcome the limits of the TLM method, the hybrid TLM-Integral Equation Method (TLM-IE) has been developed. In the TLM-IE Method the space discretising TLM Method for the numerical modeling of the near field is combined with the Integral Equation method for the description of the electromagnetic field propagation in the wide region of the homogenous medium around the objects.

We consider two or more interacting objects embedded in free space, as shown in Fig.6.11. These objects may exhibits complex structure and may contain various lossy and dielectric materials, as well as metallic layers of finite thickness. For the efficient numerical modeling of the electromagnetic field interaction in such an arrangement, two main aspects are combined in the hybrid TLM-IE method:

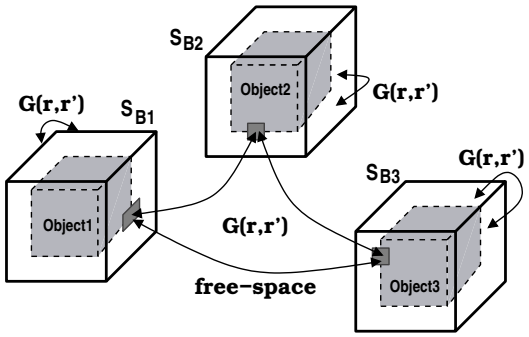

Figure 6.11: Electromagnetic coupling among different discretized subregions. The surface elements of the subregions are coupled via Green's functions in time domain

- Each object is embedded into a separate volume which is discretized spatially as indicated in Fig. 6.11. The discretized volumes are enclosed by imaginary free space boundary boxes. Inside these volumes, Maxwell's equations are solved numerically in the time domain, applying the TLM method with symmetrical condensed nodes [1].
- For the description of the electromagnetic interaction of the objects, we apply the equivalence theorem in the Schelkunoff-Huygen's representation. The objects are enclosed by a boundary box, where the total tangential electromagnetic field is evaluated by means of a proper set of integral equations in each time step.

In the following the synthesis of the two above aspects in the hybrid TLM-IE method is described more closely at the example of p interacting objects, which are coupled electromagnetically. In Fig. 6.11, three interacting objects are shown with the boundary surfaces S_{B1}, S_{B2} and S_{B2}. The TLM-subregions can be considered as multiports. The ports of these subregions are the open transmission lines of the TLM nodes at the boundaries of the TLM mesh. At the boundaries between the discretized TLM regions and the homogeneous free-space region, the two representations are interfaced by applying the continuity of the EM tangential field, thus providing an appropriate set of electric-field integral equations (EFIEs) and magnetic-field integral equations (MFIEs); the latter equations are solved explicitly at each time step [12].

Let us consider a general case where the free-space region with p interacting objects are considered. We now analyze the subregion k, with its boundary surface S_{Bk}. The tangential field at the surface S_{Bk} represents a distribution of equivalent currents and charges, according to the Huygens Shelkunoff's representation of the equivalence theorem [4]. The equivalent sources on the surface S_{Bk} are self- and mutually coupled. Inside the discretized subregion k , there are sources, producing an incident tangential

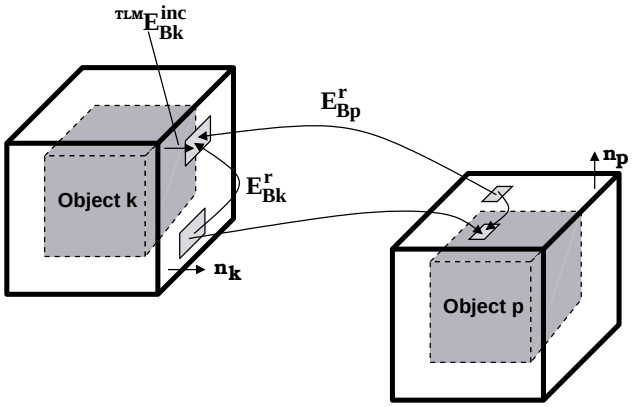

Figure 6.12: Hybrid TLM-IE scheme for transient coupling between two objects.

field ${}^{TLM}\mathbf{E}^{inc}_{Bk}$and ${}^{TLM}\mathbf{H}^{inc}_{Bk}$ on the surface S_{Bk} , as produced by the TLM algorithm. By applying the continuity of the tangential electric field at the surface boundary, we derive the following EFIE and MFIE equations for subregion k [12]:

$$\mathbf{n} \times \mathbf{E}_{Bk}(\mathbf{r}_k,\, t) = \mathbf{n} \times \left({}^{TLM}\mathbf{E}^{inc}_{Bk}(\mathbf{r}_k,\, t) + \mathbf{E}^{r}_{Bk}(\mathbf{r}_k,\, t) + \mathbf{E}^{r}_{Bp}(\mathbf{r}_k,\, t) \right) \tag{6.17}$$

$$\mathbf{n} \times \mathbf{H}_{Bk}(\mathbf{r}_k,\, t) = \mathbf{n} \times \left({}^{TLM}\mathbf{H}^{inc}_{Bk}(\mathbf{r}_k,\, t) + \mathbf{H}^{r}_{Bk}(\mathbf{r}_k,\, t) + \mathbf{H}^{r}_{Bp}(\mathbf{r}_k,\, t) \right), \tag{6.18}$$

where $\mathbf{E}^{r}_{Bp}(\mathbf{r}_k,\, t)$ and $\mathbf{H}^{r}_{Bp}(\mathbf{r}_k,\, t)$ represent the contribution to the radiated field on the interface S_{Bk} produced via the free-space Green's functions by the N_p equivalent sources (tangential field) located on the boundaries of all the other subregions p, $p \neq k$, as indicated in Fig. 6.12. $\mathbf{E}^{r}_{Bk}(\mathbf{r}_k,\, t)$ and $\mathbf{H}^{r}_{Bk}(\mathbf{r}_k,\, t)$ denote the contribution due to the N_k sources (including the self contribution) belonging to the same surface S_{Bk} . By taking the tangential part of the radiated e.m. field, we derive, as in [4]:

$$\begin{aligned}\mathbf{E}^{r}_{Bk}(\mathbf{r}_k,\mathrm{t}) = \frac{2}{4\pi} \iint_{SBk} dS' \Bigg\{ & \frac{-\mu}{R_{kk}} \frac{\partial}{\partial t} \big(\mathbf{n}_k(\mathbf{r}'_k) \times \mathbf{H}_{Bk}(\mathbf{r}'_k, \tau_{kk}) \big) \\ & + \frac{1}{R^3_{kk}} \left[1 + (t - \tau_{kk}) \frac{\partial}{\partial t} \right] \Big[(\mathbf{n}_k(\mathbf{r}'_k) \times \mathbf{E}_{Bk}(\mathbf{r}'_k, \tau_{kk})) \times \mathbf{R}_{kk} \\ & + \big(\mathbf{n}_k(\mathbf{r}'_k) \cdot \mathbf{E}_{Bk}(\mathbf{r}'_k, \tau_{kk}) \big) \cdot \mathbf{R}_{kk} \Big] \Bigg\}_{\tau_{kk} = t - R_{kk}/c}\end{aligned} \tag{6.19}$$

$$\mathbf{H}^r_{Bk}(\mathbf{r}_k,\mathrm{t}) = \frac{2}{4\pi}\iint_{SBk} dS'\Big\{\frac{\varepsilon}{R_{kk}}\frac{\partial}{\partial t}\big(\mathbf{n}_k(\mathbf{r}'_k)\times\mathbf{E}_{Bk}(\mathbf{r}'_k,\tau_{kk})\big) + \frac{1}{R^3_{kk}}\Big[1+(t-\tau_{kk})\frac{\partial}{\partial t}\Big]\Big[(\mathbf{n}_k(\mathbf{r}'_k)\times\mathbf{H}_{Bk}(\mathbf{r}'_k,\tau_{kk}))\times\mathbf{R}_{kk} + \big(\mathbf{n}_k(\mathbf{r}'_k)\cdot\mathbf{H}_{Bk}(\mathbf{r}'_k,\tau_{kk})\big)\cdot\mathbf{R}_{kk}\Big]\Big\}_{\tau_{kk}=t-R_{kk}/c}, \tag{6.20}$$

where the unit vector $\mathbf{n}_k(\mathbf{r}'_k)$ is normal to the boundary surface S_k and points out of the surface element centered by $\mathbf{r}'_k$. The vectors $\mathbf{r}_k$ and $\mathbf{r}'_k$ are the observation and source point vectors, respectively, both defined on the boundary surface S_{Bk}. $\mathbf{R}_{kk}$ is the corresponding distance vectors : $\mathbf{R}_{kk} = \mathbf{r}_k - \mathbf{r}'_k$ and $R_{kk} = |\mathbf{r}_k - \mathbf{r}_{k'}|$. For the calculation of the radiated field $\mathbf{E}^r_{Bp}(\mathbf{r}_k,\, t)$ and $\mathbf{H}^r_{Bp}(\mathbf{r}_k,\, t)$ from all the objects $p \neq k$ we derive as in [4]:

$$\mathbf{E}^r_{Bp}(\mathbf{r}_k,\mathrm{t}) = \sum_{i,i\neq k}^{p}\mathbf{E}^r_{Bi}(\mathbf{r}_k,t)$$

$$= \sum_{i,i\neq k}^{p}\frac{1}{4\pi}\iint_{SBi} dS'\Big\{\frac{-\mu}{R_{ki}}\frac{\partial}{\partial t}\big(\mathbf{n}_i(\mathbf{r}'_i)\times\mathbf{H}_{Bi}(\mathbf{r}'_i,\tau_{ki})\big) \tag{6.21}$$

$$+\frac{1}{R^3_{ki}}\Big[1+(t-\tau_{ki})\frac{\partial}{\partial t}\Big]\Big[(\mathbf{n}_i(\mathbf{r}'_i)\times\mathbf{E}_{Bi}(\mathbf{r}'_i,\tau_{ki}))\times\mathbf{R}_{ki} + \big(\mathbf{n}_i(\mathbf{r}'_i)\cdot\mathbf{E}_{Bi}(\mathbf{r}'_i,\tau_{ki})\big)\cdot\mathbf{R}_{ki}\Big]\Big\}_{\tau_{ki}=t-R_{ki}/c} \tag{6.22}$$

$$\mathbf{H}^r_{Bp}(\mathbf{r}_k,\mathrm{t}) = \sum_{i,i\neq k}^{p}\mathbf{H}^r_{Bi}(\mathbf{r}_k,t)$$

$$= \sum_{i,i\neq k}^{p}\frac{1}{4\pi}\iint_{SBi} dS'\Big\{\frac{\varepsilon}{R_{ki}}\frac{\partial}{\partial t}\big(\mathbf{n}_i(\mathbf{r}'_i)\times\mathbf{E}_{Bi}(\mathbf{r}'_i,\tau_{ki})\big) \tag{6.23}$$

$$+\frac{1}{R^3_{ki}}\Big[1+(t-\tau_{ki})\frac{\partial}{\partial t}\Big]\Big[(\mathbf{n}_i(\mathbf{r}'_i)\times\mathbf{H}_{Bi}(\mathbf{r}'_i,\tau_{ki}))\times\mathbf{R}_{ki} + \big(\mathbf{n}_i(\mathbf{r}'_i)\cdot\mathbf{H}_{Bi}(\mathbf{r}'_i,\tau_{ki})\big)\cdot\mathbf{R}_{ki}\Big]\Big\}_{\tau_{ki}=t-R_{ki}/c}, \tag{6.24}$$

where the unit vectors $\mathbf{n}_i(\mathbf{r}'_i)$ are normal to the boundary surface S_{Bi} with ($i = 1, ..., p,\ i \neq k$), The vectors $\mathbf{r}'_i$ are the source point vectors, lying on the source boundary surfaces S_{Bi}, while $\mathbf{r}_k$ are the observation point vectors, lying on the boundary surface S_{Bk}. R_{ki} are the corresponding distance vectors : $\mathbf{R}_{ki} = \mathbf{r}_k - \mathbf{r}'_i$ and

$R_{ki} = |\mathbf{r}_k - \mathbf{r}'_i|$, with $(i = 1, ..., p,\ i \neq k)$. The time variable τ_{ki} is retarded with respect to the time t of field evaluation. For $\mathbf{r}_k \neq \mathbf{r}'_i$, $R_{ki} > 0$, $\tau_{ki} = t - R_{ki} < t$. This means that the $\mathbf{E}^{\tau}_{Bi}(\mathbf{r}_k,\mathrm{t})$ fields are known from the past history of the total tangential fields at the boundary surfaces S_{Bi} of the regions i with $(i = 1, ..., p,\ i \neq k)$.

The EFIE (6.17) and the dual MFIE (6.18) are then discretized by expanding the total tangential-field components with appropriate sets of rectangular basis functions, both in time and in space; the subdomains of such functions are defined by the TLM grid. For the subregion k, $k = 1, ..., p$, we choose

$$\mathbf{E}_{Btk}(\mathbf{r}_k,\mathrm{t}) = \sum_{v=1}^{V_k}\sum_{i=0}^{N} \mathbf{E}_{\varphi k}(\mathbf{r}_v\ , t_i)\Phi_k(\mathbf{r}_k - \mathbf{r}_v)\, T_{Ek}(t - t_i), \tag{6.25}$$

$$\mathbf{H}_{Btk}(\mathbf{r}_k,\mathrm{t}) = \sum_{v=1}^{V_k}\sum_{i=0}^{N} \mathbf{H}_{\psi k}(\mathbf{r}_v\ , t_i)\Psi_k(\mathbf{r}_k - \mathbf{r}_v)\, T_{Hk}(t - t_i), \tag{6.26}$$

where $\mathbf{E}_{\varphi k}$ and $\mathbf{H}_{\Psi k}$ are the unknown expansion coefficients of the total tangential field $\mathbf{E}_{Btk}$and $\mathbf{H}_{Btk}$, respectively, on the surface S_k. The functions Φ_k and Ψ_k denote surface pulse functions of rectangular type,

$$\Phi_k(\mathbf{r}_k - \mathbf{r}_v) = \Psi_u(\mathbf{r}_k - \mathbf{r}_v) = \begin{cases} 0 & for\ \ \mathbf{r}_k - \mathbf{r}_v \geq \Delta l/2 \\ 1 & otherwise, \end{cases} \tag{6.27}$$

equal to unity for $\mathbf{r}_k$ on the elementary surface cell centered at $\mathbf{r}_v$ and zero on all the other cells. T_{Ek} and T_{Hk} are time-pulse functions, equal to unity for t in the time interval centered at $t_i$and zero on all the other time steps, as

$$T_{Ek}(t - t_i) = T_{Hu}(t - t_i) = \begin{cases} 0 & for\, t - i\Delta t \geq \Delta t/2 \\ 1 & otherwise. \end{cases} \tag{6.28}$$

We consider V_k elementary subdomains for the subregion k and N time steps for all the subregions. Following a direct time-domain method of moments approach [4], we choose the weight functions

$$W_{vj}(\mathbf{r}, \mathbf{r}_v, t, t_j) = \delta(t - t_j)\delta(\mathbf{r} - \mathbf{r}_v)\ \ with\ \ t_j = j\Delta t. \tag{6.29}$$

The time step is chosen according to the TLM algorithm: $\Delta t = \Delta l/hc$, with c being the light velocity, Δl the size of the TLM grid and h the stabilization factor of the Symmetrical Condensed Node (SCN) approach [49]. For each subregion k, we assign discrete coordinates of the fields and the time step; in particular, v_k and u_k represent source $\mathbf{r}_{vk}$ and destination $\mathbf{r}_{uk}$ points, respectively, while N is the number of discrete time steps.

We insert now the expanded fields (6.25, 6.26) in the EFIE (6.17) and MFIE (6.18). Taking the symmetric product with W_{vj} of (6.29) for $j = 0, 1, 2, ...N$, we obtain, for each subregion k, the expanding coefficients of the total tangential field,

$$\mathbf{E}_{\varphi k}(u_k, j) =^{TLM} \mathbf{E}^{inc}_{Bk}(u_k,\, j) + \mathbf{E}^{r}_{\varphi k}(u_k,\, j) + \mathbf{E}^{r}_{\varphi p}(u_k,\, j), \tag{6.30}$$

$$\mathbf{H}_{\psi k}(u_k, j) =^{TLM} \mathbf{H}^{inc}_{Bk}(u_k,\, j) + \mathbf{H}_{\psi k}(u_k,\, j) + \mathbf{H}_{\psi p}(u_k,\, j), \tag{6.31}$$

with

$$\begin{aligned}
\mathbf{E}^{r}_{\varphi k}(u_k,\, j) = \frac{1}{2\pi} \sum_{v_k=1}^{V_k} \Delta S_{v_k} [\\
\frac{-\mu}{R_{u_k v_k} \Delta t} (\mathbf{n}_k(v_k) \times (\mathbf{H}_{B\psi_k}(v_k, i_k) - \mathbf{H}_{B\psi_k}(v_k, i_k - 1))) \\
+ (\mathbf{n}_k(v_k) \times ((j - i_k + 1)\mathbf{E}_{B\varphi_k}(v_k, i_k) - (j - i_k)\mathbf{E}_{B\varphi_k}(v_k, i_k - 1)) \times \frac{\mathbf{R}_{u_k v_k}}{R^3_{u_k v_k}}) \\
+ (\mathbf{n}_k(v_k) \cdot ((j - i_k + 1)\mathbf{E}_{B\varphi_k}(v_k, i_k) - (j - i_k)\mathbf{E}_{B\varphi_k}(v_k, i_k - 1)) \cdot \frac{\mathbf{R}_{u_k v_k}}{R^3_{u_k v_k}})],
\end{aligned} \tag{6.32}$$

$$\begin{aligned}
\mathbf{H}^{r}_{\psi k}(u_k,\, j) = \frac{1}{2\pi} \sum_{v_k=1}^{V_k} \Delta S_{v_k} [\\
\frac{\varepsilon}{R_{u_k v_k} \Delta t} (\mathbf{n}_k(v_k) \times (\mathbf{E}_{B\varphi_k}(v_k, i_k) - \mathbf{E}_{B\varphi_k}(v_k, i_k - 1))) \\
+ (\mathbf{n}_k(v_k) \times ((j - i_k + 1)\mathbf{H}_{B\psi_k}(v_k, i_k) - (j - i_k)\mathbf{H}_{B\psi_k}(v_k, i_k - 1)) \times \frac{\mathbf{R}_{u_k v_k}}{R^3_{u_k v_k}}) \\
+ (\mathbf{n}_k(v_k) \cdot ((j - i_k + 1)\mathbf{H}_{B\psi_k}(v_k, i_k) - (j - i_k)\mathbf{H}_{B\psi_k}(v_k, i_k - 1)) \cdot \frac{\mathbf{R}_{u_k v_k}}{R^3_{u_k v_k}})],
\end{aligned} \tag{6.33}$$

where ΔS_{v_k} denotes the area of the elementary surface cell centered at $\mathbf{r}_{v_k}$, $\mathbf{R}_{u_k v_k} = \mathbf{r}_{u_k} - \mathbf{r}_{v_k}$, $R_{u_k v_k} = |\mathbf{r}_{u_k} - \mathbf{r}_{v_k}|$, and $i_k = j - hR_{u_k v_k}/\Delta l\, c$. For $\mathbf{E}^{r}_{\varphi p}(u_k,\, j)$ in (6.30)

and $\mathbf{H}^r_{\psi p}(u_k,\, j)$ in (6.31), we derive

$$\begin{aligned}\mathbf{E}^r_{\varphi p}(u_k,\, j) = \frac{1}{4\pi}\sum_{s,s\neq k}^{p}\sum_{v_s=1}^{V_s}\Delta S_{v_s}[\\ \frac{-\mu}{R_{u_k v_s}\Delta t}(\mathbf{n}_s(v_s)\times(\mathbf{H}_{B\psi_s}(v_s,i_s)-\mathbf{H}_{B\psi_s}(v_s,i_s-1)))\\ +(\mathbf{n}_s(v_s)\times((j-i_s+1)\mathbf{E}_{B\varphi_s}(v_s,i_s)-(j-i_s)\mathbf{E}_{B\varphi_k}(v_s,i_s-1))\times\frac{\mathbf{R}_{u_k v_s}}{R^3_{u_k v_s}})\\ +(\mathbf{n}_s(v_s)\cdot((j-i_s+1)\mathbf{E}_{B\varphi_s}(v_s,i_s)-(j-i_s)\mathbf{E}_{B\varphi_s}(v_s,i_s-1))\cdot\frac{\mathbf{R}_{u_k v_s}}{R^3_{u_k v_s}})],\end{aligned} \tag{6.34}$$

$$\begin{aligned}\mathbf{H}^r_{\psi p}(u_k,\, j) = \frac{1}{4\pi}\sum_{s,s\neq k}^{p}\sum_{v_s=1}^{V_s}\Delta S_{v_s}[\\ \frac{\varepsilon}{R_{u_k v_s}\Delta t}(\mathbf{n}_s(v_s)\times(\mathbf{E}_{B\varphi_s}(v_s,i_s)-\mathbf{E}_{B\varphi_s}(v_s,i_s-1)))\\ +(\mathbf{n}_s(v_s)\times((j-i_s+1)\mathbf{H}_{B\psi_s}(v_s,i_s)-(j-i_s)\mathbf{H}_{B\psi_k}(v_s,i_s-1))\times\frac{\mathbf{R}_{u_k v_s}}{R^3_{u_k v_s}})\\ +(\mathbf{n}_s(v_s)\cdot((j-i_s+1)\mathbf{H}_{B\psi_s}(v_s,i_s)-(j-i_s)\mathbf{H}_{B\psi_s}(v_s,i_s-1))\cdot\frac{\mathbf{R}_{u_k v_s}}{R^3_{u_k v_s}})],\end{aligned} \tag{6.35}$$

where V_s represents the number of boundary elements on the boundary surface of the TLM-subregion $s\,(s=1,...,\,p,\,s\neq p)$. ΔS_{v_s} is the area of the elementary cell centered at $\mathbf{r}_{v_s}$,$\mathbf{R}_{u_k v_s}=\mathbf{r}_{u_k}-\mathbf{r}_{v_s}$, $R_{u_k v_s}=|\mathbf{r}_{u_k}-\mathbf{r}_{v_s}|$. i_s is the retarded time step.

The solution of eqs. (6.30) (6.31) is the set of expanding coefficients for the unknown total tangential field. The expanding coefficients at time j can be directly computed from the incident field at the same time plus the past history of the total tangential field on all the surface elements of all the interacting TLM-subregions, including the self-coupling contribution. Moreover, for each time step t_j, the correct value of the tangential field, calculated by the boundary integral equations, provides the exact radiating boundary for the TLM algorithm on the surface $S_k(k=1,...,p)$. The time difference index $(j-i_s)$ is the time retardation of the signal caused by the distance $R_{u_k v_s}$. The time step is chosen according to the TLM algorithm for wave propagation in free space with the stability factor $h\geq 2$ of the TLM algorithm, with

$$\frac{(t_j-t_{i_s})}{\Delta t}=j-i_s=\frac{hR_{u_k v_s}}{\Delta l} \tag{6.36}$$

For long distances, the factor $(j - i_s - 1)$ can be approximated to $(j - i_s)$. In this case eqs. (6.34, 6.35) can be further simplified.

The wave amplitudes $\mathbf{a}_{Bk}(u_k, j)$ of the incident wave pulses at the open external ports of the TLM-subregions can be expressed by the unknown total tangential e.m. field $\mathbf{E}_{\varphi k}(u_k, j)$ and $\mathbf{H}_{\psi k}(u_k, j)$ at the free space boundaries and its normal vector $\mathbf{n}_k$ according to [49].

$$\mathbf{a}_{Bk}(u_k, j) = \frac{1}{2}(-\mathbf{n}_k \times \mathbf{n}_k \times \mathbf{E}_{\varphi k}(u_k, j) + Z\,\mathbf{n}_k \times \mathbf{H}_{\psi k}(u_k, j)). \tag{6.37}$$

In the eqs. (6.30, 6.31) is shown that the field, which is occurring at the destination points due to radiation from the all the boundary surfaces, can be expressed by a series of weighted field values of all the boundary surface elements. In order to save computational time, the weighting factors, connecting the field values of the surface elements with each other are developed and stored in advance. The weighting coefficients in the series are only dependant on the relative location of the surface element u_k to the surface element v_s, between all the interacting objects.

7 Hybrid TLM-TDMOM

7.1 Introduction

The transient phenomena in response to an impulse excitation are of great practical interest because they are central to the analysis of electromagnetic compatibility problems, inverse scattering, microwave imaging, radar identification, and so on.

Modeling of these electromagnetic problems requires fine resolution to deal with thin curved structures, the capability to model open boundary problems, and also to model complex objects placed in a non-uniform environment consisting of several materials like dielectrics, lossy material and conductors. These large differences in physical scale impose severe computational and modeling requirements.

The TLM method is very flexible for the modeling of general complex structures exhibiting compound dielectric and lossy materials, but the main drawback of the TLM method is its inability to accurately model curved thin structure, especially when the curvature is not conformable to the axes of the structured grid. The Cartesian grid leads to a staircase approximation of the geometry and small details are not resolved at all. Using the space discretizing TLM method to analyze the electromagnetic interaction between objects separated by large free-space regions requires a high computational effort. One possibility for the reduction of the computational effort is to combine the transmission line matrix method and the Integral-Equation method in a hybrid method that permits to incorporate the treatment of large free space regions with high efficiency, because it reduces the complexity of the field problem by one dimension [6]- [12]. In the hybrid TLM-IE method, discussed in the previous chapter, each of the interacting objects is embedded into a closed spatial subdomain, where the TLM method is applied for the field modeling. However, there still exist some drawbacks to this hybrid technique since, for objects with thin curved boundaries the staircasing approach employed in the conventional TLM method can introduce significant errors into the solution unless very dense grids are used to accurately resolve the variations in the geometric features, with a consequent increase in the computational demands. Curved conducting structures can be efficiently modeled using the time-domain version of the Method of Moments [17]- [29]. Indeed, the TD-MOM algorithm only require a discretization of the scatterer body, where the current flows, as opposed to a volume discretization surrounding the scatterer, as shown in Fig. 7.13, and do not

call for absorbing boundary condition, but automatically impose the radiation condition. The implementation of the time-domain MOM algorithm to curved conducting thin structure has been discussed in details in chapter 5. Therfore the basic idea is to

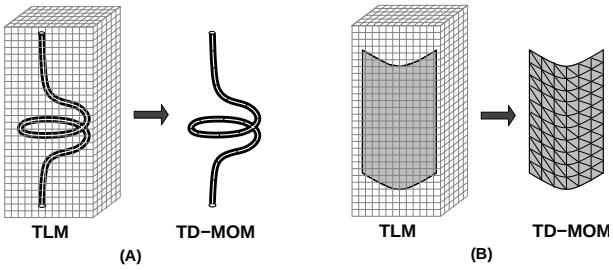

Figure 7.13: Fine discretization used for curved structure in TLM in comparison with the discretization used in the TD-MOM algorithm; (a) arbitrarily curved thin wire, (b) coducting surface with arbitrary shape.

develop a novel efficient hybrid method (TLM-TDMOM) combining the very flexible Transmission Line Matrix Method (TLM) and the efficient Time Domain Method of Moments (TDMOM), using for each part of the overall complex electromagnetic problem the most efficient technique, in order to overcome the intrinsic limitations of using a single technique only.

With that the TLM-TDMOM method can be applied to complex transient electromagnetic problems, as shown in Fig. 7.14. The novel efficient hybrid method has got the high flexibility of a space discretizing method for modeling of complex objects exhibiting materials with non-linear properties and the efficiency of method of moments for the scattering analysis of thin curved conducting structure and the treatment of large free-space regions.

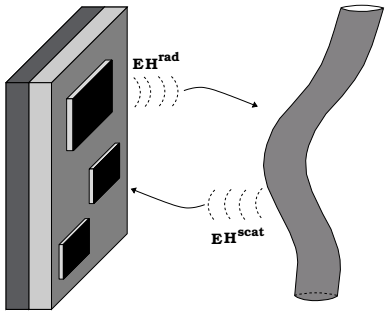

Figure 7.14: A complex object in interaction with an arbitrarily curved conducting structure.

7.2 TLM-TDMOM Concept

We present now the theoretical concept and the implementation of the different steps for the proposed novel efficient hybrid TLM-TDMOM method, restricting our investigation to the transient analysis of a complex configuration comprising thin curved conducting structure placed in front of an arbitrary inhomogeneous complex structure.

The application of the equivalence principle allows us to divide the three-dimensional space into subregions, and to apply the TLM method for modeling of the complex inhomogeneous object and the TD-MOM for the scattering modeling of the curved conducting object (thin wire or surface). The electromagnetic interaction between the subregions is provided by the dyadic free-space Green's functions in time domain.

The problem is the evaluation of the transient interference between the interacting objects. The analysis is performed in time domain, which seems to be the most suitable approach to treat fast transient phenomena. In fact EMC radiated fields are characterized by a very wide bandwith (up to several GHz), and moreover, that part of the spectrum having an apparently negligible amplitude can produce strong effects when the natural frequencies of resonant structures are excited. In this case a frequency domain approach requires a very accurate sampling, especially around the resonant frequencies, thus resulting in a very large number of samples and consequently a great computational effort.

In the hybrid TLM-TDMOM method, the time domain approach leads to the use of the time domain formulation of the MOM, also known as Marching On in Time (MOT) procedure. In this manner we obtain a perfect matching between the two numerical techniques, because both of them provide explicit iterative expressions for the electromagnetic field quantities. In this hybrid method the source object, analyzed by TLM, and the scattering object, analyzed by TDMOM, are studied separately as two simpler sub-problems of the original complex problem. This formulation was obtained by means of the application of the equivalence principle: the source object is enclosed by equivalence surface, where equivalent electric and magnetic currents flow. A proper determination of the equivalent currents allows us to evaluate the radiated field due to the sources in the complex object, and to account for the scattered field from the curved conducting structure, considering that all fields propagate in free space.

We consider two objects embedded into free space as shown in Fig. 7.15. The complex structure is enclosed by a discretized subregion where the TLM method is applied for the field modeling. The scattering structure (wire or surface) can be efficiently characterized by integral equation approaches, like the Method of Moments (MOM). The Marching on in Time procedure adopted to solve the integral equation for the current along the scattering structure, gives an explicit value of the unknown induced current samples at each time step.

The electromagnetic interaction between the TLM-interface S_B and scatterer is provided by the dyadic free-space Green's function in time domain. According to the

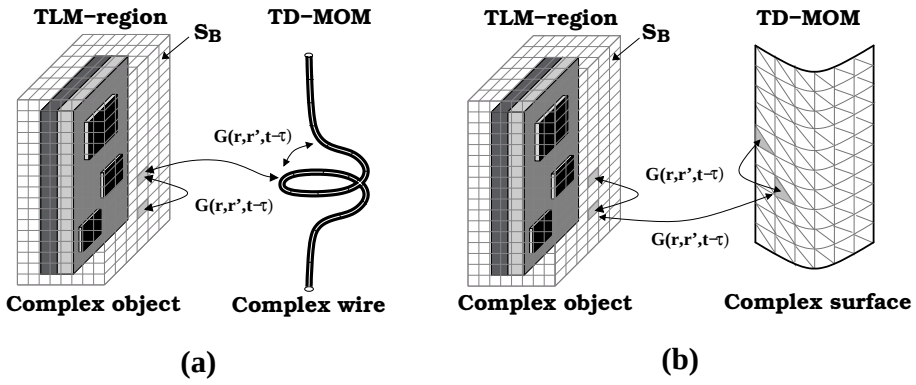

Figure 7.15: Hybrid TLM-TDMOM scheme; interference between a complex object and (a) curved thin wire, (b) conducting surface.

equivalence theorem, the tangential field at the TLM-interface represent equivalent surface currents which are sources of radiation. Inside the discretized subregion there are sources producing an incident field ${}^{TLM}\mathbf{E}_B^{inc}$ and ${}^{TLM}\mathbf{H}_B^{inc}$ on the interface modeled by the TLM algorithm, as indicated in Fig. 7.16. On the interface we impress the total tangential field $\mathbf{E}_{Btot}$ and $\mathbf{H}_{Btot}$ during the TLM Simulation. By applying the continuity of the tangential field at the interface, we derive the following EFIE and MFIE equations:

$$\mathbf{E}_{Btot}|_{tan} = \left({}^{TLM}\mathbf{E}_B^{inc} + \mathbf{E}_{Bself}^{r} + \mathbf{E}_{BScat}^{r}\right)\Big|_{tan}, \qquad (EFIE) \tag{7.1}$$

$$\mathbf{H}_{Btot}|_{tan} = \left({}^{TLM}\mathbf{H}_B^{inc} + \mathbf{H}_{Bself}^{r} + \mathbf{H}_{BScat}^{r}\right)\Big|_{tan}, \qquad (MFIE) \tag{7.2}$$

where $\mathbf{E}_{Btot}$ and $\mathbf{H}_{Btot}$ represent the unknown total tangential e.m. field on the interface. $\mathbf{E}_{Bself}^{r}$ and $\mathbf{H}_{Bself}^{r}$ are the radiated fields coming from the self interaction between the boundary elements. $\mathbf{E}_{BScat}^{r}$ and $\mathbf{H}_{BScat}^{r}$ are the radiated fields at the boundary surface coming from the scattering structure. This field is obtained from the current distribution on the scattering structure.

The focus of the next sections is to calculate the different field quantities in the EFIE (7.1) and MFIE (7.2) and then the total tangential field at every surface boundary element at the TLM interface for the case (a) Fig. 7.15(a): the scatterer is an arbitrarily oriented thin wire and for the case (b) Fig. 7.15(b): the scatterer is a perfectly conducting surface with arbitrary shape.

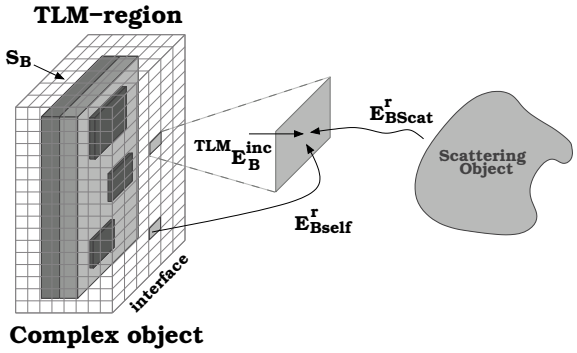

Figure 7.16: Total tangential field components at TLM-interface.

7.3 Calculation of the scattered fields

7.3.1 Thin wire scatterer

We consider in the first problem the electromagnetic interaction between a complex structure exhibiting complex dielectric and lossy materials and an arbitrarily oriented thin wire structure, as shown in Fig. 7.15(a). The time domain formulation of the problem allows us to treat efficiently fast transient phenomena, at the same time the hybrid technique allows us to treat separately the electromagnetic field source object and a scattered structure, strongly coupled with the source, solving each structure with the most suitable method.

In order to calculate the scattered field $\mathbf{E}^r_{Bscat}$ and $\mathbf{H}^r_{BScat}$ from the thin wire structure back to the TLM subregion, we have to determine in advance the current distribution on the wire body. This is shown in the next subsection.

Current Distribution

The most straightforward technique to calculate the induced transient currents would be to model the wire as a perfect electric conductor, and hence set all tangential electric components on the wire surface equal to zero. This leads to the Electric Field Integral Equation (EFIE). For excitation with smooth time dependence, the time derivative of the EFIE is generally used, because it avoids the time integral due to the charge contribution, as shown in chapter 5 (section 5.2),

$$\frac{\partial \mathbf{E}^{inc}_C(\mathbf{r},t)}{\partial t}\,\mathbf{e}_l = \frac{\mu}{4\pi}\frac{\partial^2}{\partial t^2}\int_{l(\mathbf{r})}\frac{I(\mathbf{r}',\tau)}{R}\mathbf{e}_l\cdot\mathbf{e}_l{}'\,dl' - \frac{1}{4\pi\epsilon}\frac{\partial}{\partial l}\int_{l(\mathbf{r})}\frac{\partial I(\mathbf{r}',\tau)}{\partial l'}\frac{1}{R}dl', \tag{7.3}$$

where $\mathbf{I}(\mathbf{r},t)$ is the unknown current distribution, $l(\mathbf{r})$ is the integration path. $\mathbf{E}_C^{inc}$ is the incident field at the wire surface coming from the TLM-subregion with $\mathbf{E}_C^{inc} = \mathbf{E}_B^r$, as indicated in Fig. 7.17. l and l' are curvilinear coordinates along the wire axis. $\mathbf{e}_l$ and $\mathbf{e}_l'$ are unit vectors tangential to the wire axis in the field and the source points, respectively, as shown in Fig. 7.17. R is the distance between the source $\mathbf{r}'$ and the field points $\mathbf{r}$. $\tau = t - R/c$ is the retarded time and c the light velocity in free space. All points on the wire are defined by the three dimensional coordinate vectors $\mathbf{r}$. We discretize the thin conductor into N wire segments with the index k as shown in Fig. 7.17.

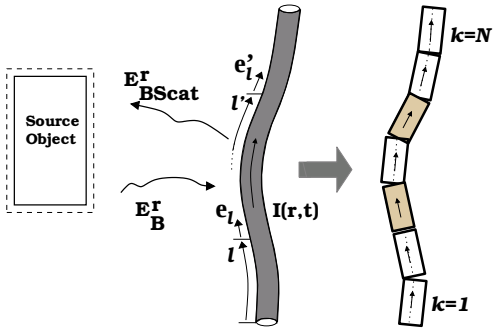

Figure 7.17: Discretization of the curved thin wire through straight segments for the the application to the hybrid TLM-TDMOM algorithm.

On each wire segment we define the current $\mathbf{I}_k$ and the tangential unity vector $\mathbf{e}_k$. Assuming constant current values $\mathbf{I}_k$ along the wire segments k in every time step and replacing derivatives with their finite difference scheme. The incident field at the sampling points of the wire is calculated from the total tangential e.m. field quantities at the TLM-interface by the Green's function in time domain. Equation (7.3) can be solved for the actual current values $\mathbf{I}_{k,n}$ in every time step using the marching on in time version of the MOM. In this way the eq. (7.3) involving integral and differential operations is transformed into a linear, iterative relation that provides an explicit evaluation of the current. A detailed calculation of the current distribution on the wire scatterer, using the Marching On in Time technique (MOT) is presented in the chapter 5 (section 5.2). At the actual time step $t_n = n\Delta t$ the unknown current $\mathbf{I}_{k,n}$ is calculated by using the retarded known currents. The eq. (5.54) written in a compact form as

$$\mathbf{I}_{k,n} = \frac{1}{\mathbf{K}_{kk}} \left[\Delta \mathbf{E}_{Bk,n}^r - \sum_{m=1, m\neq k}^{N} \mathbf{I}_{m,i} \mathbf{G}_{km,i} \right], \tag{7.4}$$

where $\mathbf{G}_{km,i}$ contains the coupling coefficient vectors of the current values at earlier time steps i. $i = n - R/\Delta s$. $\mathbf{K}_{k,k}$ is the self term integral ($m = k$). $\Delta \mathbf{E}_{Bk,n}^r$denotes

the time derivative of the radiated electric field from the TLM-interface and represents the excitation of the wire segment k at t_n.

Scattered field from the thin wire structure at TLM-interface

After computation of the current distribution on the wire body due to an incident field $\mathbf{E}_B^r$ coming from the complex object, we can now evaluate the quantity of interest, the scattered e.m. field $\mathbf{E}_{BScat}^r$ and $\mathbf{H}_{BScat}^r$ for the eqs. (7.1) (7.2). The scattered fields can be calculated using the electric and magnetic field integral equations, with the observation point located somewhere outside the scatterer surface or on the TLM-interface, in order to account the scattered fields in the TLM simulation. The scattered fields, both in in the near- and the far field region, can be computed with the following integral expressions for the electric field $\mathbf{E}_{BScat}^r(\mathbf{r},\, t)$ and magnetic field $\mathbf{H}_{BScat}^r(\mathbf{r},\, t)$, respectively, [4]:

$$\mathbf{E}_{BScat}^r(\mathbf{r},\, t) = \frac{1}{4\pi}\int_{l(\mathbf{r})} dl' \Bigg\{ -\frac{\mu_o}{R}\frac{\partial}{\partial\tau}\mathbf{I}(\mathbf{r}',\tau) + \frac{1}{\varepsilon_o}\frac{\partial}{\partial l}\left[\mathbf{I}(\mathbf{r}',\tau)\frac{\mathbf{R}}{c\,R^2} + \int_0^{t-R/c}\mathbf{I}(\mathbf{r}',\tau)d\tau\frac{\mathbf{R}}{R^3}\right]\Bigg\}_{\tau=t-R/c} \tag{7.5}$$

$$\mathbf{H}_{BScat}^r(\mathbf{r},t) = \frac{1}{4\pi}\int_{l(\mathbf{r})} dl' \left\{ \mathbf{I}(\mathbf{r}',\tau)\times\frac{\mathbf{R}}{R^3} + \frac{\partial}{\partial\tau}\mathbf{I}(\mathbf{r}',\tau)\times\frac{\mathbf{R}}{c\,R^2}\right\}_{\tau=t-R/c}, \tag{7.6}$$

where $l(\mathbf{r})$ denotes the integration path along the wire body. $\mathbf{I}(\mathbf{r}',\tau) = I(\mathbf{r}',\tau).\mathbf{e}_l'$ represents the line current vector in the wire axis. $\mathbf{e}_l'$ is the unit vector tangential to the wire axis in the source points $\mathbf{r}'$. $\tau = t - R/c$ is the retarded time. R/c denotes the retarded time feature between the observation points $\mathbf{r}$ outside the scatterer and the source points $\mathbf{r}'$ on the wire axis, with $R = |\mathbf{r} - \mathbf{r}'|$. c is the speed of light in free-space. From the current distribution along the wire axis we derive the radiated fields $\mathbf{E}_{BScat}^r$ and $\mathbf{H}_{BScat}^r$ at the TLM-subregion interface, as indicated in Fig.7.18.

We give numbers u to all boundary surface elements on the TLM-subregion, as indicated in Fig. 7.18. The radiated electromagnetic field on the center of these surface elements coming from the current distribution along the wire segments is obtained by summing the effect of each individual current element on the wire. After expanding the current by basis functions (5.35) at given time in a given subdomain we can

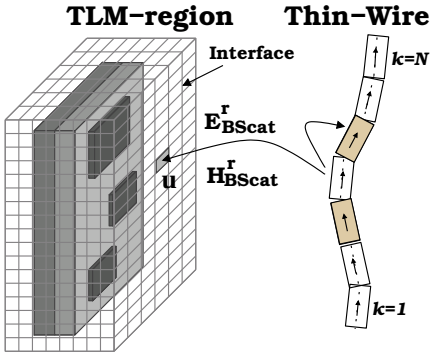

Figure 7.18: Scattered field from the thin wire towards the TLM interface.

approximate the eqs. (7.5) (7.6) by,

$$\mathbf{E}^r_{BScat}(\mathbf{r}_u, t_n) = \frac{1}{4\pi}\sum_{k=1}^{N}\int_{l_k-\frac{\Delta s}{2}}^{l_k+\frac{\Delta l}{2}} -\frac{\mu}{R}\frac{\partial}{\partial t} I(\mathbf{r}', \tau)\mathbf{e}'_l\, dl' + \frac{1}{4\pi\varepsilon}\sum_{k=1}^{N}\int_{l_k-\frac{\Delta l}{2}}^{l_k+\frac{\Delta l}{2}} \frac{\partial}{\partial l} I(\mathbf{r}', \tau)\mathbf{e}'_l\, \frac{\mathbf{R}}{c\,R^2} dl' + \frac{1}{4\pi\varepsilon}\sum_{k=1}^{N}\int_{l_k-\frac{\Delta l}{2}}^{l_k+\frac{\Delta l}{2}} \frac{\partial}{\partial l}\Big[\int_0^{t_n-R/c} I(\mathbf{r}', \tau)\mathbf{e}'_l\, d\tau\Big]\frac{\mathbf{R}}{R^3} dl', \tag{7.7}$$

$$\mathbf{H}^r_{BScat}(\mathbf{r}_u, t_n) = \frac{1}{4\pi}\sum_{k=1}^{N}\int_{l_k-\frac{\Delta l}{2}}^{l_k+\frac{\Delta l}{2}} I(\mathbf{r}', \tau)\mathbf{e}'_l \times \frac{\mathbf{R}}{R^3} dl' + \frac{1}{4\pi}\sum_{k=1}^{N}\int_{l_k-\frac{\Delta l}{2}}^{l_k+\frac{\Delta l}{2}} \frac{\partial}{\partial t} I(\mathbf{r}', \tau)\mathbf{e}'_l \times \frac{\mathbf{R}}{cR^2} dl', \tag{7.8}$$

where l_k is the location of the wire segments k, with $k = (1, ..., N)$. R is the distance between the destination $\mathbf{r}_u$ on the boundary surface element u of the TLM-subregion and source position vectors $\mathbf{r}'$ on the wire segments, $\tau = t - R/c$ is a properly delayed time. By approximating the current to be constant at given time in a given subdomain we obtain the scattered e. m. field at every patch u at the TLM-interface. The eqs.

(7.5) (7.6) can be written in a simplified compact form as

$$\mathbf{E}^r_{BScat}(u,n) = \sum_{k=1}^{N}\sum_{i=0}^{n} \Phi_{u,k,i}\mathbf{I}_{k,i}, \tag{7.9}$$
$$\mathbf{H}^r_{BScat}(u,n) = \sum_{k=1}^{N}\sum_{i=0}^{n} \Psi_{u,k,i}\mathbf{I}_{k,i},$$

where Φ and Ψ denote the matrices of the coupling coefficients of the current values at earlier time steps i. The time integral can be discretized using the TLM time step. The indices n and i are the time indices at the destination and at the source points, respectively. The field values $\mathbf{E}^r_{BScat}(u,n)$ and $\mathbf{H}^r_{BScat}(u.n)$ are defined in the center of the patches u at the TLM interface.

7.3.2 Thin conducting surface scatterer

We consider in the second problem the transient interference between a complex structure exhibiting materials with non-linear properties and an arbitrarily shaped conducting surface, as shown in Fig. 7.15(b). In this thesis, the thin surface scatterer is approximated by planar triangular patches. The triangularization have the ability to conform to any geometrical surface or boundary, permit easy description of the patching scheme to the computer and may be used with greater densities on those portions of the surface where more resolution is desired. The most widely used surface discretization method is based on *Rao-Wilton-Glisson* (RWG) elements, which are simple, flat, and have triangular facets.

Current distribution on the surface scatterer

A Time-Domain version of the EFIE for the scattering problem of interest is solved through a MOM approach. Let S be the exterior surface of a perfectly conducting body, which can be either closed or open, illuminated by the radiated field $\mathbf{E}^r_B$ coming from the TLM-subregion, as shown in Fig. 7.19. $\mathbf{J}$ is the surface current density induced on S.

Since the body is a perfect electric conductor, the tangential component of the total electric field on S must vanish. This leads to an integro-differential vector equation in the unknown induced current density $\mathbf{J}(\mathbf{r}',t)$ [4]. The forcing term of this equation is given by the tangential component of the incident electric field $[\mathbf{E}^r_B]_{tan}$,

$$[\mathbf{E}^r_B(\mathbf{r},t)]_{tan} = \frac{\partial}{\partial t}\left[\frac{\mu}{4\pi}\int_S \frac{\mathbf{J}(\mathbf{r}'\,t - R/c)}{R}\,dS'\right]$$
$$-\nabla\left[\frac{1}{4\pi\epsilon}\int_S \frac{1}{R}\,[\int_0^{t-R/c} \nabla'\cdot\mathbf{J}(\mathbf{r}',\tau)\,d\tau]\,dS'\right], \tag{7.10}$$

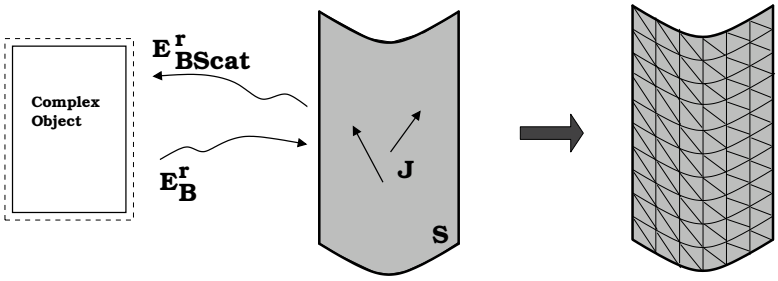

Figure 7.19: Discretization of the curved surface through triangular patches for the application to the hybrid TLM-TDMOM algorithm.

where $R = |\mathbf{r} - \mathbf{r}'|$ represents the distance between an arbitrarily located observation point $\mathbf{r}$ and a source point $\mathbf{r}'$, both on S; $t - R/c$ is the retarded time, μ and ϵ are the permeability and permittivity of the medium surrounding the scatterer, respectively.

As mentioned in the chapter 5 (section 5.3), the scattering problem is solved through discretization of the EFIE and its direct time-domain solution by means of a marching-on-in-time procedure. A suitable expansion of the unknown current $\mathbf{J}(\mathbf{r}, t)$ is employed, as given by eqs. (5.57) and (5.58) in chapter 5. In particular, the spatial variation of surface currents induced on the body can be accurately approximated by discretizing its surface into N_T triangular patches over which a set of basis functions can be defined. An iterative vector equation is obtained, allowing all the samples of the unknown surface current distribution to be derived at each time step by simple algebraic expressions, involving the discrete values of the same current distribution at previous time intervals, as shown in chapter 5 (subsection 5.3.1),

$$\mathbf{I}_m(t_{n+1}) = \frac{4\pi\Delta t}{\mu_o \mathbf{e}_{mm}} \mathbf{E}^r_B(\mathbf{r}_m,\, t_n) - \frac{4\pi}{\mu_o \mathbf{e}_{mm}} \left[(\breve{\mathbf{A}}(\mathbf{r}_m,\, t_{n+1}) - \breve{\mathbf{A}}(\mathbf{r}_m,\, t_n)) \right] + \frac{8\pi\Delta t}{\mu_o \mathbf{e}_{mm} (\rho^+_m + \rho^-_m)} [\phi(\mathbf{r}^{c+}_m, t_n) - \phi(\mathbf{r}^{c-}_m, t_n)]. \tag{7.11}$$

Equation (7.11) is a recursion formula relating unknown present time currents $\mathbf{I}_m(t_{n+1})$ in terms of retarded known currents.

Scattered-Field Calculation

Once the transient current density on the induced scatterer has been determined, we can easily compute the scattered field $\mathbf{E}^r_{BScat}$ and $\mathbf{H}^r_{BScat}$ at the boundary of the TLM-subregion by summing the effect of each individual current element on the surface of the thin conducting structure, as indicated in Fig. 7.20. We give numbers u

to all boundary surface patches on the TLM-subregion with the position vector $\mathbf{r}_u$ on the center. The radiated electromagnetic field on the center of these patches coming from the surface current distribution along the curved structure is obtained, as in [4], by

$$\mathbf{E}^r_{BScat}(\mathbf{r}_u,\, t) = \frac{1}{4\pi}\int_S \Big\{ -\frac{\mu_o}{R}\frac{\partial}{\partial\tau}\mathbf{J}(\mathbf{r}',\tau) + \frac{1}{\varepsilon_o}\frac{\partial}{\partial S}\big[\mathbf{J}(\mathbf{r}',\tau)\frac{\mathbf{R}}{c\,R^2} + \int_0^{t-R/c}\mathbf{J}(\mathbf{r}',\tau)d\tau\frac{\mathbf{R}}{R^3}\big]\Big\} dS', \tag{7.12}$$

$$\mathbf{H}^r_{BScat}(\mathbf{r}_u, t) = \frac{1}{4\pi}\int_S \left\{ \mathbf{J}(\mathbf{r}',\tau)\times\frac{\mathbf{R}}{R^3} + \frac{\partial}{\partial\tau}\mathbf{J}(\mathbf{r}',\tau)\times\frac{\mathbf{R}}{c\,R^2}\right\} dS', \tag{7.13}$$

where

$$R = |\mathbf{R}| = |\mathbf{r}_u - \mathbf{r}'| \text{ and } \tau = t - R/c\ , \tag{7.14}$$

R is the distance between the destination $\mathbf{r}_u$ on the boundary surface element u of the TLM-subregion and source position vectors $\mathbf{r}'$ on the surface of the conducting thin structure, τ is a properly delayed time.

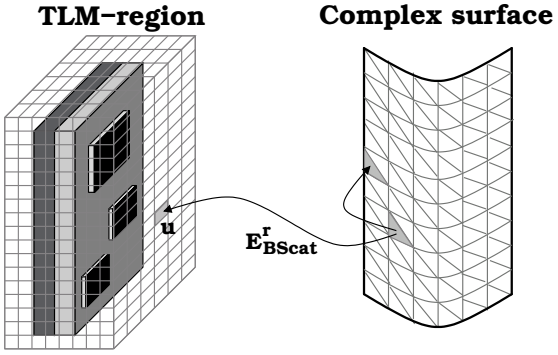

Figure 7.20: Scattered field from the curved conducting surface towards TLM-interface.

After approximating the current distribution by the triangular current expansion on S, as given by eqs. (5.57) and (5.58) in chapter 5, we obtain the following approximation of the scattered electromagnetic field at every patch u of the TLM interface,

$$\mathbf{E}^r_{BScat}(\mathbf{r}_u, t_n) = \frac{1}{4\pi}\sum_{k=1}^{N_e}\int_{T_k^+ + T_k^-} -\frac{\mu}{R}\frac{\partial}{\partial t}\mathbf{I}(\mathbf{r}', \tau)dS' + \frac{1}{4\pi\varepsilon}\sum_{k=1}^{N_e}\int_{T_k^+ + T_k^-}\frac{\partial}{\partial l}\mathbf{I}(\mathbf{r}', \tau)\frac{\mathbf{R}}{c\,R^2}dS' + \frac{1}{4\pi\varepsilon}\sum_{k=1}^{N_e}\int_{T_k^+ + T_k^-}\frac{\partial}{\partial l}[\int_0^{t_n - R/c}\mathbf{I}(\mathbf{r}', \tau)d\tau]\frac{\mathbf{R}}{R^3}dS', \tag{7.15}$$

$$\mathbf{H}^r_{BScat}(\mathbf{r}_u, t_n) = \frac{1}{4\pi}\sum_{k=1}^{N_e}\int_{T_k^+ + T_k^-}\mathbf{I}(\mathbf{r}', \tau)\times\frac{\mathbf{R}}{R^3}dS' + \frac{1}{4\pi}\sum_{k=1}^{N_e}\int_{T_k^+ + T_k^-}\frac{\partial}{\partial t}\mathbf{I}(\mathbf{r}', \tau)\times\frac{\mathbf{R}}{cR^2}dS', \tag{7.16}$$

where N_e represents all the edges, discounting the boundary edges in the triangulated model of the conducting surface. T_k^+ and T_k^- represent the triangles associated with the edge k, as shown in Fig. 5.7 (chapter 5). R is the distance between the destination $\mathbf{r}_u$ on the boundary surface element u of the TLM-subregion and source position vectors $\mathbf{r}'$ on the triangular patch elements on the surface scatterer, $\tau = t - R/c$ is a properly delayed time. By expanding the current at given time in a given subdomain as shown in Chapter 3, we obtain the radiated e. m. field coming from the surface scatterer at every boundary element u on the TLM interface. For simplification, the eqs. (7.15) (7.16) can be written in a compact form as,

$$\mathbf{E}^r_{BScat}(u, n) = \sum_{k=1}^{N_e}\sum_{i=0}^{n}\Theta_{u,k,i}\mathbf{I}_{k,i} \tag{7.17}$$

$$\mathbf{H}^r_{BScat}(u, n) = \sum_{k=1}^{N_e}\sum_{i=0}^{n}\Upsilon_{u,k,i}\mathbf{I}_{k,i}, \tag{7.18}$$

where the matrices Θ and Υ contain the coupling coefficients of the current values. The indices n and i are the time indices at the destination patch u and at the source points on the center of the kth edge, respectively. The field values $\mathbf{E}^r_{BScat}(u,\, n)$ and $\mathbf{H}^r_{BScat}(u,\, n)$ are defined in the center of the patches u at the TLM interface.

We have now calculated the contributions for the scattered e.m field $\mathbf{E}^r_{BScat}$ and $\mathbf{H}^r_{BScat}$ in the EFIE (7.1) and MFIE (7.2) for the first case of a thin wire and for the second case of conducting surface. In the next section we deal with how to calculate the radiated fields $\mathbf{E}^r_B$ and $\mathbf{H}^r_B$ from the TLM-subregion, which represent at the same

time the excitation of the scatterer. We have also to evaluate the self interaction fields $\mathbf{E}^r_{Bself}$ and $\mathbf{H}^r_{Bself}$ at the TLM-interface for the total tangential e.m field in the eqs. (7.1) and (7.2).

7.4 Radiated field from the TLM-subregion

The radiation from the complex object towards a destination point outside its discretized TLM-subregion is expressed replacing the sources inside the object by equivalent current sources at the TLM-interface. At any destination point on (and outside) the TLM-subregion, the field can be derived from the past history of the total tangential field on the interface using the dyadic free space Green's function in time domain, as in [4], by

$$\begin{aligned}\mathbf{E}^r_B(\mathbf{r},\mathrm{t}) = \frac{T}{4\pi}\iint_S dS'\Big\{ &\frac{-\mu}{R}\frac{\partial}{\partial t}\big(\mathbf{n}(\mathbf{r}')\times\mathbf{H}_{Btot}(\mathbf{r}',\tau)\big)\\ &+\frac{1}{R^3}\left[1+(t-\tau)\frac{\partial}{\partial t}\right]\Big[(\mathbf{n}(\mathbf{r}')\times\mathbf{E}_{Btot}(\mathbf{r}',\tau))\times\mathbf{R}\\ &+\big(\mathbf{n}(\mathbf{r}')\cdot\mathbf{E}_{Btot}(\mathbf{r}',\tau)\big)\cdot\mathbf{R}\Big]\Big\}_{\tau=t-R/c}\end{aligned} \tag{7.19}$$

$$\begin{aligned}\mathbf{H}^r_B(\mathbf{r},\mathrm{t}) = \frac{T}{4\pi}\iint_S dS'\Big\{ &\frac{\varepsilon}{R}\frac{\partial}{\partial t}\big(\mathbf{n}(\mathbf{r}')\times\mathbf{E}_{Btot}(\mathbf{r}',\tau)\big)\\ &+\frac{1}{R^3}\left[1+(t-\tau)\frac{\partial}{\partial t}\right]\Big[(\mathbf{n}(\mathbf{r}')\times\mathbf{H}_{Btot}(\mathbf{r}',\tau))\times\mathbf{R}\\ &+\big(\mathbf{n}(\mathbf{r}')\cdot\mathbf{H}_{Btot}(\mathbf{r}',\tau)\big)\cdot\mathbf{R}\Big]\Big\}_{\tau=t-R/c},\end{aligned} \tag{7.20}$$

where $\mathbf{E}_{Btot}$ and $\mathbf{H}_{Btot}$ represent the total tangential fields at the interface. $\mathbf{n}(\mathbf{r}')\times\mathbf{E}_{Btot}$, $\mathbf{n}(\mathbf{r}')\times\mathbf{H}_{Btot}$, $\mathbf{n}(\mathbf{r}')\cdot\mathbf{E}_{Btot}$, and $\mathbf{n}(\mathbf{r}')\cdot\mathbf{H}_{Btot}$ represent the equivalent currents and charges on the external surface of the TLM-subregion, respectively . The vectors $\mathbf{r}$ and $\mathbf{r}'$ are the destination and source positions vectors, respectively. The vectors $\mathbf{r}'$ are the source point vectors, lying on the TLM-interface. R is the corresponding distance vector ($\mathbf{R}=\mathbf{r}-\mathbf{r}'$; $R=|\mathbf{r}-\mathbf{r}'|$). The unit vector $\mathbf{n}$ is normal to the boundary of the TLM-subregion and pointing out of the interface. The coefficient T is defined so that the above equations can be applied to all the space: $T=2$, for interaction between patches belonging to the same interface $\mathbf{E}^r_{Bself}(\mathbf{r},\mathrm{t})=\mathbf{E}^r_B(\mathbf{r},\mathrm{t})\mid_{T=2}$, $T=1$ can be used to calculate the radiated field from the TLM-interface at every destination point in free-space as well as on every element on the discretized scatterer (wire or surface), as indicated in Fig. 7.21 for both cases of the scatterer. This field represents the incident

field on the conducting surface, which is the forcing term used to calculate the current distribution on the scatterer, by applying eq. (7.4) for thin wire or eq. (7.11) for thin conducting surface.

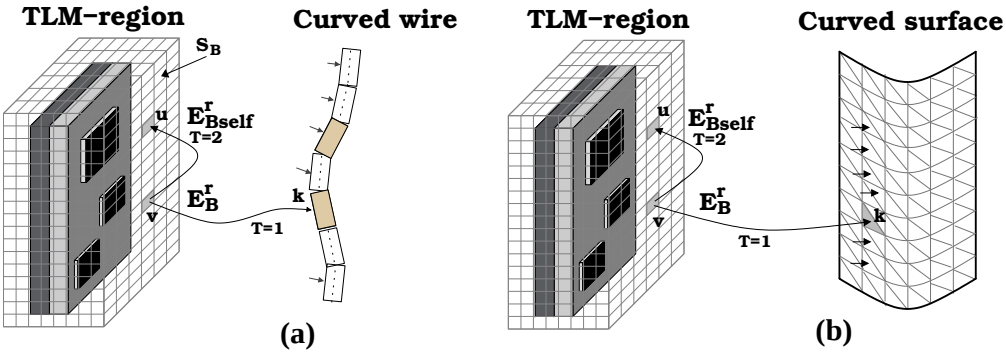

Figure 7.21: Radiation from the complex TLM-region towards a scatterer; (a) thin wire scatterer, (b) thin conducting surface scatterer.

According to the sampling theorem a smooth field distribution of the e.m. field $\mathbf{E}_{Btot}$ and $\mathbf{H}_{Btot}$ is obligatory at the TLM-interface in order to avoid discretization errors. Since at the complex object, modeled by TLM, there may occur field singularities, therefore the TLM-interface have to be kept in distance to the object [12].

The electromagnetic integral equations (7.19) and (7.20) are then discretized by expanding the total tangential-field components with appropriate sets of basis functions, both in time and in space; the subdomains of such functions are defined by the TLM grid, and can be chosen rectangular, triangular or as parabola segments. In this thesis we choose basis functions of rectangular type,

$$\mathbf{E}_{Btot}(\mathbf{r},t) = \sum_{v=1}^{V}\sum_{i=0}^{N} \mathbf{E}_{\varphi}(\mathbf{r}_v\ ,t_i)P(\mathbf{r}-\mathbf{r}_v)\,Q(t-t_i). \tag{7.21}$$

$$\mathbf{H}_{Btot}(\mathbf{r},t) = \sum_{v=1}^{V}\sum_{i=0}^{N} \mathbf{H}_{\varphi}(\mathbf{r}_v\ ,t_i)P(\mathbf{r}-\mathbf{r}_v)\,Q(t-t_i), \tag{7.22}$$

where the function P denotes a surface pulse function of rectangular type, being equal to unity for $\mathbf{r}$ on the elementary surface patch v centered at $\mathbf{r}_v$ and zero on all the other patches. Q is a time pulse function of rectangular type, being equal to unity for t in the time interval centered at t_i and zero on all the other time steps. $\mathbf{E}_{\varphi}$ and $\mathbf{H}_{\varphi}$ represent the unknown expansion coefficients of the total tangential e.m. field. We consider V patches at the TLM-interface and N time steps for all the interacting objects.

By using the expansion functions (7.21) and (7.22) and approximating the time derivative by finite differences, we obtain the following approximation of the eqs. (7.19) and (7.20) for the radiated e.m. field at any destination point outside (or on) the discretized TLM-subregion,

$$\mathbf{E}^r_{Bk,j} = T \sum_{v=1}^{V} \left(-\frac{\mu_0}{R_{kv}\Delta t} \frac{\Delta a_v}{4\pi} \right) \left[\mathbf{n}_v \times (\mathbf{H}_{\varphi v,i} - \mathbf{H}_{\varphi v,i-1}) \right] + \left[(\mathbf{n}_v \times ((j-i+1)\mathbf{E}_{\varphi v,i} - (j-i)\mathbf{E}_{\varphi v,i-1}) \right] \times \left(\frac{\mathbf{R}_{kv}}{R^3_{kv}} \frac{\Delta a_v}{4\pi} \right) + \left[(\mathbf{n}_v \cdot ((j-i+1)\mathbf{E}_{\varphi v,i} - (j-i)\mathbf{E}_{\varphi v,i-1}) \right] \left(\frac{\mathbf{R}_{kv}}{R^3_{vk}} \frac{\Delta a_v}{4\pi} \right)], \tag{7.23}$$

$$\mathbf{H}^r_{Bk,j} = T \sum_{v=1}^{V} \left(\frac{\epsilon}{R_{kv}\Delta t} \frac{\Delta a_v}{4\pi} \right) \left[\mathbf{n}_v \times (\mathbf{E}_{\varphi v,i} - \mathbf{E}_{\varphi v,i-1}) \right] + \left[(\mathbf{n}_v \times ((j-i+1)\mathbf{H}_{\varphi v,i} - (j-i)\mathbf{H}_{\varphi v,i-1}) \right] \times \left(\frac{\mathbf{R}_{kv}}{R^3_{kv}} \frac{\Delta a_v}{4\pi} \right) + \left[(\mathbf{n}_v \cdot ((j-i+1)\mathbf{H}_{\varphi v,i} - (j-i)\mathbf{H}_{\varphi v,i-1}) \right] \left(\frac{\mathbf{R}_{kv}}{R^3_{vk}} \frac{\Delta a_v}{4\pi} \right)], \tag{7.24}$$

where the indices j and i are the time indices of the destination and the source points respectively. The unit vector $\mathbf{n}_v$ is normal to the boundary element v of the TLM-interface and pointing out of the surface. The vector $\mathbf{R}_{kv} = \mathbf{r}_k - \mathbf{r}_v$ and its value $R_{kv} = |\mathbf{R}_{kv}|$ the distance between the source points $\mathbf{r}_v$, lying on the TLM-interface, and the destination points $\mathbf{r}_k$ at every element k (segment k for wire or edge k for triangular surface patch) on the scatterer for $T = 1$. $T = 2$ can be used to calculate the electromagnetic self-interaction $\mathbf{E}^r_{Bself}$ and $\mathbf{H}^r_{bself}$ between the boundary elements belonging to the same TLM-interface, in this case $\mathbf{r}_k$ represents the destination points on the TLM-interface $\mathbf{r}_u$, $(\mathbf{r}_v\,,\, \mathbf{r}_u = \mathbf{r}_k) \in S_B$. The time retardation feature $(t - t')$ is calculated from the time step $\Delta t = \Delta l/hc$ according to the TLM algorithm for wave propagation in free-space, with the stability factor h, as

$$\frac{(t-t')}{\Delta t} = j - i = \frac{hR_{kv}}{\Delta l}, \tag{7.25}$$

Δl represents the side length of the surface element on the TLM-boundary. Δa_v denotes the area of the elementary surface patch centered at $\mathbf{r}_v$. The field values $\mathbf{E}_{\varphi v,i}$ and $\mathbf{H}_{\varphi v,i}$ represent the sampling of the total tangential fields at discrete sampling points at the boundary surface S_B on the cell v at earlier time step i. For large free space region between the TLM-subregion and the scatterer, the term $(j-i+1)$ can be

approximated to $(j-i)$. In this case the eqs. (7.23) (7.24) can be further simplified to,

$$\mathbf{E}^r_{Bk,j} = \sum_{v=1}^{V} \underbrace{\left(-\frac{\mu_0}{R_{kv}\Delta t}\frac{\Delta a_v}{4\pi}\right)}_{\mathbf{F1}} \big[\mathbf{n}_v \times (\mathbf{H}_{\varphi v,i} - \mathbf{H}_{\varphi v,i-1})\big] + \big[(\mathbf{n}_v \times (\mathbf{E}_{\varphi v,i} - \mathbf{E}_{\varphi v,i-1})\big] \times \underbrace{\left(\frac{\mathbf{R}_{kv}}{R^2_{kv}}\frac{\Delta a_v}{2\pi}\right)}_{\mathbf{F2}} + \big[(\mathbf{n}_v \cdot (\mathbf{E}_{\varphi v,i} - \mathbf{E}_{\varphi v,i-1})\big] \underbrace{\left(\frac{\mathbf{R}_{kv}}{R^2_{kv}}\frac{\Delta a_v}{2\pi}\right)}_{\mathbf{F2}})] \tag{7.26}$$

$$\mathbf{H}^r_{Bk,j} = \sum_{v=1}^{V} \underbrace{\left(\frac{\epsilon}{R_{kv}\Delta t}\frac{\Delta a_v}{4\pi}\right)}_{\mathbf{G1}} \big[\mathbf{n}_v \times (\mathbf{E}_{\varphi v,i} - \mathbf{E}_{\varphi v,i-1})\big] + \big[(\mathbf{n}_v \times (\mathbf{H}_{\varphi v,i} - \mathbf{H}_{\varphi v,i-1})\big] \times \underbrace{\left(\frac{\mathbf{R}_{kv}}{R^2_{kv}}\frac{\Delta a_v}{2\pi}\right)}_{\mathbf{F2}} + \big[(\mathbf{n}_v \cdot (\mathbf{H}_{\varphi v,i} - \mathbf{H}_{\varphi v,i-1})\big] \underbrace{\left(\frac{\mathbf{R}_{kv}}{R^2_{kv}}\frac{\Delta a_v}{2\pi}\right)}_{\mathbf{F2}})]. \tag{7.27}$$

The eqs. (7.26) and (7.27) show that the field, which is occurring at the destination points on the scatterer due to the radiation from the TLM interface, can be expressed by a series of the weighted field values of all the boundary cells at the TLM interface. In order to save computational time, the weighting factors **F1**, **F2** and **G1**, connecting the field values of the TLM-interface boundary cells to those of the destination points on the scatterer are developed and stored in advance. The electric field quantities $\mathbf{E}^r_{Bk,j}$ represent the excitation of the scatterer, which are needed to calculate the current distribution on the scatterer.

7.5 Total tangential field at TLM-interface

By inserting all the integral representation for the electric field (7.12, 7.19), the dual equations for the magnetic field (7.13, 7.20) into the general EFIE (7.1) and the MFIE (7.2) at the TLM-interface, respectively, we observe in the kernel of the operators on the right side of (7.1) and (7.2), the time variable t is retarded with respect to the

same variable in the left side. This allows us to solve the EFIE (7.1) and MFIE (7.2) for the total tangential field in an iterative way. Since the point ($\mathbf{r} = \mathbf{r}'$) is excluded in the evaluation of the integrals (7.19, 7.20), R/c is never zero (we consider principal-value integrals). Therefore the variable τ is always less than t or, in other words, we have always $(t - \tau) = R/c > 0$. This implies that the unknown total tangential electromagnetic field at the TLM-interface can be directly calculated from the known incident field, coming from the sources inside the TLM-subregion, and an integral that is also known from the past history of the same field. By inserting the expanded fields referring to (7.21, 7.22) in (7.1, 7.2) and following a direct time-domain method of moments approach, we derive an equation system whose solution permits us to recover iteratively the expanding coefficients of the total tangential electromagnetic field at the TLM interface:

$$\mathbf{E}_{\varphi u,j} =^{TLM} \mathbf{E}_B^{inc}(u,j) + \mathbf{E}_{BScat}^{r}(u,j) + \sum_{v=1}^{V} \sum_{i=0}^{j-1} \{\mathbf{G}_E(u,v\ ,j-i)\mathbf{E}_\varphi(v\,,i) + \mathbf{G}_H(u,v\ ,j-i)\mathbf{H}_\varphi(v\,,i)\}\,, \tag{7.28}$$

$$\mathbf{H}_{\varphi u,j} =^{TLM} \mathbf{H}_B^{inc}(u,j) + \mathbf{H}_{BScat}^{r}(u,j) + \sum_{v=1}^{V} \sum_{i=0}^{j-1} \{\mathbf{D}_E(u,v\ ,j-i)\mathbf{E}_\varphi(v\,,i) + \mathbf{D}_H(u,v\ ,j-i)\mathbf{H}_\varphi(v\,,i)\}\,, \tag{7.29}$$

where $\mathbf{G}_E$, $\mathbf{G}_H$, $\mathbf{D}_E$ and $\mathbf{D}_H$ represent operators involving integral and differential operations of the Green's function formulation of the radiated field in (7.19, 7.20) with $T = 2$ (self-interaction). The equations (7.28, 7.29) show that, for every cell number u, the expanding coefficients $\mathbf{E}_{\varphi u,j}$ and $\mathbf{H}_{\varphi u,j}$ at time $j = t_j/\Delta t$ can be directly computed from the incident field at the same time j plus the past history of the tangential field on all the surface elements of the interacting objects, including the self contribution, up to the time $(j-1)$. This process is called *marching-on-in-time* (MOT) technique. Once the total electromagnetic field quantities at the TLM-interface have been calculated the radiated field from the TLM interface towards the destination points on the scatterer can be calculated using the equations (7.23, 7.24) or for large free space regions the simplified equations (7.26, 7.27). For each time step, the correct value of the total tangential field at the interface provides *the exact radiating boundary* for the TLM algorithm at interface S_B. The hybrid TLM-TDMOM algorithm consists of a TLM program in which, for every time step, the total tangential field at TLM-interface is evaluated by means of a proper set of integral equations.

The electromagnetic fields coming from outside the TLM-subregion are obtained by superposition of the scattered field coming from the scatterer (wire or surface) and the radiated field from the neighbored patches belonging to the same interface, as shown in Fig. 7.22. These field values $\mathbf{E}_{Buj}^{r,out}$ and $\mathbf{H}_{Buj}^{r,out}$ at the port on the boundary surfaces of the TLM-subregion are mapped on the TLM wave amplitudes $\mathbf{a}_{uj}$, which are defined

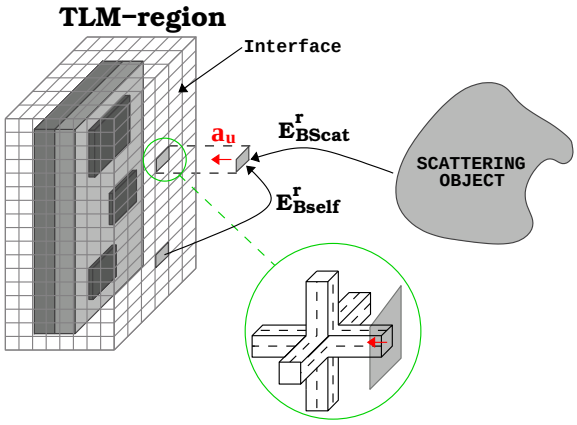

Figure 7.22: Injection of the self-coupling and scattered fields back to the TLM simulation.

at the transmission lines which are cut by the interface, and injected back to the TLM simulation:

$$\mathbf{a}_{u,j} = \frac{1}{2}(-\mathbf{n}_u \times \mathbf{n}_u \times \mathbf{E}^{r,out}_{Bu,j} + Z\,\mathbf{n}_u \times \mathbf{H}^{r,out}_{Bu,j}), \tag{7.30}$$

$$\textit{with} \quad \mathbf{E}^{r,out}_{Bu,j} = \mathbf{E}^{r}_{BScat}(u,j) + \mathbf{E}^{r}_{Bself}(u,j), \tag{7.31}$$

$$\textit{and} \quad \mathbf{H}^{r,out}_{Bu,j} = \mathbf{H}^{r}_{BScat}(u,j) + \mathbf{H}^{r}_{Bself}(u,j). \tag{7.32}$$

The bijective field-mapping formulation of the *cell boundary mapping* CBM in the SCN-TLM (chapter 4, section 4.6.2) make it possible to excite the boundary elements at TLM-interface, following the equation (4.81).

In conclusion, we develop the following essential steps in the implementation of the proposed new efficient hybrid TLM-TDMOM method for the accurate and efficient modeling of the electromagnetic transient interference between a complex structure, which may contain dielectric and lossy materials, and a scatterer, which may be an arbitrarily oriented thin wire or a perfectly conducting surface with arbitrary shape:

1. For every time step the incident field on the surface of the TLM-subregion is calculated by the TLM algorithm using the absorbing boundary conditions at the TLM-interface.

2. The known incident field values will be inserted in the integral equations (7.28 and 7.29).

3. For every destination cell u on the surface of the TLM-subregion and for every time step j the total field on the boundary of the TLM-subregion is calculated

by summing the effect of every neighbor source cell v on the same boundary surface using the past history of the same field of the TLM-subregion eqs. (7.23, 7.24) with $T = 2$, and the incident field (step2) using the TLM scheme. Since the singularity point $R_{uv} = 0$ is excluded in the evaluation of the integrals (7.23, 7.24), we consider principal-value integrals, we have always the condition $t > t - hR_{uv}/c$.

4. For every destination segment k on the surface of the scattering structure and for every TLM time step the radiated field, which represents the excitation of the scatterer, is calculated by summing the effect of every source cell v on the surface of the TLM-subregion by applying the eqs. (7.23, 7.24), with $T = 1$, or for large free space regions between the structures the simplified eqs. (7.26, 7.27). After that the iterative equation (7.4) for thin wire or (7.11) for surface, can be used to calculate the actual current values $\mathbf{I}(\mathbf{r}_k, t_n)$ of the scatterer in every time step using the marching on in time technique.

5. The radiated fields from the scatterer and the self-interaction fields are superposed, mapped to TLM wave pulses and injected back to TLM simulation using the bijective *cell boundary mapping* CBM-formulation of the SCN-TLM.

6. After the derivation of the total tangential field on the boundary of the TLM-subregion and the current distribution on the wire structure, the field in every point of the free-space region can be calculated by superposition of the radiated field from the TLM-subregion using the eqs. (7.23) and (7.24) with $T = 1$, and the radiated field from the scattering structure by applying eqs. (7.7, 7.8) for thin wire or eqs. (7.15, 7.16) for thin conducting surface.

8 Numerical Applications

8.1 Introduction

The previous chapter presented details about the different steps implementation of the hybrid TLM-TDMOM method. In this chapter, the new proposed efficient hybrid method is demonstrated by studying typical EMC problems restricting our investigation to the electromagnetic transient interference between a complex structure in interaction with a scatterer, which may be a thin wire structure or an arbitrarily shaped conducting surface. The application of the hybrid method (TLM-TDMOM) to significant cases is presented in the following sections, as well as a comparison between the hybrid method and the pure conventional TLM method showing the capability of this hybrid technique to accurately model complex configurations excited by transient electromagnetic fields.

8.2 Apertured metallic box and thin wire

Apertures and thin wire structure are widely used in many electromagnetic applications such as antennas, but due to their radiating characteristics, they are also source of interferences with respect to other equipments. In particular, the interferences exist in the case of a realistic equipment which consists of a metallic box with a rectangular aperture. The aperture is fed by an arbitrary distribution of electric and magnetic dipoles inside the box. For such equipments, it is very important to achieve an accurate computation of the EM field surrounding the metallic enclosure and, in particular, it is essential to compute the box resonances, aperture resonances and , most of all, the resonances due to the interaction between aperture and the extern objects such as a thin wire structure. These resonant frequencies are dominant in the far field interaction with other devices. In this section we apply the hybrid method (TLM-TDMOM) for studying the electromagnetic interaction between a metallic box with aperture and a thin wire in order to obtain an accurate prediction of the EM field between the interacting objects.

As example we consider a typical EMC-problem which is depicted in Fig. 8.23 consisting of a metallic enclosure with an aperture and a simple straight wire. We use the TLM-TDMOM method presented in this thesis for the investigation of the

problem. The dimensions of the metallic enclosure as specified in Fig. 8.23 are given in the following: $H = 12.5\,cm$, $A = 20\,cm$, $B = 20\,cm$. The thickness of the metallic walls is $5\,mm$. The dimensions of the aperture are $15 \times 1\,cm$. The radius and the total length of straight wire are $a = 2.5\,mm$ and $L = 20\,cm$, respectively. The wire is

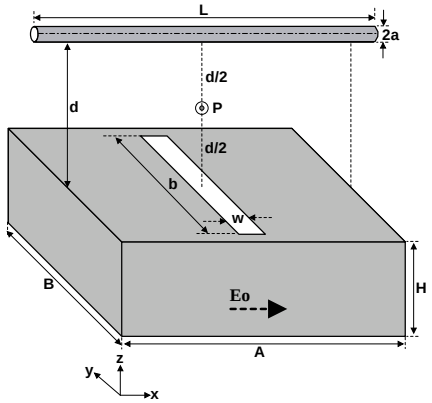

Figure 8.23: An apertured metallic enclosure interfering with a thin wire structure.

placed at a distance of $10\,cm$ from the aperture. The wire is assumed to be perfectly conducting and thin enough for the thin-wire approximation to be applied. The field in a metallic box with a rectangular aperture is excited by an electric field having a gaussian evolution in the time domain, with amplitude Eo. In the following we assume ideal conducting walls at the air filled box. We place the aperture in the plane $z = 12.5\,cm$. The electromagnetic field inside the box is described by means of the

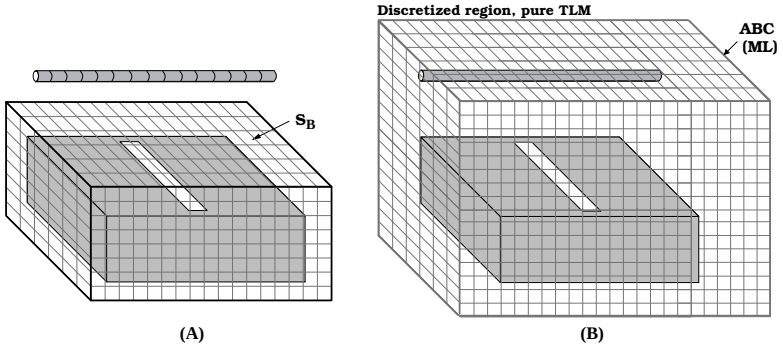

Figure 8.24: Concept of the discretization used in the hybrid TLM-TDMOM algorithm (A) and in the pure TLM method (B).

TLM method, the field in the external region is described by means of the free-space Green's functions in the time domain. The thin wire is described by means of the time domain integral equation and solved by the marching on in time technique (MOT). An incident field coming from the source region inside the box impinges on the separating top surface with aperture, producing an equivalent distribution of sources; this in turns produces a back-scattered field inside the box and a radiating field to the free-space region, which in turns excite the thin wire structure and induces a transient current distribution, which produces a backscattered field to the metallic box.

We investigate the backscattering and the resonances of the metallic enclosure which is interfered by the thin wire at a point P in distance of $d/2 = 5\,cm$ from the aperture. The main part of the electromagnetic interaction between the box and the wire occurs via the upper-plane boundary surface of the TLM-subregion and the surface of the wire. For a fast field computation with the TLM-TDMOM method, we consider only these two surfaces as radiating boundaries. For a self-consistent comparison we apply the novel hybrid TLM-TDMOM and the pure TLM method to this problem.

For applying the conventional TLM method, we enlarge the spatial domain around the configuration and we apply the absorbing boundary condition, as shown in Fig. 8.24(B). We have to embed the interacting objects and most of the near field region of the configuration in the discretized TLM region. The distance between the objects and the boundaries of the discretized TLM region is $20\,cm$.

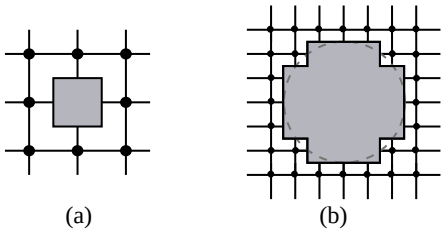

Figure 8.25: Various methods of describing wire cross-section in the TLM mesh; (a) one node description, (b) finer description.

The thin wire description in the TLM algorithm is determined to a large extent by the size of its diameter, relative to the size of the nodes. In this example, the wire diameter is equal to the node size, one node is used with appropriate short circuits to describe the wire cross-section. Fig. 8.25 shows various methods of describing wires in the TLM mesh, where one node or more finer discretization with a staircase approximation can be used. The dimension of the TLM cell is $\Delta l = 5mm$. By applying the hybrid TLM-TDMOM to this configuration, the metallic enclosure is embedded into an imaginary TLM box with the boundary surface S_B as shown in Fig. 8.24(A), we discretize the space inside the box and 3 additional layers in the aperture side of the enclosure to avoid the field singularities [12], as shown in Fig. 8.26. The

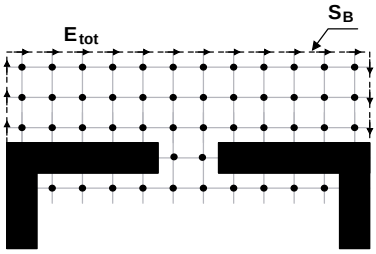

Figure 8.26: The imaginary boundary S_B in the aperture area; 3 additional layers in the aperture side of the enclosure.

wire structure is broken down into $N = 40$ linear straight segments and is modeled using Time Domain Method of Moments (TDMOM). We evaluate the electric field E_x (normalized respect to E_o) at a point P.

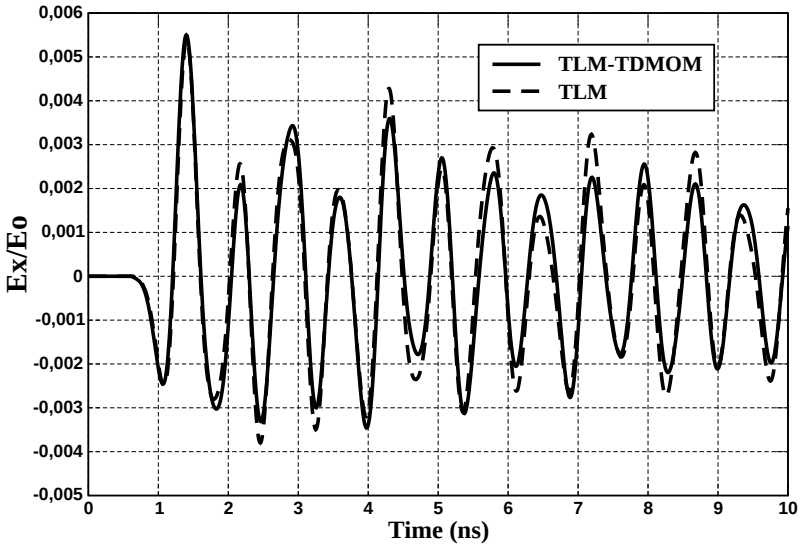

Figure 8.27: Time evolution of the E_x-field calculated by the TLM and the hybrid TLM-TDMOM methods at point P.

The field evaluated using the hybrid method is closer to the field calculated by TLM, as shown in Fig. 8.27. The same comparison is performed in frequency domain, after FFT (Fig. 8.28). A good agreement over the large band is remarkable. The deviations in amplitude are caused by the different boundary conditions, which are used in the

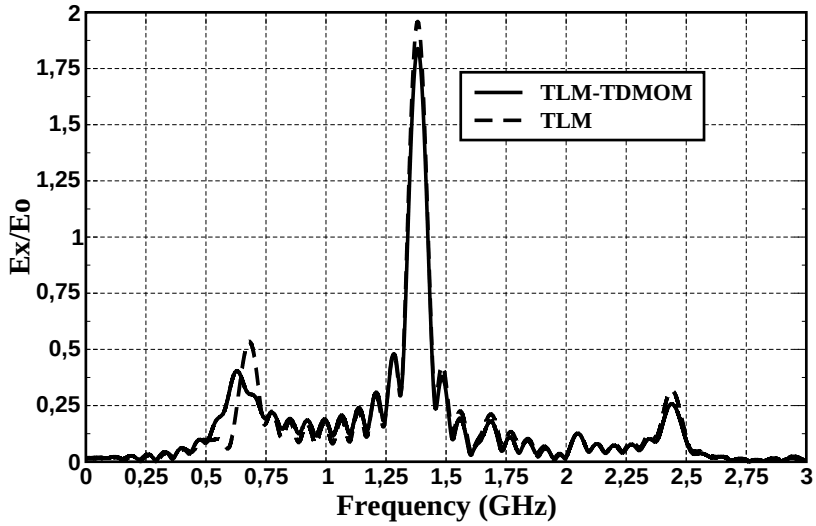

Figure 8.28: Spectrum of the E_x-field at the point P evaluated by the TLM-TDMOM vs pure TLM after FFT.

different methods.

The time domain waveform for the x-directed current I_x at the wire center is given by Fig. 8.29. In order to compute the current distribution using the TLM algorithm, the Ampere's Law is used to perform the current linked to a closed path surrounding the wire. The distribution of the line current I_x on the whole wire body is performed at different time steps in Fig 8.30. The current is assumed to be zero at the ends of the wire.

Fig. 8.31 shows the time domain waveform of the scattered field from the wire structure in comparison with the radiated field from the metallic enclosure at destination P. The superposition of the scattered and the radiated field provides the total field at destination P performed in Fig. 8.27.

The resonant frequencies which were calculated by the TLM-TDMOM method were compared with results of the pure TLM-method for an area of high extension. The results show very good agreement, thus confirming the validity of the proposed hybrid TLM-TDMOM method.

8.3 Mictrostrip patch antenna and thin wire

Real radiating systems do not work under free space conditions. The presence of obstacles, the environment of the mechanical structure of an antenna can modify

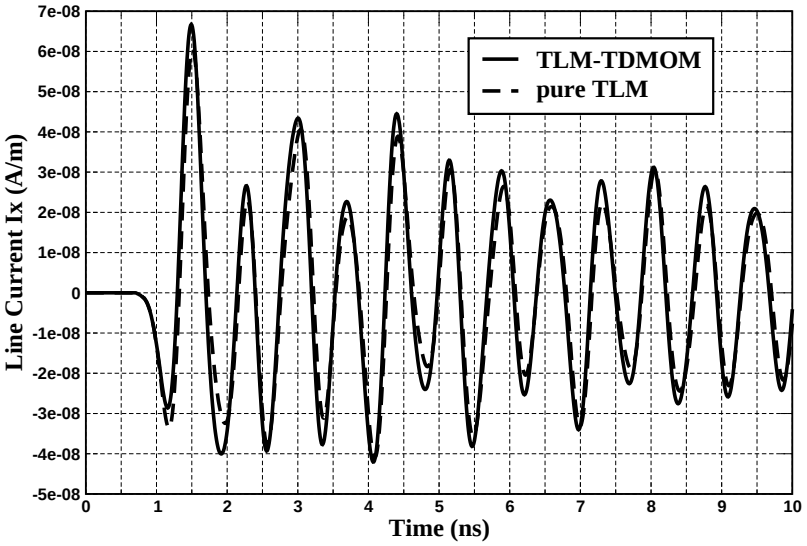

Figure 8.29: Current induced at the wire center.

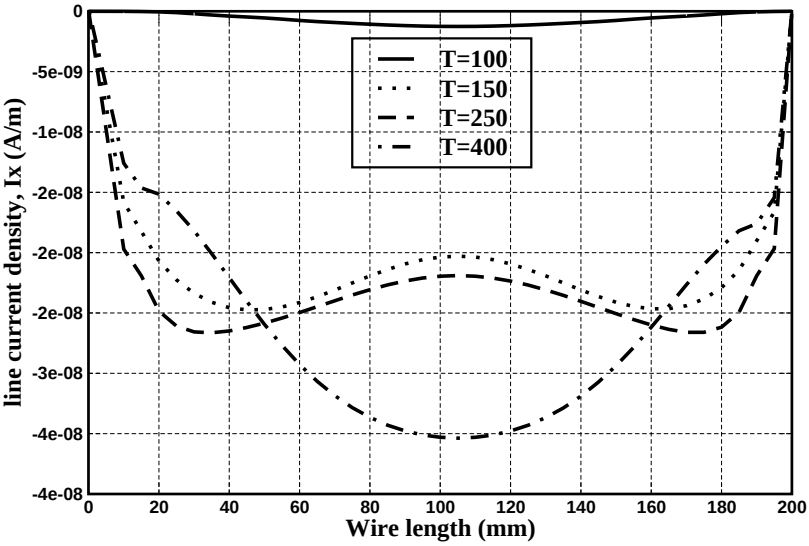

Figure 8.30: Axial component line current magnitude I_x along the wire axis at different time steps ($t = T\Delta t$) with $\Delta t = 8.33\,ps$.

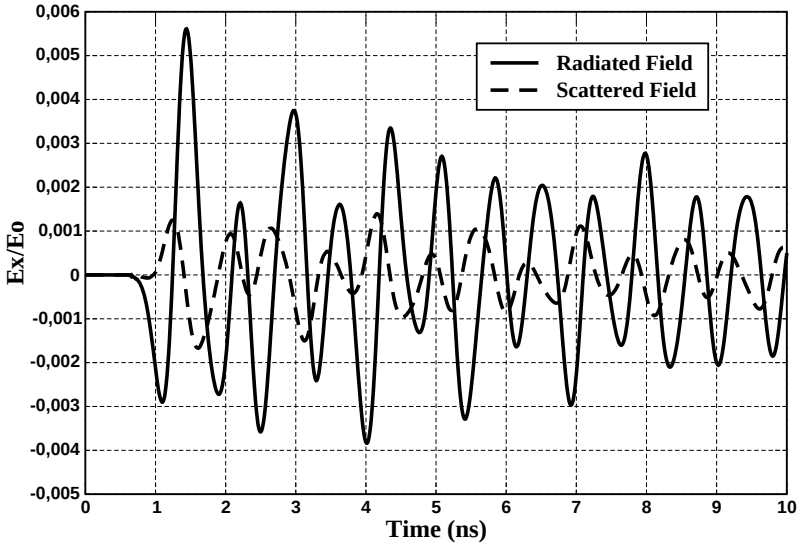

Figure 8.31: Comparison of the time evolution of the radiated and the scattered part of the total E_x-field component at the point P evaluated by the hybrid TLM-TDMOM method.

its properties so that the results of an ideal analysis process cannot be considered perfectly valid. The direct way to consider this effect is introducing in the model of the radiating system the distorting elements in order to be compensated. The proposed hybrid method pretends modeling the scattering over the obstacle and its influence over the global radiation characteristics of an antenna.

As example we consider a configuration containing a microstrip-fed rectangular patch antenna printed on a dielectric layer in interaction with a thin wire structure as drawn in Fig. 8.32. The configuration will be investigated using the hybrid TLM-TDMOM algorithm. The radiating structure is modeled using the TLM method, whereas the thin wire obstacle is modeled using the time-domain method of moments, which is able to model, by one hand, the relation between the incident field coming from the patch antenna and the current distribution over the wire; and, by the other hand, the relation between the current distribution and the scattered field that it generates. In order to validate the simulation we apply the full-wave pure TLM method for the analysis of the electromagnetic interaction between the objects.

The microstrip patch antenna parameters are: $s = 3\,mm$, $h = 5\,mm$, $t = 1\,mm$, $a = 20\,mm$, $b = 22\,mm$, $\epsilon_r = 2.1$, as depicted in Fig. 8.32. The metalization plane is placed at $z = 0$. The boundary of the discretized TLM-subregion is the surface S_B. In this case the surface S_B surrounding the radiating patch-antenna structure has

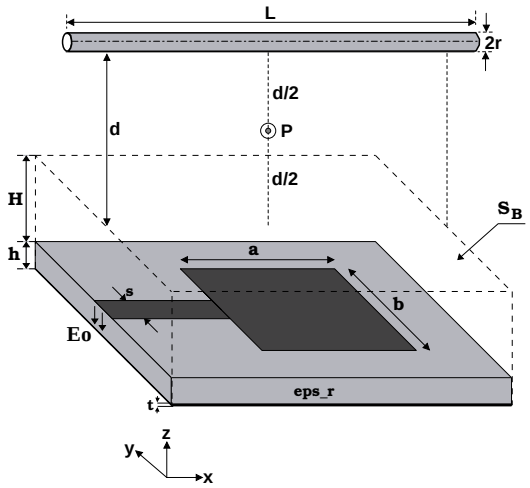

Figure 8.32: A rectangular microstrip patch antenna printed on a substrate interfering with a thin wire structure.

the form of a rectangular box, as shown in Fig. 8.32, where the boundary surface is depicted with dashed lines. The upper plane of the surface S_B is placed at a distance of $7\,mm$ from the plane $z = 0$. The dimension of the TLM cell is $\Delta l = 1\,mm$. The radius and the total length of the simple straight wire are $r = 1\,mm$ and $L = 40\,mm$, respectively. The wire is placed at a distance of $d = 20\,mm$ from the upper plane of the surface S_B. The wire is assumed to be perfectly conducting and thin enough for the thin-wire approximation to be applied. The microstrip structure is excited by an electric pulse propagating in the z-direction. The excitation, with amplitude E_o has a gaussian time dependence, and is placed at the boundary between the ground plane and the feeding microstrip, as shown in Fig. 8.32.

We investigate the perturbation of the radiating patch antenna through the thin wire obstacle at a point P in distance of $15\,mm$ from the patch antenna, as indicated in Fig. 8.32. The main part of the electromagnetic interaction between the patch and the wire occurs via the upper-plane boundary surface of the TLM-subregion and the surface of the wire. For a self-consistent comparison we apply the novel efficient hybrid method, presented in the previous chapter, and the pure TLM method to this problem. For applying the conventional TLM method, we enlarge the spatial domain and we apply the absorbing boundary conditions. These ABCs are realized through matched layer absorber (ML), discussed in chapter 4 (section 4.7.3). The wire structure is broken down into 40 linear straight segments and is modeled using MOM. The wire structure is modeled as a net of straight segments.

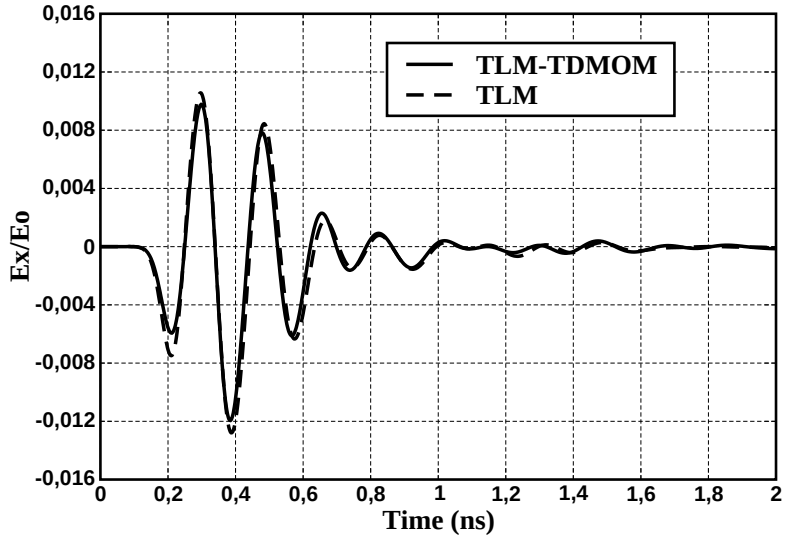

Figure 8.33: Time evolution of the E_x-field calculated by the TLM and the hybrid TLM-TDMOM methods at the point P.

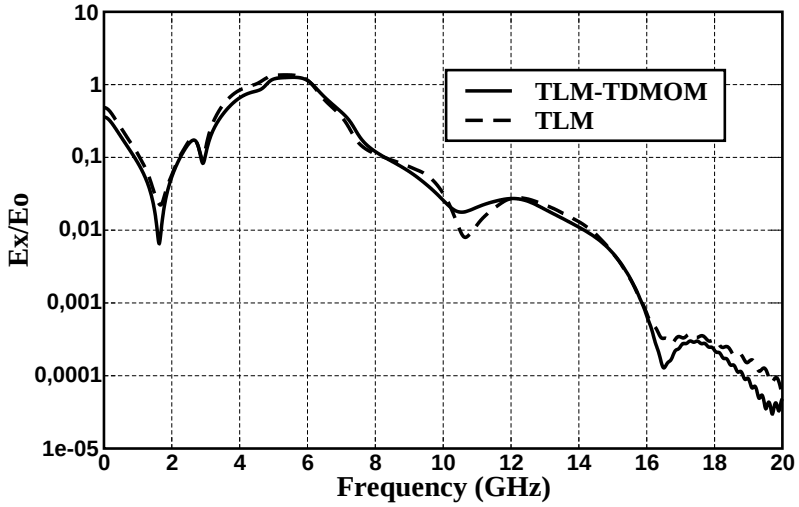

Figure 8.34: Spectrum of the E_x-field at the point P evaluated by the TLM-TDMOM vs pure TLM after FFT.

We evaluate the electric field E_x component (normalized with respect to E_o), at a point $P(z = 20\,mm)$. The field evaluated using the hybrid method is closer to the field computed by TLM, as shown in Fig. 8.33. The same comparison is performed in frequency domain, after FFT (Fig. 8.34), a good agreement is shown. The deviations in amplitude are caused by the different boundary conditions, which are used in the different methods. However the peak amplitude difference is quite acceptable in an EMC context.

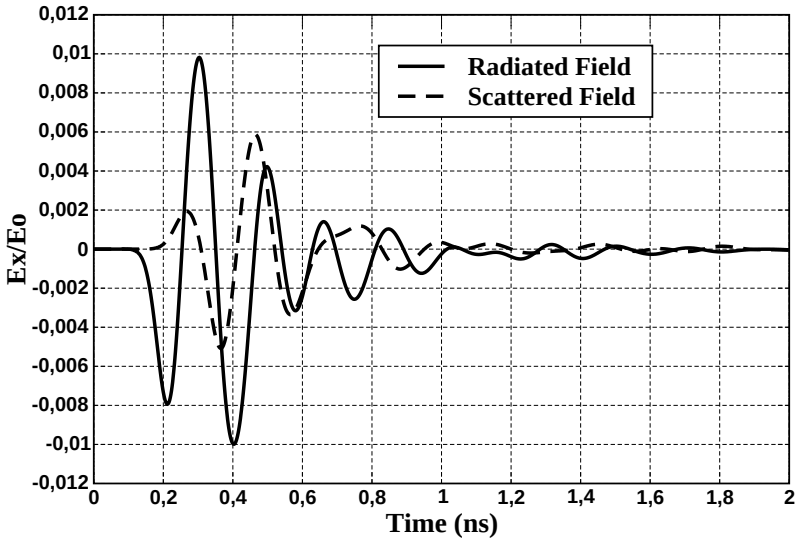

Figure 8.35: Radiated and scattered field parts of the total E_x-field at point P evaluated by the hybrid TLM-TDMOM method.

Fig. 8.35 shows the radiated field from the patch antenna in comparison with the perturbation, represented through the scattered field from the wire obstacle. The superposition of these field quantities deliver the total field at the point P performed in Fig. 8.33. For thin wire, we expect that the longitudinal component of the current in the direction of the wire dominates the transversal component. The x-component of the current induced at the wire center is plotted versus time in Fig. 8.36. Note that the currents at the end segments are always set to be zero. At the early stage of the response, the induced current is relatively large because of the gaussian pulsed electric field. The induced current follows mostly the temporal characteristic of the incident field.

The obstacle now is a thin wire structure with two 90° bent segments (2L-shaped wire), with $L1 = 20\,mm$, as shown in Fig. 8.37. Two special issues has to be handled before to incorporate this type of scatterer in the analysis of the configuration using the

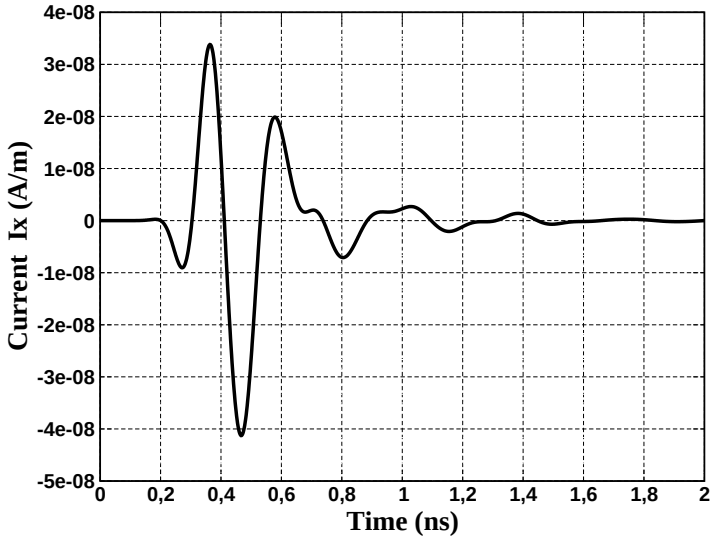

Figure 8.36: Transient current induced at the center of the wire scatterer .

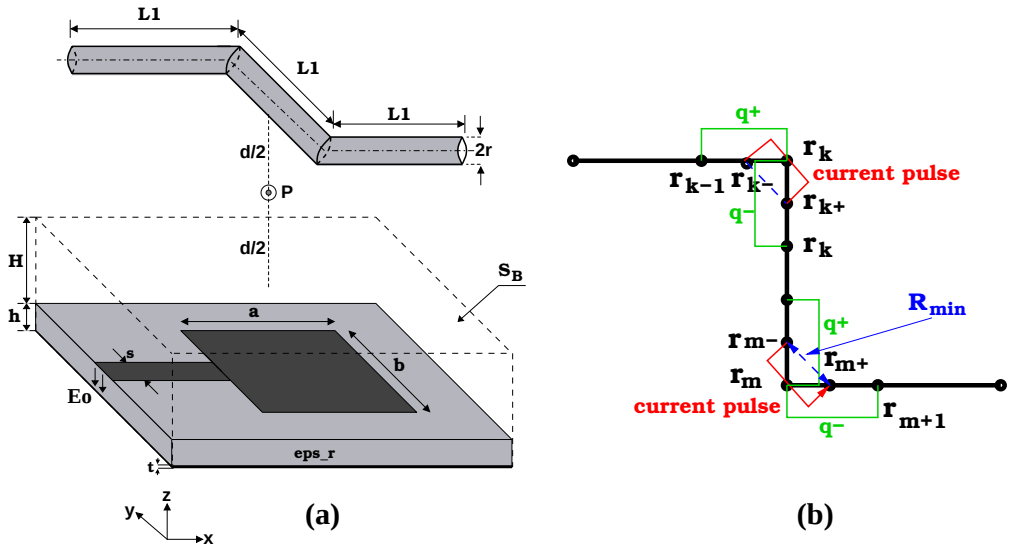

Figure 8.37: A rectangular microstrip patch antenna printed on a substrate interfering with a thin wire structure with two 90° junctions.

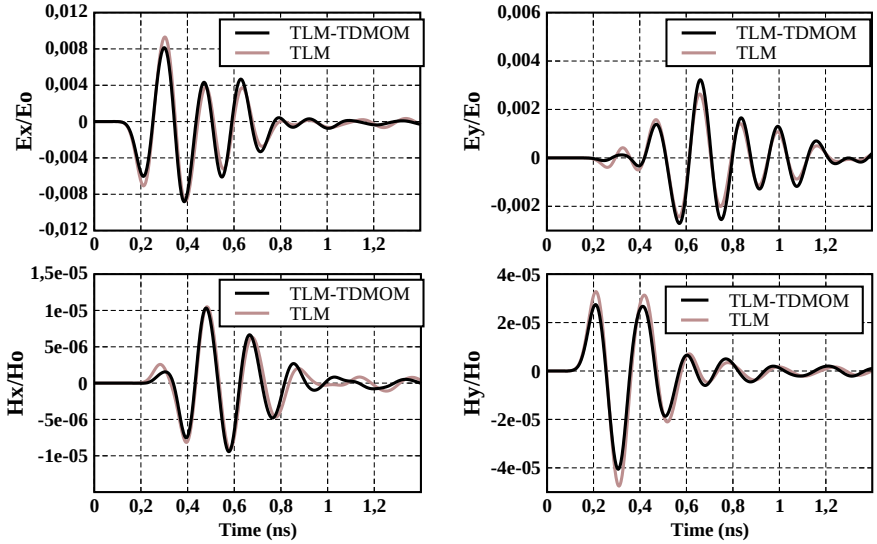

Figure 8.38: Time evolution of the E_x, E_y, H_x, and H_y fields calculated by the TLM and the hybrid TLM-TDMOM methods at point P, for the case of a wire obstacle with two 90^o junctions.

hybrid TLM-TDMOM-method. The first issue is related to the choice of the time step. The time step, used in the marching on in time procedure, must be equal or less than the minimum distances, R_{min}, between two distance match points. In this case, if the length of any segment is longer than distance across 90°bend, the distance across the 90° bend will be $R_{min} \cong \Delta l = 1\,mm$. For curved thin wires we can assume $R_{min} \cong \Delta l$ because of the great number of elements required to describe the curved structures. This condition makes elements so small that there is a negligible difference between arc and straight element length. To handle this, the code must calculate the distance between every segment k end point vector, as well as the distance between every half-segment vector. The minimum distance is then obtained by evaluating the two sets of values. The second issue is related to the basic pulse function, as shown in Fig. 8.37(b). The basic function is based on a geometry whereby the segments are not perpendicular to one another. Looking at Fig. 8.37(b), the current might lies at an imaginary wire segment that cuts across the 90° bent. This might introduces a certain amount of error, however, this error has not been evaluated and is assumed to be small enough to be ignored. We investigate the perturbation caused by the 2L-shaped wire on the radiated field from the patch antenna at the point $P(z = 20)$ between the interacting objects. For this purpose we evaluate the normalized field components, E_x, E_y, H_x, and H_y, at a point P. In Fig. 8.38 we compare the normalized field components at

P by the hybrid TLM-TDMOM method and by the pure TLM method. We observe a good agreement between the hybrid method and the TLM method, thus confirming the validity of the proposed hybrid algorithm.

8.4 Microstrip loop and circular cylinder configuration

We consider the electromagnetic interaction between a microstrip line forming a loop and a circular cylinder as indicated in Fig. 8.39. The dimensions as specified in Fig. 8.39 are given in the following : $a = 30\,mm$, $b = 22\,mm$, $s = 3\,mm$, $t = 1\,mm$, $h = 5\,mm$, $H = 5\,mm$. The total length and the radius of the circular cylinder are $L = 40\,mm$ and $r = 5\,mm$, respectively. The cylinder is placed at a distance of $d = 20\,mm$ from the upper plane of the TLM-subregion. The electromagnetic field inside the TLM-subregion is computed by the TLM algorithm, the field in the external region is described by means of the free-space Green's functions, the circular cylinder is modeled using the method of moments which relies on a triangular-patch geometrical model of its exterior surface. We excite the field by an electric pulse of gaussian-type propagating in the z-direction with amplitude Eo. The excitation is placed at the boundary between the ground plane and the feeding microstrip, as depicted in Fig. 8.39. The dielectric substrate has a permittivity of $\varepsilon_r = 2.1$. In the

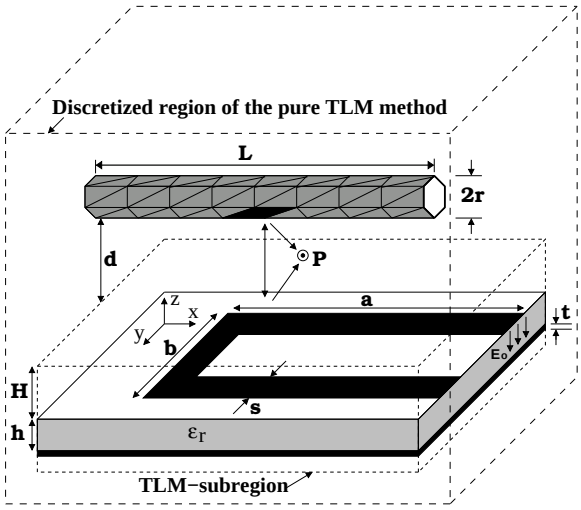

Figure 8.39: A microstrip loop interfering with a perfectly conducting circular cylinder.

present case the TLM-subregion interface surrounds the structure in the geometrical form of rectangular box, as shown in Fig. 8.39. For comparing the results we apply the hybrid method as well as the pure TLM method to this problem. The circular

cylinder is modeled by 96 triangular surface patches. For the pure TLM simulation we have to discretize a region which encloses the microstrip loop, the circular cylinder with a staircase approximation, the entire near-field region, and to apply the absorbing boundary conditions as shown in Fig. 4. The dimensions of the discretized space for the pure TLM method are $120\,mm \times 120\,mm \times 110\,mm$. For both the pure TLM and the hybrid method, the TLM grid is uniform with $\Delta x = \Delta y = \Delta z = \Delta l = 1\,mm$. Also the time step is the same with $\Delta t = \Delta l/2c = 1.66\,ps$.

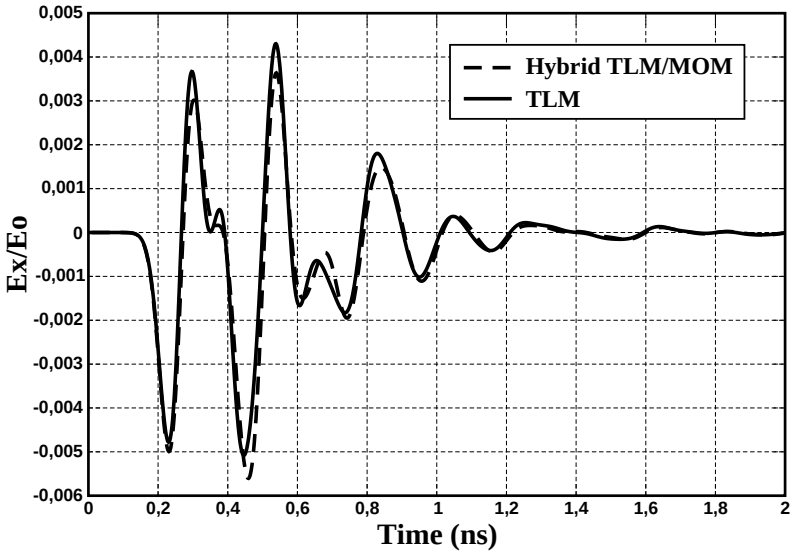

Figure 8.40: Time evolution of the E_x-field calculated by the TLM and the hybrid TLM-TDMOM methods at point P.

We evaluate the electric field E_x (normalized with respect to E_o), at a distance of $d/2 = 10\,mm$ between the interacting objects at the point P ($x = 15\,mm$, $y = 15\,mm$, $z = 20\,mm$). The field evaluated using the hybrid method is closer to the field calculated by TLM, as shown in Fig. 8.40. In Fig. 8.41 the same comparison is performed in the frequency domain after a FFT, a good agreement is remarkable. The deviations in amplitude are caused by the different boundary conditions, which are used in the different methods.

Fig. 8.42 reports the different parts of the electric field E_x at the point P, the radiated field coming from the equivalent sources at the TLM interface, and the scattered field coming from the circular cylinder. The superposition of these both parts gives the total electric field E_x, performed in Fig. 8.40, using the hybrid method. The surface current density induced at the center patch of the circular cylinder, as indicated in Fig. 8.39, is plotted versus time in Fig. 8.43. The results show very good agreement,

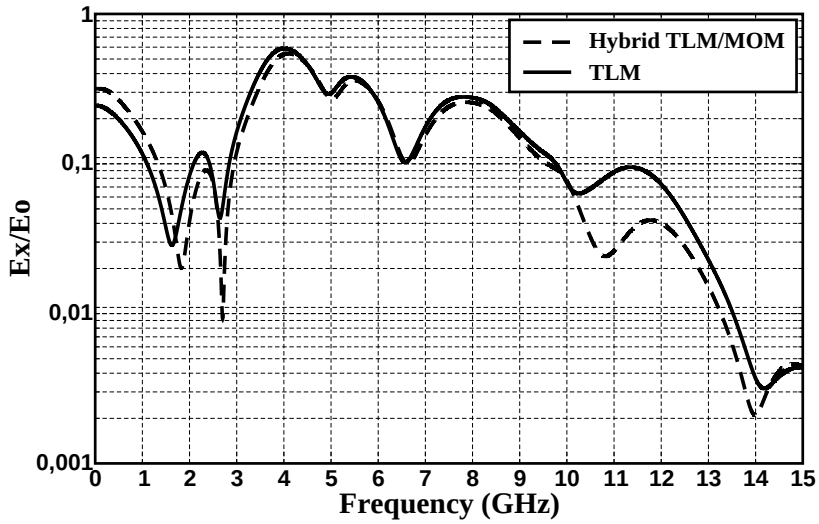

Figure 8.41: Spectrum of the E_x-field at the point P evaluated by the hybrid TLM-TDMOM method vs the pure TLM method after FFT.

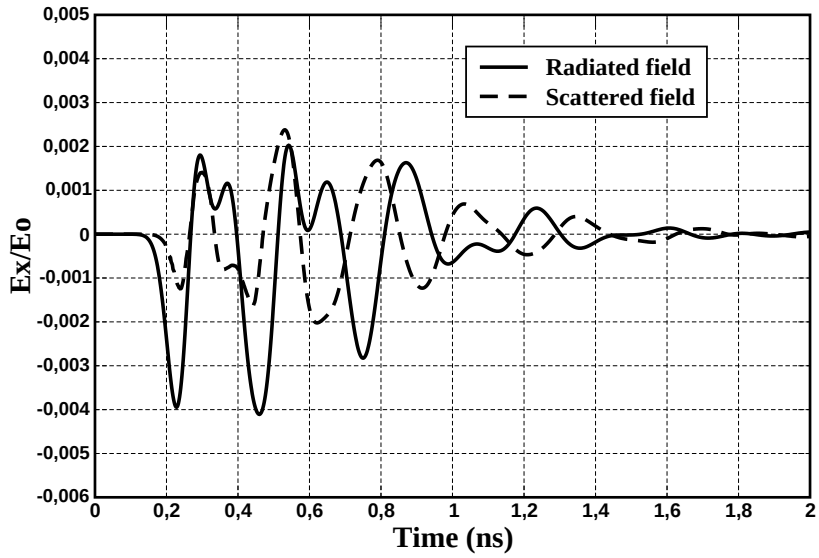

Figure 8.42: Comparison of the time evolution of the radiated and the scattered part of the total E_x-field component at the point P evaluated by the hybrid TLM-TDMOM method.

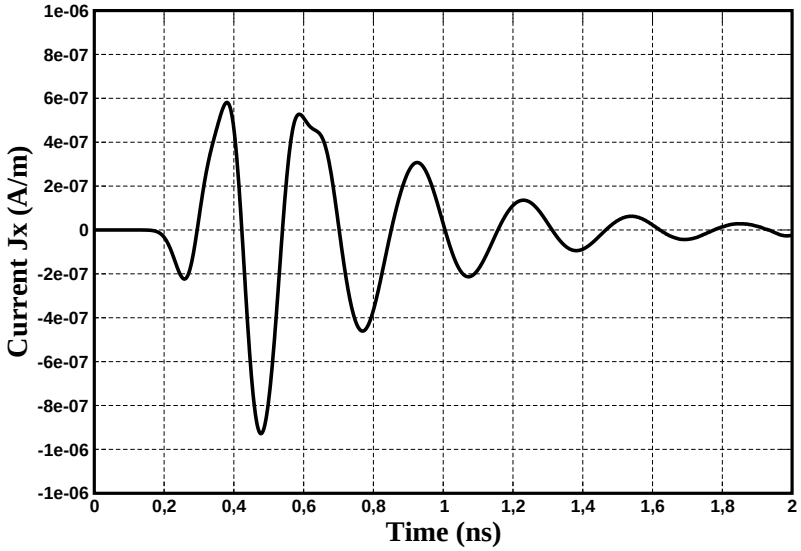

Figure 8.43: Transient current induced at the center patch of the circular cylinder.

thus confirming the validity of the hybrid TLM-TDMOM method for the analysis of transient interferences between a complex object exhibiting compound dielectric and lossy materials and a metallic regular object.

While the CPU-time, required for the pure TLM method is about 70% higher than the computation time effort required for the hybrid TLM-TDMOM method. Because for the pure TLM method we have to discretize a region which encloses both the structures and the entire near field region, which leads to a considerably higher computational time. The ratio between the CPU computational time for the pure TLM method and the TLM-TDMOM method is strongly increasing when we consider the far field evaluation. Using the TLM-TDMOM method, it is possible to calculate the near as well as the far field with about the same computational effort. A general evaluation of the efficiency of the hybrid TLM-TDMOM algorithm in comparison with the conventional TLM method is presented and discussed in section 8.6 in this chapter.

8.5 Stability analysis

Time domain, iterative numerical techniques such as the marching on in time procedure can exhibit problems of numerical stability in terms of spurious growing oscillations. The advantages using the MOT-technique can be achieved only by taking a great care in the choice of the key parameters, which affect numerical stability of the

solution. This is a critical aspect because it is difficult to state general rules. In fact the parameter evaluation depends on many factors such as the geometrical complexity of the structure. The first basic parameter to be defined in the application of the hybrid TLM-TDMOM method is the space step Δl. The scatterer (wire or surface) is discretized into N subdomains (segments or triangular patches). The choice N depends on the compromise between the accuracy of the geometrical representation of the structure and the computational efficiency. A second important parameter is the choice of the time step Δt. Marching on in time technique forces the choice of the time step to depend on the space step and should satisfy the condition $\Delta t \leq R_{min}/c$, where R_{min} represents the minimum distance between the edge centers (segments in case of wire). This distance coincides perfectly with space step in the case of straight wires. For curved structures we can also assume $R_{min} \cong \Delta l$ because of the great number of elements required to describe curved structures. This condition makes elements so small that there is a negligible difference between arc and straight element length. Furthermore the Courant's stability condition [21] forces the choice of the time step to be less than $R_{min}/c\sqrt{2}$ and in the present work we chose $\Delta t = R_{min}/hc$, with the stability factor h and $h \geq 2$. Moreover, we found that Δt cannot be arbitrarily small, but it depends on the geometrical complexity. This requirement may be related to the different propagation paths characterizing the electromagnetic field and the current wave induced on the curved scatterer. In this case the propagation delay from the source to field point, is not an integer multiple of time step Δt, so that an approximation is necessary to determine the retarded contributions of electromagnetic quantities. Adopting a linear interpolation of field (or current) values in the calculation of such retarded contributions, a significant improvement can be obtained. The delay time is truncated at the nearest integer multiple of time step Δt.

We should mention furthermore that, even after satisfying the Courant stability condition, the hybrid TLM-TDMOM technique may suffer from late-time instabilities, although these usually have a slow growth rates. To control the late time oscillations we use a special averaging procedure: Let $\mathbf{E}_{\varphi u\,,j}$ be the expanding field quantity at the cell u at a time instant j on the TLM-interface of the complex object as in eq. (7.28). We calculate $\mathbf{E}_{\varphi u\,,j+1}$ at the next time step and simply approximate the averaged value $\widetilde{\mathbf{E}}_{\varphi u\,,j}$ as:

$$\widetilde{\mathbf{E}}_{\varphi u\,,j} = \frac{1}{4}\,(\widetilde{\mathbf{E}}_{\varphi u\,,j-1} + 2\mathbf{E}_{\varphi u\,,j} + \mathbf{E}_{\varphi u\,,j+1}). \tag{8.1}$$

The averaging technique is used in this thesis because the scheme is simple, accurate, and involves a negligible amount of extra computation. The same averaging technique is applied to the expanding magnetic field quantity $\mathbf{H}_{\varphi u\,,j}$ eq. (7.29). We need to add an extra step to the normal marching on in time algorithm, and obviously, this step involves very little processing time.

Fig. 8.44 shows the transient interference field evaluated using the hybrid TLM-TDMOM method for the example of a patch antenna in interaction with a straight

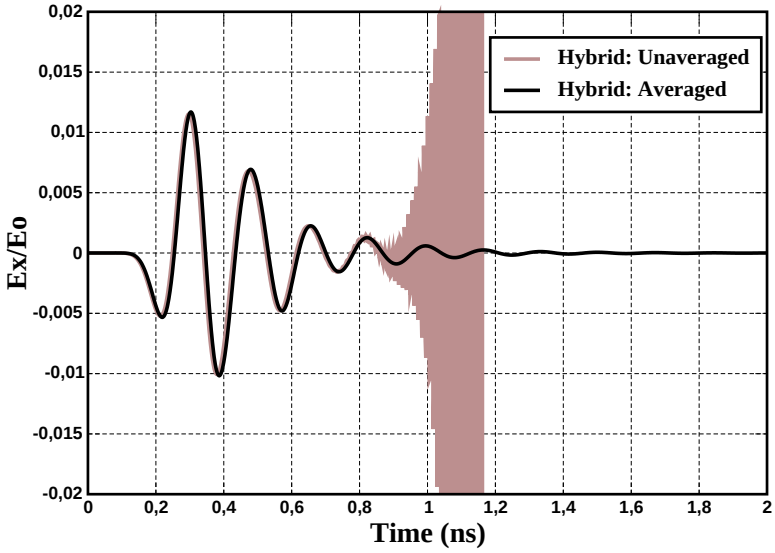

Figure 8.44: Time evolution of the E_x-field calculated by the hybrid TLM-TDMOM method at point P, with and without averaging technique.

wire, studied in section 8.3. In the shown results, the use of the averaging technique eq. (8.1) leads to the total disapperence of oscillations as shown in Fig. 8.44. Even if this is a particular example, we want to stress that the use of the averaging technique yields good improvement also for more complex curved structures. Furthermore, after using this averaging scheme, the late-time instabilities are pushed further down in time or eliminated completely by reducing the mesh points. In particular the more uniform and regular is the discretization, the more stable is the algorithm with the averaging procedure.

In some applications, only the early time response of the system, prior the appearance of the instabilities, is of interest, so a time domain method is preferred as it can effectively be truncated allowing us to compute solutions only for as long as necessary. In our opinion this instability does not affect appreciably the problem solution, because the iterative procedure allows to stop the process after acquiring the needed transient information.

8.6 Computational Efficiency

It is very difficult to absolutely quantify the general resource requirements for a computational electromagnetic (CEM) solution for problems relative to physical size.

Resource requirements are influenced by many things, including the frequencies of interest, the applied formulation, complementary techniques used, and a host of factors in the specific methods employed during coding of the numerical routines.

In general, resource predictions for classical full wave techniques are determined based on the number of computational elements, as this number takes both the physical problem size and the solution frequency into account. Unfortunately, the scaling of the resources with respect to the number of computational elements is not linear, but rather close to quadratic or even cubic.

The goal of any analysis or optimization is to achieve sufficient accuracy with minimum effort, where effort usually is interpreted as computational cost in terms of computational times and memory requirements. However, there may also be a considerable effort associated with other issues such as the programming of the numerical algorithm or the construction of geometrical description suitable for the computation at hand.

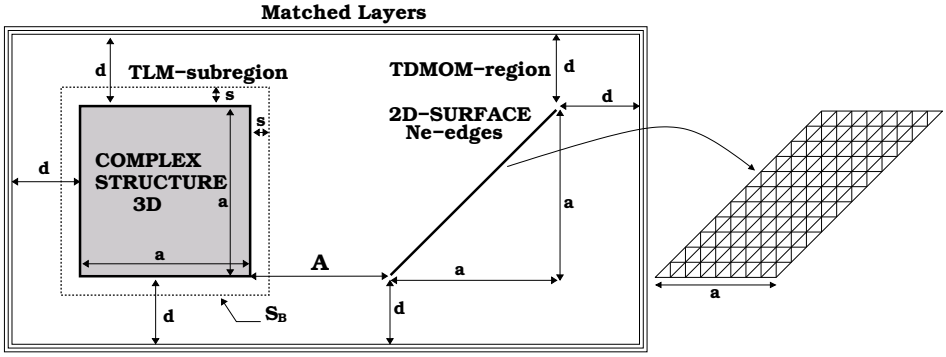

Figure 8.45: General comparison of TLM and the hybrid TLM-TDMOM: Discretized regions for the simulation of the electromagnetic interaction between two objects separated by free-space regions.

The need to tackle increasingly larger and more complex problems has focused attention to increasing the efficiency of TLM algorithm by minimizing storage and run-time requirements. Although any conclusions reached are likely to be dependent on hardware and software configurations, it is nevertheless useful to make some estimate of computational requirements. There is a trade-off between storage and run-time requirements in many situations. A TLM code that allows structuring of the problem into two or three regions which are treated in the most efficient way can result in significant storage savings and improvements in execution speed.

For a general comparison of the computational effort of the hybrid TLM-TDMOM algorithm and the pure conventional TLM method, we consider a cubic complex object with a side length of a cells and which is modeled using the TLM scheme and a 2D

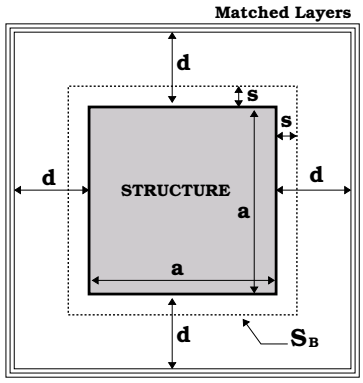

Figure 8.46: General comparison of TLM and the hybrid method in the case of one radiating object, without a scatterer.

metallic surface with the position and dimensions, as indicated in Fig. 8.45. The metallic surface is discretized by triangular patches with Ne edges and modeled using the time-domain Method of Moments. The interacting objects are separated by a distance of A cells as shown in Fig. 8.45. By applying the pure conventional TLM method the most near field region must be embedded in the discretized TLM region. Therefore the distance d between the objects and the boundary of the discretized TLM region must be chosen as $d \geq \lambda max/2$, as indicated in Fig. 8.45. We consider the case, that the size a of the objects is not more than half of the largest wavelength considered ($a \leq \lambda max/2$). That implies that $d \geq a$. We consider the case $d = a$ for which the calculation effort of the TLM-algorithm is the smallest. For the TLM simulation matched layers are used to achieve absorbing boundary conditions at the boundary of the discretized TLM region, as shown in Fig. 8.45. For the case of the hybrid TLM-TDMOM algorithm we discretize the space inside the complex structure and s additional layers to avoid the field singularities [12].

8.6.1 Computation time

For a comparison of the computational time, we consider the number of multiplications of floating points variables which have to be performed in every time step in the TLM and the hybrid TLM-TDMOM methods.

Pure TLM algorithm

In the pure conventional SCN TLM method the number of multiplication N_{TLM} in every time step is calculated from the number of 72 multiplication in the scattering

process times the number of nodes in the discretized TLM region.

$$N_{TLM} = 72\,(2d + 2a + A)(2d + a)^2, \tag{8.2}$$

for the case of one radiating complex object, as shown in Fig. 8.46, we have,

$$N_{TLM} = 72\,(2d + a)^3. \tag{8.3}$$

Hybrid TLM-TDMOM

In the hybrid TLM-TDMOM algorithm, we get the number of multiplications N_{Hybrid} from the number of multiplications $NMSPTLM$ in the scattering process in the nodes of the TLM-subregion S_B, the number of multiplications $NMSI$ at the interface of the TLM-subregion using the dyadic free-space Green's functions in the time domain, and the number of multiplications $NMCMOM$ in the coupling with the TDMOM region, so we get,

$$\begin{aligned} N_{Hybrid} &= NMSPTLM + NMSI + NMCMOM \\ &= \underbrace{72.(a+2s)^3}_{NMSPTLM} + \underbrace{R_{red}.12(a+2s)^4}_{NMSI} + \underbrace{R_{red}.48.(a+2s)^2 Ne}_{NMCMOM}, \end{aligned} \tag{8.4}$$

where

$NMSPTLM$	**N**umber of **M**ultiplications in the **TLM S**cattering **P**rocess	$72.(a+2s)^3$
$NMSI$	**N**umber of **M**ultiplications for the **S**elf-**I**nteraction between the boundary elements belonging to the same TLM interface.	$R_{red}.12(a+2s)^4$
$NMCMOM$	**N**umber of **M**ultiplications for the **C**oupling with the **MOM** region outside the TLM interface.	$R_{red}48(a+2s)^2 Ne$
R_{red}	Reduction factor with $R_{red} = r_{ts}.r_{td}.r_{rd}$.	0.125
r_{ts}	Reduction factor of the time sampling points of the field-distribution at the TLM-interface as source points.	0.5
r_{td}	Reduction factor of the calculated time-fieldvalues at destination points through time interpolation.	0.5

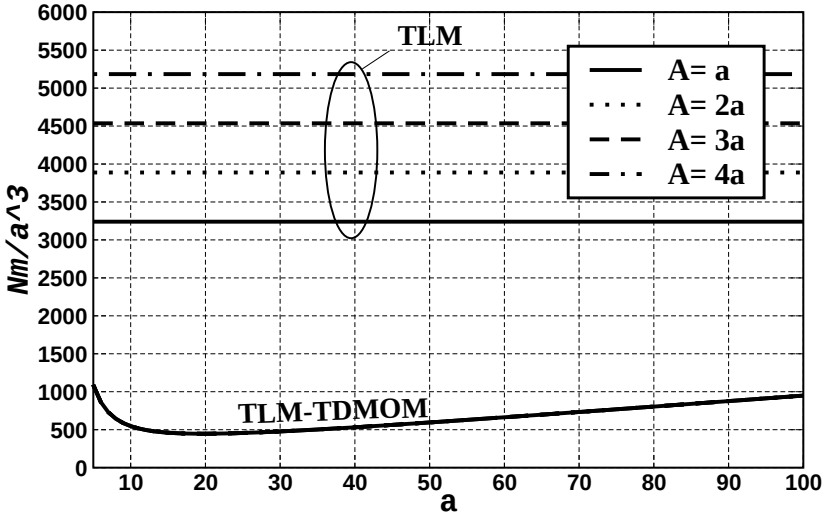

Figure 8.47: Number of multiplications for each time step; Comparison of the pure TLM method with the hybrid TLM-TDMOM.

r_{rd}	Reduction factor of the calculated space-fieldvalues at destination points through space interpolation.	0.5

For $s = 3$ and $Ne = a^2$, and $R_{red} = 0.125$ we get,

$$N_{Hybrid} = 72.(a + 2s)^3 + 1.5(a + 2s)^4 + 6(a + 2s)^2 a^2 \tag{8.5}$$

As it is shown the number of multiplications N_{Hybrid} is independent from the separation distance A between the interacting objects, as plotted in Fig. 8.47. In Fig. 8.48 the relative number of multiplications N_m of the TLM algorithm compared to the number of multiplications in the Hybrid algorithm is shown. It shows that the number of multiplications of the Hybrid method is considerably smaller than the number of multiplications of the TLM algorithm. For example, we discretize the side of the cube with $a = 60$ cells. If the distance between the objects is two times the side length $A = 2a$, the computational time of the TLM method is six times higher than the one of the hybrid TLM-TDMOM algorithm

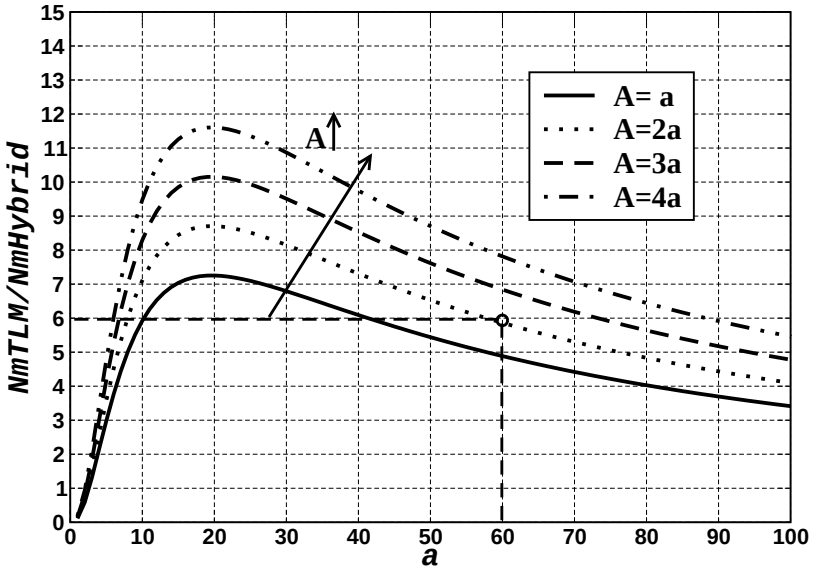

Figure 8.48: Relative number of multiplication for the hybrid TLM-TDMOM method in comparison with the TLM algorithm.

8.6.2 Memory requirement

For a comparison of the storage requirement of the TLM method and the hybrid method, we consider the maximal number of floating points values which has to be stored.

Pure TLM algorithm

In the pure TLM method the number S_{TLM} of the stored floating point values is calculated through the number of 18 incoming and 18 outgoing impulses in one TLM node times the number of nodes in the discretized TLM region. For the case of two interacting object as shown in Fig. 8.45,

$$S_{TLM} = 36(2d + a)^2(2d + 2a + A) \tag{8.6}$$

For the case of one single radiated object as shown in Fig. 8.46 we have,

$$S_{TLM} = 36.(2d + a)^3 \tag{8.7}$$

Hybrid TLM-TDMOM

In the Hybrid method the number of the stored values is calculated through the number of impulses in the TLM-subregion, the coefficients of the dyadic green's functions, and in the previous time-steps stored field values at the TLM-interface.

For the case of two objects separated by A cells as shown in Fig. 8.45, we have,

$$\begin{aligned} S_{Hybrid} &= STLM + SCSI + SCMOM + SSSI + SSIMOM + SSMOM \\ &= \underbrace{36.(a+2s)^3}_{STLM} + \underbrace{R_{red}8(a+2s)^4}_{SCSI} + \underbrace{R_{red}.8.(a+2s)^2N_e}_{SCMOM} + \underbrace{R_{red}.48\sqrt{3}(a+2s)^3}_{SSSI} + \\ &\quad \underbrace{h.N_e.a\sqrt{3}}_{SSIMOM} + \underbrace{R_{red}.48.(a+2s)^2N_e\sqrt{[(s+2a+A)^2+(a\sqrt{2})^2]}}_{SSMOM}, \end{aligned} \quad (8.8)$$

where

$STLM$	**S**tored impulses in the **TLM**-subregion	$36.(a+2s)^3$
$SCSI$	**S**tored **C**oefficients for **S**elf **I**nteraction	$R_{red}n_pn_mn_{fs}^2 = R_{red}8(a+2s)^4$
$SCMOM$	Stored **C**oefficients for coupling with **MOM** region	$R_{red}n_p.n_m.n_{fs}N_e = R_{red}.8.(a+2s)^2N_e$
N_e	Number of patch-elements at the scatterer surface, for example ($N_e = a^2$).	$N_e = a^2$
$SSSI$	**S**tored **S**ampling values for **S**elf **I**nteraction	$R_{red}.h.n_k.n_f.D_v = R_{red}.48\sqrt{3}(a+2s)^3$
$SSIMOM$	**S**tored **S**ampling **C**urrent values in the **MOM** region	$h.N_e.a\sqrt{3} = h.a^3.\sqrt{6}$
$SSMOM$	**S**tored **S**ampling values for coupling with **MOM** region	$R_{red}.h.n_f.n_kD_{max} = R_{red}.48.(a+2s)^2N_e.D_{max}$
h	Stability factor	2
n_{fs}	Number of surface elements in one side at TLM-interface	$(a+2s)^2$
n_f	Number of surface elements in all sides at TLM-interface	$6(a+2s)^2$
n_p	Number of ports at one side at TLM-interface	2

n_k	Number of field-components at every side of the TLM- interface (example: E_x, E_y, H_x, H_y)	4
n_m	Number of Multiplication in the EFIE/MFIE	4
D_s	Diagonal in one side of the TLM-subregion	$D_s = \sqrt{2}(a + 2s)$
D_v	Volume diagonal of the TLM-subregion	$D_v = \sqrt{3}(a + 2s)$
D_{max}	Maximal space between a TLM-cell and Scatterer-element	$D_{max} = \sqrt{H^2 + V^2}$ $H = (s + 2a + A)$ $V = (a\sqrt{2})$

For $s = 3$, $N_e = a^2$, $h = 2.0$, and $R_{red} = 0.125$ we get,

$$S_{Hybrid} = 46.39(a+6)^3 + (a+6)^4 + (a+6)^2 a^2\sqrt{2} + 2.a^3\sqrt{6} + 6\sqrt{2}(a+6)^2 a^2 \sqrt{[(A+3+2a)^2 + (a\sqrt{2})^2]}. \quad (8.9)$$

As we can see from the general equation (8.8), the maximal number of stored floating point values in the hybrid TLM-TDMOM algorithm depends on the separation distance A between the objects. The time window, where the sampled field values in the previous time-steps must be stored, is the maximal distance D_{max} between a surface element at the TLM interface and an edge on the MOM region.

In Fig. 8.49, the relative number S_v of stored values of the TLM method compared to the number of stored values in the hybrid TLM-TDMOM algorithm is shown. As can be seen, the storage requirement of the hybrid method is considerably lower than the one of the TLM method. The difference between the storage requirement of the hybrid method and the pure conventional TLM method is increasing if we increase the distance of the interacting structures, as can be seen in Fig. 8.50. Using only the front side of the discretized TLM-subregion as radiating boundary the computational effort of the hybrid method can be further reduced to one third.

As it has been shown the computational effort of the hybrid TLM-TDMOM method is much lower than the computational effort of the pure TLM-Method. On the other hand the demand for a homogeneous discretization at the boundaries of the discretized region makes it possible to use a graded mesh for the TLM-simulation. In the hybrid

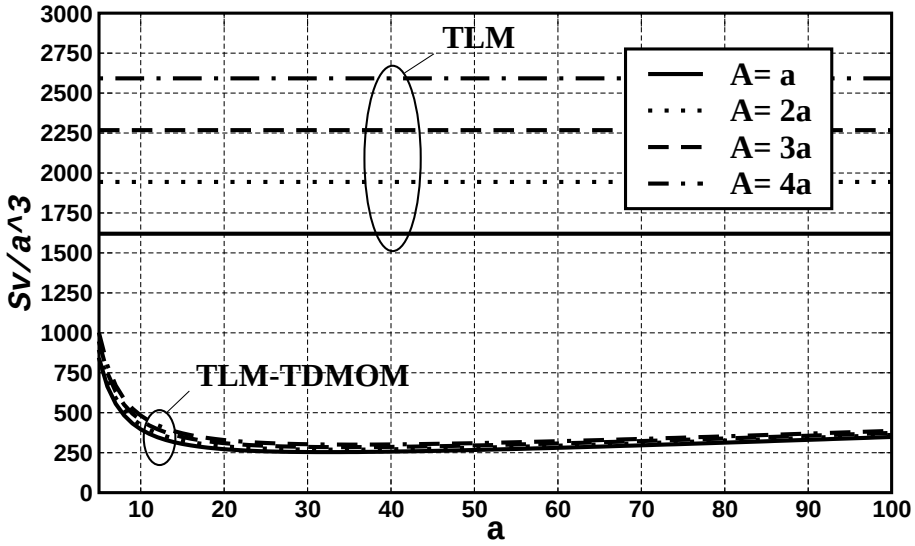

Figure 8.49: Number of stored values S_v; Comparison of the pure TLM method with the hybrid TLM-TDMOM method.

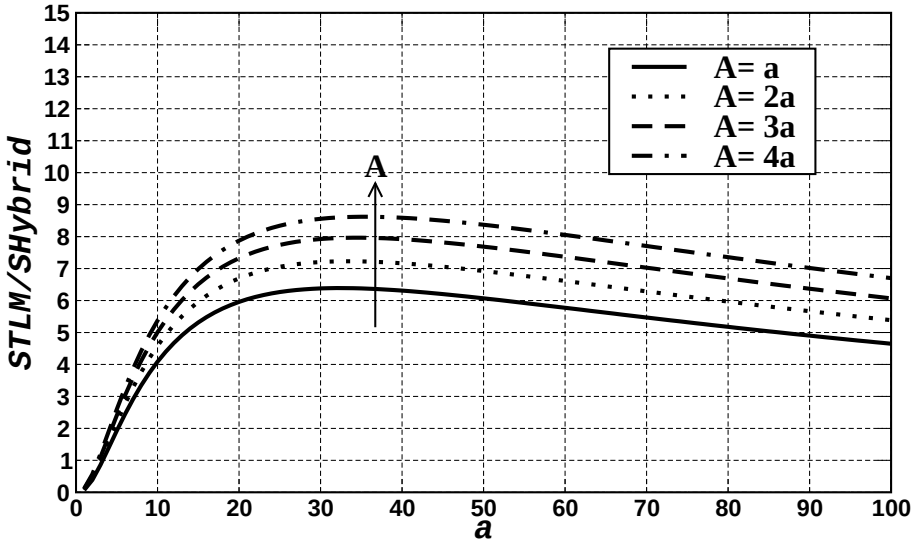

Figure 8.50: Relative number S_v of stored values of the TLM algorithm in comparison with the hybrid TLM-TDMOM method.

method the use of a graded mesh is possible which can lead to further reductions in computational effort, dependant on the structure to be modeled. The most important aspect of the hybrid method is the low storage requirement. In many cases where we have to model radiation and coupling phenomena in large free-space regions the memory requirement of the pure TLM method exceeds the limit of the computational machine. These are the cases where only the hybrid methods are working.

9 Discussion and Conclusions

9.1 Conclusions and outline

In this thesis, we have presented the theoretical analysis and the numerical application of the novel efficient hybrid TLM-TDMOM method combining the flexible Transmission Line Matrix method (TLM) and the efficient Time Domain Method of Moments (TDMOM). This hybrid method is very efficient for the accurate modeling of the transient interference between a complex object exhibiting materials with arbitrary electrical properties and a perfectly conducting thin wire or surface of arbitrary shape, separated by large free space regions. The time domain formulation of the methods allows us to treat efficiently fast transient phenomena, at the same time the hybrid technique allows us to treat separately the electromagnetic field source object and a scattered object, strongly coupled with the source, solving each structure with the most suitable method. The application of the equivalence principle allows us to divide the three-dimensional space into subregions, and to apply each method in its best domain of application. The complex inhomogeneous object is embedded into a closed TLM-subregion and modeled by the transmission line matrix (TLM) scheme. Outside the subregion the coupling is represented by equivalent sources located on the surfaces which bound the TLM-subregion. These equivalent current/charges distributions are coupled via the dyadic Green's functions (be it analytical and/or numerical) of the homogeneous region. At the boundary between the discretized TLM-subregion and the scatterer region, the two representations are then interfaced by applying the continuity of the EM tangential field, thus providing appropriate sets of Electric Field Integral Equations (EFIE) and Magnetic Field Integral Equations (MFIE). The latter integral equations are then transformed to matrix systems by applying the Marching On in Time (MOT) procedure and solved explicitly, at each time step, for the unknown total tangential field. The tangential field components represent, in turns, the exact radiating boundary condition for the TLM-subregion.

For the modeling of the conducting scatterer (wire or surface), the time domain electric field integral equation is used along with the method of moments which relies on a triangular-patch geometrical model of the exterior surface or net of straight segments for the case of a thin wire and operates according to the marching-on-in-time (MOT) technique. Adopting the conventional procedure of MOM, we use pulse basis functions to expand the current distribution both in time and space domain as well as delta test

functions according to the point matching technique. This time formulation of the MOM delivers an explicit iterative procedure for computing the current distribution on the scatterer. Arbitrarily field values can then be efficiently derived from the current solution at any point in space as a secondary computational step. This means that integral techniques do not need to apply resources to the modeling of homogeneous propagating space.

This new approach was validated by comparing the results with those obtained by applying the pure transmission line matrix method (TLM) to the whole electromagnetic problem.

The benefits of the novel proposed hybrid method are

- Accurate and efficient characterization of arbitrarily curved thin wire or surface using the TDMOM method.
- The complex object exhibiting materials with nonlinearities, anisotropies, or dispersive characteristics can be enclosed into a TLM-subregion and efficiently modeled using the Transmission Line Matrix (TLM) method.
- Accurate and efficient treatment of large free free space regions using the dyadic free space Green's functions in time domain.
- The approach imposes automatically the correct radiation and causality conditions, which must be imposed artificially in the truncation of finite grids by applying only the pure TLM for the analysis of the whole configuration.
- The time domain formulation of the problem allows us to treat efficiently the transient interference between the objects.
- Significant reductions in computer resources over those required for the pure TLM algorithm.

Two major problems were faced in the development of this hybrid method. The TDMOM algorithm solves an integro-differential equation for the current on the scatterer, whereas the TLM algorithm provides combinations of electric and magnetic fields, represented as pulses propagating on a 3D grid of transmission lines. The problem of these different mathematical formulations was overcome by means of the marching on in time procedure, which gives an iterative solution of the electromagnetic integral equations. The equivalence principle was used to solve the second problem concerning the interaction between the source and the scatterer; the complex object is enclosed by equivalence surfaces, where equivalent electric and magnetic sources have to be calculated at every time steps.

The complex object is embedded into a discretized region, where the TLM method is applied for the field modeling. According to the Huygens Shelkunoff's representation of the equivalence theorem, the radiation from the complex object outside its discretized subdomain is expressed replacing the sources inside the object by equivalent

surface currents at the TLM interface. The tangential field on the surface represents a distribution of equivalent currents and charges. The radiated field from the complex structure represents the incident field or the excitation of the scatterer. The scattering problem is solved through discretization of the EFIE and its direct time-domain solution by means of a marching-on-in-time procedure. An explicit equation that relates the current at a certain time instant to the currents of previous instants and the incident field is obtained. Once the transient current density on the induced scatterer has been determined, we can easily compute the scattered field back to the boundary of the TLM-subregion by summing the effect of each individual current element on the surface of the thin conducting structure.

The novel hybrid method has been applied to the modeling of different electromagnetic coupling problems. All interactions and backscattering processes have been taken into consideration. A comparison between the results obtained from the hybrid method TLM-TDMOM and those obtained from the pure conventional TLM method has been presented. The results confirm the validity of the proposed approach. For a comparison of the computational time, the number of multiplications of floating points variables which have to be performed in every time step in the TLM and the hybrid TLM-MOM methods was considered. The relative number of multiplications of the hybrid method is considerably smaller than the number of multiplications of the TLM algorithm. For example, If the distance between the objects is two times the side length of the object, the computational time of the TLM method is six times higher than the one of the hybrid TLM-TDMOM algorithm. For a comparison of the storage requirement of the TLM method and the hybrid method, the maximal number of floating points values which has to be stored was considered. The storage requirement of the hybrid method is considerably lower than the one of the TLM method. The difference between the storage requirement is increasing if we increase the distance of the interacting structures.

The thesis has illustrated the capability of this hybrid method and established guidelines for its selection in preference to the pure TLM with a particular focus on the simulation of the transient electromagnetic interference.

We should mention that, the hybrid TLM-TDMOM technique may suffer from late-time instabilities, although these usually have a slow growth rates. To study this phenomenon, we have compared the responses of several regular objects, by using the hybrid TLM-TDMOM. For the example studied in this thesis, we have found that the instabilities appear after 7000 time steps. It means the early-time transient response is usually calculated accurately, prior to the appearance of the instabilities. Furthermore, after using the averaging scheme, the late-time instabilities are pushed further down in time or eliminated completely by reducing the mesh points. In particular the more uniform and regular is the discretization, the more stable is the algorithm with the averaging procedure. In some applications, only the early time response of the system is of interest, so a time domain method is preferred as it can effectively be truncated allowing us to compute solutions only for as long as necessary. In our

opinion this instability does not affect appreciably the problem solution, because the iterative procedure allows to stop the process after acquiring the needed information.

The above considerations show that the advantages of the hybrid method TLM-TDMOM with respect to the pure TLM method are especially evident if we have to model radiation, coupling phenomena in large free-space regions and to deal with curved thin structure such as a wire or surface. In many such cases the memory requirement of the pure space discretizing TLM method exceeds the limit of the computational machine and only the hybrid method is working.

Already now with the conjuction of the present rigorous numerical hybrid methods, the engineer has tools for investigating coupling problems efficiently. The user will gain more understanding of the coupling phenomena, and is hence able to react and to prevent strong interactions.

A Appendix

A.1 Wires with arbitrary orientation and length

A.1.1 Overview

To analyze general EMC configurations comprising thin wire structure*s,* it is interesting to study configurations with wires of arbitrary length and arbitrary orientation with respect to a reference coordinate system. In this section, rotated and translated coordinate systems with respect to a reference coordinate system will be introduced. Subsequently, electric field integral equation for a single thin wire pointing in the x-direction of an arbitrary coordinate system is subjected to this transformation. All transformations are considered with respect to the reference coordinate system $(\mathbf{O}r, \mathbf{u}_{xr}, \mathbf{u}_{yr}, \mathbf{u}_{zr})$. A wire can thus be arbitrarily positioned in space. If in the new coordinate system the wire is oriented along the x-axis, only the pertaining incident field term needs to be considered. Next, the coupling between two, now arbitrarily oriented, wires in free space is studied again. This coupling exists because the radiated field of one wire may be regarded as a part of the incident field on the other wire. When the radiated field is also written in terms of the reference coordinate system, mutual coupling can be described. The organization of this section is as follows. First, the transformation from the reference coordinate system to an arbitrary coordinate system and vice versa is introduced. Next, the transformation is applied to the EFIE equation for a single thin wire and a transformation is applied to the EFIE equation for a second thin wire in another arbitrary coordinate system. With these three steps, wires can be arbitrarily positioned with respect to a reference coordinate system.

A.1.2 Coordinate transformations

The currents along a set of straight wires are coupled via the radiated field and the incident-field term in the EFIE equation pertaining to each wire. As described earlier, for an arbitrarily oriented wire as in Fig. A.51, the incident-field term in coordinate system $(O1, \mathbf{u}_{x1}, \mathbf{u}_{y1}, \mathbf{u}_{z1})$ is transformed to the reference system. In a later stage, the currents along other wires can be related to the current along the wire displayed in Fig. A.51.

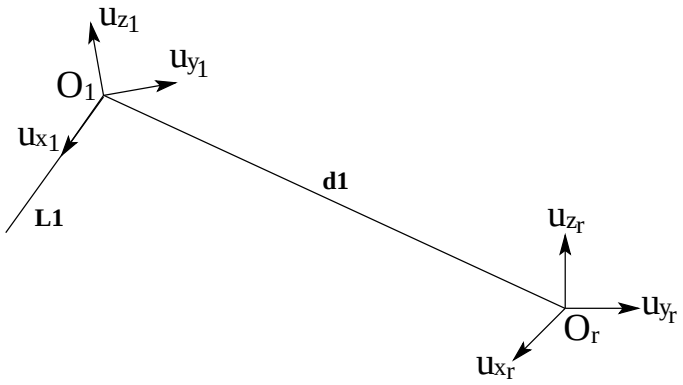

Figure A.51: An arbitrarily oriented thin wire with respect to the reference system $(\mathbf{O}_r, \mathbf{u}_{xr}, \mathbf{u}_{yr}, \mathbf{u}_{zr})$.

Before the incident field term is transformed to the reference system for every point along the wire, first an arbitrary point $\mathbf{r} = x_1\mathbf{u}_{x1} + y_1\mathbf{u}_{y1} + z_1\mathbf{u}_{z1}$ in coordinate system $(\mathbf{O}_1, \mathbf{u}_{x1}, \mathbf{u}_{y1}, \mathbf{u}_{z1})$ will be expressed in terms of the unit vectors of the reference system$(\mathbf{O}_r, \mathbf{u}_{xr}, \mathbf{u}_{yr}, \mathbf{u}_{zr})$. The transformation involves the following steps.

- Translation of the system $(\mathbf{O}_r, \mathbf{u}_{xr}, \mathbf{u}_{yr}, \mathbf{u}_{zr})$ over a displacement vector $\mathbf{d}1$ resulting in $(\mathbf{O}_1, \mathbf{u}_x^{(1)}, \mathbf{u}_y^{(1)}, \mathbf{u}_z^{(1)})$.
- Rotation of $(\mathbf{O}_1, \mathbf{u}_x^{(1)}, \mathbf{u}_y^{(1)}, \mathbf{u}_z^{(1)})$ around the z-axis over an angle $\phi 1$ resulting in $(\mathbf{O}_1, \mathbf{u}_x^{(2)}, \mathbf{u}_y^{(2)}, \mathbf{u}_z^{(2)})$.
- Rotation of system $(\mathbf{O}_1, \mathbf{u}_x^{(2)}, \mathbf{u}_y^{(2)}, \mathbf{u}_z^{(2)})$ around the y-axis over a second angle θ_1 resulting in $(\mathbf{O}_1, \mathbf{u}_{x1}, \mathbf{u}_{y1}, \mathbf{u}_{z1})$.

In Fig. A.52, each step is visualized. The extra superscripts (1) and (2) indicate that the first and the second step have been carried out, respectively. The two intermediate coordinate systems are only introduced for the derivation of the transformation. Note that the subscript 1 refers to coordinate system 1.

An arbitrary vector $\mathbf{r}$ can be written as

$$\begin{aligned}\mathbf{r} &= x_r\mathbf{u}_{xr} + y_r\mathbf{u}_{yr} + z_r\mathbf{u}_{zr} = x^{(1)}\mathbf{u}_x^{(1)} + y^{(1)}\mathbf{u}_y^{(1)} + z^{(1)}\mathbf{u}_z^{(1)} \\ &= x^{(2)}\mathbf{u}_x^{(2)} + y^{(2)}\mathbf{u}_y^{(2)} + z^{(2)}\mathbf{u}_z^{(2)} = x_1\mathbf{u}_{x1} + y_1\mathbf{u}_{y1} + z_1\mathbf{u}_{z1}. \end{aligned} \tag{A.1}$$

The derivation of the transformation formulas is carried out by composition of at most three individual steps whose mathematical description is given below.

The transformation of the reference system to system 1 is then as follows:

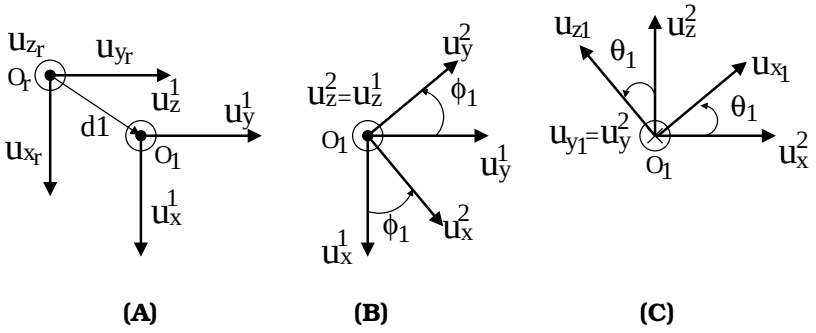

Figure A.52: An arbitrarily oriented thin wire with respect to the reference system $(\mathbf{O}_r, \mathbf{u}_{xr}, \mathbf{u}_{yr}, \mathbf{u}_{zr})$.

(A) Translation over $\mathbf{d}1 = \mathbf{d}_{1x}\mathbf{u}_{xr} + \mathbf{d}_{1y}\mathbf{u}_{yr} + \mathbf{d}_{1z}\mathbf{u}_{zr}$:

$$\mathbf{r} = x_r\mathbf{u}_{xr} + y_r\mathbf{u}_{yr} + z_r\mathbf{u}_{zr} = x^{(1)}\mathbf{u}_x^{(1)} + y^{(1)}\mathbf{u}_y^{(1)} + z^{(1)}\mathbf{u}_z^{(1)}, \tag{A.2}$$

with

$$\begin{pmatrix} x^{(1)} \\ y^{(1)} \\ z^{(1)} \end{pmatrix} = \begin{pmatrix} x_r \\ y_r \\ z_r \end{pmatrix} - \begin{pmatrix} d_{1x} \\ d_{1y} \\ d_{1z} \end{pmatrix}, \quad \textit{and} \quad \begin{pmatrix} \mathbf{u}_x^{(1)} \\ \mathbf{u}_y^{(1)} \\ \mathbf{u}_z^{(1)} \end{pmatrix} = \begin{pmatrix} \mathbf{u}_{xr} \\ \mathbf{u}_{yr} \\ \mathbf{u}_{zr} \end{pmatrix}. \tag{A.3}$$

(B) Rotation around the z-axis over ϕ_1:

$$\mathbf{r} = x^{(1)}\mathbf{u}_x^{(1)} + y^{(1)}\mathbf{u}_y^{(1)} + z^{(1)}\mathbf{u}_z^{(1)} = x^{(2)}\mathbf{u}_x^{(2)} + y^{(2)}\mathbf{u}_y^{(2)} + z^{(2)}\mathbf{u}_z^{(2)}, \tag{A.4}$$

with

$$\begin{pmatrix} x^{(2)} \\ y^{(2)} \\ z^{(2)} \end{pmatrix} = \mathbf{T}^{(1)} \begin{pmatrix} x^{(1)} \\ y^{(1)} \\ z^{(1)} \end{pmatrix}, \quad \begin{pmatrix} u_x^{(2)} \\ u_y^{(2)} \\ u_z^{(2)} \end{pmatrix} = \mathbf{T}^{(1)} \begin{pmatrix} u_x^{(1)} \\ u_y^{(1)} \\ u_z^{(1)} \end{pmatrix}, \tag{A.5}$$

and

$$\mathbf{T}^{(1)} = \begin{pmatrix} \cos\phi_1 & \sin\phi_1 & 0 \\ -\sin\phi_1 & \cos\phi_1 & 0 \\ 0 & 0 & 1 \end{pmatrix}. \tag{A.6}$$

(C) Rotation around the y-axis over θ_1:

$$\mathbf{r} = x^{(2)}\mathbf{u}_x^{(2)} + y^{(2)}\mathbf{u}_y^{(2)} + z^{(2)}\mathbf{u}_z^{(2)} = x_1\mathbf{u}_{x1} + y_1\mathbf{u}_{y1} + z_1\mathbf{u}_{z1}, \tag{A.7}$$

with

$$\begin{pmatrix} x_1 \\ y_1 \\ z_1 \end{pmatrix} = \mathbf{T}^{(2)} \begin{pmatrix} x^{(2)} \\ y^{(2)} \\ z^{(2)} \end{pmatrix}, \quad \begin{pmatrix} u_{x1} \\ u_{y1} \\ u_{z1} \end{pmatrix} = \mathbf{T}^{(2)} \begin{pmatrix} u_x^{(2)} \\ u_y^{(2)} \\ u_z^{(2)} \end{pmatrix}, \tag{A.8}$$

and

$$\mathbf{T}^{(2)} = \begin{pmatrix} \cos\theta_1 & 0 & \sin\theta_1 \\ 0 & 1 & 0 \\ -\sin\theta_1 & 0 & \cos\theta_1 \end{pmatrix}. \tag{A.9}$$

With these three steps the following composed transformation formula the reference system to coordinate system 1 can be constructed:

$$\begin{pmatrix} x_1 \\ y_1 \\ z_1 \end{pmatrix} = \mathbf{T}^{(2)} \begin{pmatrix} x^{(2)} \\ y^{(2)} \\ z^{(2)} \end{pmatrix} = \mathbf{T}^{(2)}\mathbf{T}^{(1)} \begin{pmatrix} x^{(1)} \\ y^{(1)} \\ z^{(1)} \end{pmatrix} = \mathbf{T}_1 \left[\begin{pmatrix} x_r \\ y_r \\ z_r \end{pmatrix} - \begin{pmatrix} d_{1x} \\ d_{1y} \\ d_{1z} \end{pmatrix} \right], \tag{A.10}$$

and

$$\begin{pmatrix} u_{x1} \\ u_{y1} \\ u_{z1} \end{pmatrix} = \mathbf{T}_1 \begin{pmatrix} u_{x_r} \\ u_{y_r} \\ u_{z_r} \end{pmatrix}, \tag{A.11}$$

with

$$\mathbf{T}_1 = \mathbf{T}^{(2)} \cdot \mathbf{T}^{(1)} = \begin{pmatrix} \cos\phi_1\cos\theta_1 & \sin\phi_1\cos\theta_1 & \sin\theta_1 \\ -\sin\phi_1 & \cos\phi_1 & 0 \\ -\cos\phi_1\sin\theta_1 & \sin\phi_1\sin\theta_1 & \cos\theta_1 \end{pmatrix}. \tag{A.12}$$

Because $\mathbf{T}_1\mathbf{T}_1^T = \mathbf{I}$, the transformation matrix $\mathbf{T}_1$ is orthogonal and hence the inverse transformation matrix can be written as

$$\mathbf{T}_1^{-1} = \mathbf{T}_1^T = \begin{pmatrix} \cos\phi_1\cos\theta_1 & -\sin\phi_1 & -\cos\phi_1\sin\theta_1 \\ \sin\phi_1\cos\theta_1 & \cos\phi_1 & -\sin\phi_1\cos\theta_1 \\ \sin\theta_1 & 0 & \cos\theta_1 \end{pmatrix}, \tag{A.13}$$

where the superscript T stands for transposed. The transformation from coordinate system $(O_1, \mathbf{u}_{x1}, \mathbf{u}_{y1}, \mathbf{u}_{z1})$ to the reference system is found as:

$$\begin{pmatrix} x_r \\ y_r \\ z_r \end{pmatrix} = \mathbf{T}_1^T \begin{pmatrix} x_1 \\ y_1 \\ z_1 \end{pmatrix} + \begin{pmatrix} d_{1x} \\ d_{1y} \\ d_{1z} \end{pmatrix}, \quad \begin{pmatrix} \mathbf{u}_{x_r} \\ \mathbf{u}_{y_r} \\ \mathbf{u}_{z_r} \end{pmatrix} = \mathbf{T}_1^T \begin{pmatrix} \mathbf{u}_{x1} \\ \mathbf{u}_{y1} \\ \mathbf{u}_{z1} \end{pmatrix}, \tag{A.14}$$

where the subscript 1 in the transformation matrix indicates that the transformation pertains to coordinate system 1. Since all transformations are from and to the reference coordinate system, no extra indication is made. In general, a transformation from coordinate system $n = 1, 2, ...$ to the reference system is described by a transformation matrix $\mathbf{T}_n$ and a translation vector $\mathbf{d}_n$. Note that the components of the vector $\mathbf{d}_n$ are found with respect to the reference coordinate system.

A.1.3 Transformation of the incident field term

With the coordinate transformations that are found, the electric field in a certain coordinate system can be transformed to the reference system and vice versa. Once the transformed electric field from a coordinate system is known in the reference system, the transformation to a second coordinate system can be carried out. If these electric fields originate from wire antennas, the mutual coupling between wires, each in their own coordinate system, can be described.

In terms of the notation of previous chapters, the radiated electric field originating from a wire antenna will be referred to as the direct field $\mathbf{E}^d(\mathbf{r})$ of a wire.

The transformation as described in the previous section will be applied to the incident field term in the EFIE equation for a thin wire in coordinate system 1 and length $L1$, as shown in Fig. A.51. The incident field term at position $\mathbf{r}$ can be written as:

$$E_{x1}^{inc}(\mathbf{r})\,\mathbf{u}_{x1} + E_{y1}^{inc}(\mathbf{r})\,\mathbf{u}_{y1} + E_{z1}^{inc}(\mathbf{r})\,\mathbf{u}_{z1} = E_{xr}^{inc}(\mathbf{r})\,\mathbf{u}_{xr} + E_{yr}^{inc}(\mathbf{r})\,\mathbf{u}_{yr} + E_{zr}^{inc}(\mathbf{r})\,\mathbf{u}_{zr}, \tag{A.15}$$

with

$$\mathbf{r} = x_1\mathbf{u}_{x1} + y_1\mathbf{u}_{y1} + z_1\mathbf{u}_{z1} = x_r\mathbf{u}_{xr} + y_r\mathbf{u}_{yr} + z_r\mathbf{u}_{zr}.$$

The position $\mathbf{r}$ can be described in terms of the reference system as well as in terms of coordinate system 1 as was shown earlier. For the incident electric field vector, the transformation is limited to the orientation and magnitude of the three field components. The value of the field vector is already determined by the position $\mathbf{r}$ which is a parameter of the incident electric field. This can be easily shown by introducing the start and end points of the incident field vector as

$$\mathbf{p} = (p_{x1}, p_{y1}, p_{z1}) \begin{pmatrix} \mathbf{u}_{x1} \\ \mathbf{u}_{y1} \\ \mathbf{u}_{z1} \end{pmatrix} = (p_{xr}, p_{yr}, p_{zr}) \begin{pmatrix} \mathbf{u}_{xr} \\ \mathbf{u}_{yr} \\ \mathbf{u}_{zr} \end{pmatrix}, \tag{A.16}$$

$$\mathbf{q} = (q_{x1}, q_{y1}, q_{z1}) \begin{pmatrix} \mathbf{u}_{x1} \\ \mathbf{u}_{y1} \\ \mathbf{u}_{z1} \end{pmatrix} = (q_{xr}, q_{yr}, q_{zr}) \begin{pmatrix} \mathbf{u}_{xr} \\ \mathbf{u}_{yr} \\ \mathbf{u}_{zr} \end{pmatrix}, \tag{A.17}$$

respectively. The incident field vector as such is then defined by $\mathbf{q} - \mathbf{p}$. When the coordinate transformation is carried out on the right-hand sides of (A.14) as follows

$$\begin{pmatrix} p_{xr} \\ p_{yr} \\ p_{zr} \end{pmatrix} = \mathbf{T}_1^T \begin{pmatrix} p_{x1} \\ p_{y1} \\ p_{z1} \end{pmatrix} + \begin{pmatrix} d_{1x} \\ d_{1y} \\ d_{1z} \end{pmatrix}, \tag{A.18}$$

$$\begin{pmatrix} q_{xr} \\ q_{yr} \\ q_{zr} \end{pmatrix} = \mathbf{T}_1^T \begin{pmatrix} q_{x1} \\ q_{y1} \\ q_{z1} \end{pmatrix} + \begin{pmatrix} d_{1x} \\ d_{1y} \\ d_{1z} \end{pmatrix}, \tag{A.19}$$

and

$$\begin{pmatrix} \mathbf{u}_{xr} \\ \mathbf{u}_{yr} \\ \mathbf{u}_{zr} \end{pmatrix} = \mathbf{T}_1 \begin{pmatrix} \mathbf{u}_{x1} \\ \mathbf{u}_{y1} \\ \mathbf{u}_{z1} \end{pmatrix},$$

it is seen that the translation vector $\mathbf{d}1$ cancels in the subtraction $\mathbf{q} - \mathbf{p}$. Hence, the translation has no effect in the transformation of a field vector.

With this result, the transformation of the incident electric field term in the EFIE equation from the reference system to system 1 is found as

$$(E^{inc}_{x1}(\mathbf{r}), E^{inc}_{y1}(\mathbf{r}), E^{inc}_{z1}(\mathbf{r})) \begin{pmatrix} \mathbf{u}_{x1} \\ \mathbf{u}_{y1} \\ \mathbf{u}_{z1} \end{pmatrix} = (E^{inc}_{xr}(\mathbf{r}), E^{inc}_{yr}(\mathbf{r}), E^{inc}_{zr}(\mathbf{r})) \begin{pmatrix} \mathbf{u}_{xr} \\ \mathbf{u}_{yr} \\ \mathbf{u}_{zr} \end{pmatrix}, \tag{A.20}$$

with

$$\begin{pmatrix} x_r \\ y_r \\ z_r \end{pmatrix} = \mathbf{T}_1^T \begin{pmatrix} x_1 \\ y_1 \\ z_1 \end{pmatrix} + \begin{pmatrix} d_{1x} \\ d_{1y} \\ d_{1z} \end{pmatrix}, \quad \begin{pmatrix} E^{inc}_{xr} \\ E^{inc}_{yr} \\ E^{inc}_{zr} \end{pmatrix} = \mathbf{T}_1^T \begin{pmatrix} E^{inc}_{x1} \\ E^{inc}_{y1} \\ E^{inc}_{z1} \end{pmatrix}, \tag{A.21}$$

and

$$\begin{pmatrix} \mathbf{u}_{xr} \\ \mathbf{u}_{yr} \\ \mathbf{u}_{zr} \end{pmatrix} = \mathbf{T}_1^T \begin{pmatrix} \mathbf{u}_{x1} \\ \mathbf{u}_{y1} \\ \mathbf{u}_{z1} \end{pmatrix}.$$

What remains is to write the electric field in the reference system in terms of the electric field in system 1. With the incident field term as defined in (A.15), the transformation from system 1 to the reference system is determined by

$$\begin{pmatrix} x_1 \\ y_1 \\ z_1 \end{pmatrix} = \mathbf{T}_1 \left[\begin{pmatrix} x_r \\ y_r \\ z_r \end{pmatrix} - \begin{pmatrix} d_{1x} \\ d1y \\ d_{1z} \end{pmatrix} \right], \quad \begin{pmatrix} E^{inc}_{x1} \\ E^{inc}_{y1} \\ E^{inc}_{z1} \end{pmatrix} = \mathbf{T}_1 \begin{pmatrix} E^{inc}_{xr} \\ E^{inc}_{yr} \\ E^{inc}_{zr} \end{pmatrix}, \tag{A.22}$$

and

$$\begin{pmatrix} \mathbf{u}_{x1} \\ \mathbf{u}_{y1} \\ \mathbf{u}_{z1} \end{pmatrix} = \mathbf{T}_1 \begin{pmatrix} \mathbf{u}_{xr} \\ \mathbf{u}_{yr} \\ \mathbf{u}_{zr} \end{pmatrix}.$$

In chapter 7, a special form of the EFIE equation is used to describe the mutual coupling between a complex object and an arbitrarilly oriented thin wire. Since the wire may now be arbitrarily oriented, the previous transformations can then be used to find an expression for the direct field on (or from) the wire.

Bibliography

[1] P. B. Johns, " A Symmetrical Condensed Node for the TLM-Method ", *IEEE Trans. Microwave Theory Tech.*, vol. MTT-35 , pp. 370-377, no. 4, Apr. 1987.

[2] M. Krumpholz and P. Russer, " A Field theoretical Derivation of TLM ", *IEEE Trans. Microwave Theory Tech.*, vol. MTT-42, pp. 1660–1668, no. 9, Sept. 1994.

[3] R. F. Harrington, *Field Computation by Moment Methods*. Krieger, New York, 1982.

[4] J. J. H. Wang, *Generalized Moment Methods in Electromagnetics*. Wiley, New York, 1991.

[5] R. Attari, K. Barkeshli, F. Ndagijmana, and J. Dansou, " A Hybrid Implementation of the TLM Method for the Analysis of High Frequency Interference", *Asia-Pacific Conference on Applied Electromagnetics*, pp. 124–127, August 2003.

[6] L. Pierantoni, A. D. Donato, and T. Rozzi, " Full-Wave Analysis of photonic Bandgap Integrated Optical Components by the TLM-IE Method", *J. of Lightwave Technology*, vol. 22, NO. 10, October 2004.

[7] L. Pierantoni, S. Lindenmeier and P. Russer, " Efficient analysis and modeling of the radiation of microstrip lines and patch antennas by the TLM-integral equation TLM-IE method", *Int. J. Numerical Modelling*, vol. 12, pp. 329–340, July 1999.

[8] L. Pierantoni, M. Farina, T. Rozzi, F. Coccetti, W. Dressel, P. Russer, "Comparison of the efficiency of electromagnetic solvers in the time- and frequency-domain for the accurate modeling of planar circuits and MEMS", Microwave Symposium Digest, 2002 IEEE MTT-S International Volume 2, 2-7 June 2002 Page(s):891 - 894

[9] Pierantoni, L. Lindenmeier, S., Russer, P., "A Combination Of Integral Equation Method And FD/TLM Method For Efficient Solution Of Emc Problems", Microwave Conference and Exhibition, 27th European Volume 2, September 8-12, 1997 Page(s):937 - 942

[10] S. Lindenmeier, C. Christopoulos, P. Russer, "Methods for the modeling of thin wire structures with the TLM Method", *IEEE MTT-S Digest*, pp. 387–390, June 2000.

[11] Lindenmeier, S.; Russer, P.; " Design of planar circuit structures with an efficient magnetostatic-field solver", *IEEE Transactions on Microwave Theory and Techniques*, Volume 45, Issue 12, Part 2, Page(s):2468 - 2473, Dec. 1997.

[12] Lindenmeier, S.; Pierantoni, L.; Russer, P.; " Hybrid space discretizing integral equation methods for numerical modeling of transient interference", *IEEE Transactions on Electromagnetic Compatibility*, Volume 41, Issue 4, Page(s):425 - 430, Nov. 1999.

[13] R. Khlifi and P. Russer, " A Novel Efficient Hybrid TLM/TDMOM Method for Numerical Modeling of Transient Interference", In Proceedings of the 22nd Annual Review of Progress in *Applied Computational Electromagnetics* ACES, March 12-16, 2006, Miami, FL, pages 182-187, March 2006.

[14] R. Khlifi and P. Russer, " A hybrid method combining TLM and MoM method for efficient analysis of scattering problems", In 2006 *IEEE MTT-S Int. Microwave Symp.* Dig. June 11-16, San Francisco, USA pages 161-164, June 2006.

[15] R. Khlifi and P. Russer," Numerical Modeling of Transient Radiated Interferences by the Hybrid TLM-TDMOM Method", In FACE 2006, *Frontiers in Applied Computational Electromagnetics*, June 19-20, 2006, University of Victoria, Victoria, BC, Canada, June 2006.

[16] Khlifi R. and Russer P., " Hybrid Space Discretizing Method Method of Moments for the Efficient Analysis of Transient Interference" , In *IEEE Transactions on Microwave Theory and Techniques*, Accepted for publication, Dec. 2006.

[17] S. M. Rao and D. R. Wilton, " Transient scattering by conducting surfaces of arbitrary shape", *IEEE Trans. Antennas Propagat.*, vol. 39, pp. 56–61, Jan. 1991.

[18] S. M. Rao and T. K. Sarkar, " Numerical solution of time domain integral equations for arbitrarily shaped conductor/dielectric composite bodies", *IEEE Trans. Antennas Propagat.*, vol. 50, pp. 1831–1837, Dec. 2002.

[19] T. K. Sarkar, W. Lee, M. Rao " Analysis of Transient Scattering From Composite Arbitrarily Shaped Complex Structures", *IEEE Trans. Antennas Propagat.*, vol. 48, pp. 1625–1634, Oct. 2000.

[20] G. Manara, A. Monorchio, R. Reggiannini, " A Space-Time Discretization Criterion for a Stable Time-Marching Solution of the Electric Field Integral Equation", *IEEE Trans. Antennas Propagat.*, vol. 45, pp. 527–532, Mar. 1997.

[21] D. A. Vechinski and S. M. Rao " A stable procedure to calculate the transient scattering by conducting surfaces of arbitrary shape", *IEEE Trans. Antennas Propagat.*, vol. 40, pp. 661–665, 1992.

[22] B. P. Rynne and P. D. Smith, " Stability of time marching algorithms for the electric field equation", *J. Electromag. Waves & Appl.*, vol. 4, no. 12, pp. 1181-1205, 1990.

[23] B. P. Rynne, " Time domain scattering from arbitrary surfaces using the electric field equation", *J. Electromagn. Waves Applicat.*, vol. 5 , no. 1, pp. 93-112, 1991.

[24] J P J Davies, " On the Stability of Time-Marching Schemes for the General Surface Electric-Field Integral Equation", *IEEE Trans. Antennas Propagat.*, vol. 44, no.11, pp. 1467-1473, Nov. 1996.

[25] X. M. Dai, W. Cao " The MOT method and the conjugate degree method of transient electromagnetic field research", *Journal of Nanjing Posts and Telecommunications College*, vol. 10, pp. 43-51, 1990.

[26] J. Zhong, Ho Jung Baek, " A stable solution of time domain electric field integral equation for thin-wire antennas using the Laguerre Polynomials ", *IEEE Trans. AP*, vol. 52, pp. 2641-2649, October 2004.

[27] J.-L. Hu and C. H. Chan, " An improved temporal basis function for the time domain electric field integral equation method ", *Electron. Lett.*, vol. 35, pp. 883 885, May 1999.

[28] D. S. Weile, A. A. Ergin, B. Shanker, and E. Michielssen, " An accurate discretization scheme for the numerical solution of time domain integral equations ", *Dig. 2000 IEEE Antennas Propagat. Int. Symp.*, Salt Lake City, UT, pp. 741-744, July 2000.

[29] Y. S. Chung, T. K. Sarkar, B. H. Jung, M. Salazar-Palma, Z. Ji, S. Jang, and K. Kim, " Solution of time domain electric field integral equation using the laguerre polynomials ", *IEEE Trans. Antennas Propagat.* , vol. 52, no. 9, pp. 2319-2328, 2004.

[30] A. Monorchio and R. Mittra, "A hybrid finite-element/finite-difference time-domain (FE/FDTD) technique for solving complex electromagnetic problems", *IEEE Microwave Guided Waves Lett.*, vol. 8, pp. 93-95, Feb. 1998.

[31] T. Itoh, *Numerical Techniques for Microwave and Millimeter-Wave Passive Structures*. New York: JohnWiley & Sons, 1989.

[32] R. Sorrentino, *Numerical Methods for Passive Microwave and Millimeter Wave Structures*. IEEE Press, 1989.

[33] E. Yamashita, *Analysis Methods for Electromagnetic Wave Problems*. Boston, London: Artech House, 1990.

[34] R. F. Harrington, *Matrix methods for field problems*, Proceedings of the IEEE, vol. 55, pp. 136-149,Feb. 1967.

[35] R. F. Harrington, *Field Computation by Moment Methods*, San Francisco: IEEE Press, 1968.

[29] J. R. Mosig, " Integral equation technique ", in Numerical Techniques for Microwave and Millimeter Wave Passive Structures (T. Itoh, ed.), pp. 131-213 New York: JohnWiley & Sons, 1989,

[36] D. Mirshekar-Syahkal, *Spectral Domain Methods for Microwave Integrated Circuits*. Taunton, Somerset, England: Research Studies Press, 1990.

[37] M. Mongiardo, P. Russer, C. Tomassoni, and L. B. Felsen, " Analysis of N-furcation in elliptical waveguides via the generalized network formulation ", *IEEE Trans. Microwave Theory Techn.*, vol. 47, pp. 2473-2478, Dec. 1999.

[38] J. Kessler, R. Dill, and P. Russer, " Field theory investigation of high-tc superconducting coplanar wave guide transmission lines and resonators ", *IEEE Trans. Microwave Theory Techn.*, vol. 39, pp. 1566-1574, Sept. 1991.

[39] R. Schmidt and P. Russer, " Modelling of cascaded coplanar waveguide discontinuities by the mode matching approach ", 1995 *Int. Microwave Symposium Digest*, Orlando, pp. 281-284, May 1995.

[40] U. Schulz and R. Pregla, " A new technique for the analysis of the dispersion characteristics of planar waveguides and its application to microstrips with tunig septums ", Radio Sci, vol. 16, pp. 1173-1178, Nov. -Dec. 1981.

[41] R. Pregla and W. Pascher, " The method of lines ", in Numerical Techniques for Microwave and Millimeter Wave Passive Structures (T. Itoh, ed.), pp. 381-446, New York: JohnWiley & Sons, 1989.

[42] K. S. Yee, "Numerical solution of initial boundary value problems involving Maxwell's equations in isotropic media ", *IEEE Trans. Antennas Propagat.*, vol. 14, pp. 302-307, May 1966.

[43] A. Taflove, *Computational Electrodynamics* - The Finite-Difference Time-Domain Method. Boston, London: Artech House, 1995.

[44] T. Weiland, " A discretization method for the solution of Maxwell's equations for six-component fields ", *Electronics and Communications* (AEU), vol. 31, pp. 116-120, 1977.

[45] T.Weiland, " On the unique numerical solution of maxwellian eigenvalue problems in three dimensions ", *Particle Accelerators*, vol. 17, pp. 227-242, 1985.

[46] T. Weiland, " Time domain electromagnetic field computation with finite difference methods " , *Int. J. Numer. Modelling*, vol. 9, pp. 295-319, 1996.

[47] J. Jin, *The Finite Element Method in Electromagnetics.* New York: JohnWiley & Sons, 1993.

[48] W. J. R. Hoefer, "The transmission line matrix method-theory and applications," *IEEE Trans. Microwave Theory Techn.*, vol. 33, pp. 882-893, Oct. 1985.

[49] W. J. R. Hoefer, *The transmission line matrix (TLM) method*, in Numerical Techniques for Microwave and Millimeter Wave Passive Structures (T. Itoh, ed.), pp. 496-591, New York: JohnWiley & Sons, 1989.

[50] C. Christopoulos, *The Transmission-Line Modeling Method TLM.* New York: IEEE Press, 1995.

[51] Wane, S.; Bajon, D.; Baudrand, H.; Gamand, P.; " A new full-wave hybrid differential-integral approach for the investigation of multilayer structures including nonuniformly doped diffusions ", *IEEE Transactions on Microwave Theory and Techniques*, Volume 53, Issue 1, Page(s):200 - 214, Jan. 2005.

[52] Bouzidi, F.; Aubert, H.; Bajon, D.; Baudrand, H.; " Equivalent network representation of boundary conditions involving generalized trial quantities-application to lossy transmission lines with finite metalization thickness", *IEEE Transactions on Microwave Theory and Techniques*, Volume 45, Issue 6, Page(s):869 - 876, June 1997.

[53] Bertin, G.; Piovano, B.; Accatino, L.; Mongiardo, M.; " Full-wave design and optimization of circular waveguide polarizers with elliptical irises ", *IEEE Transactions on Microwave Theory and Techniques*, Volume 50, Issue 4, Page(s):1077-1083, April 2002.

[54] Mongiardo, M.; Tomassoni, C.; "Modal analysis of discontinuities between elliptical waveguides ", *IEEE Transactions on Microwave Theory and Techniques*, Volume 48, Issue 4, Part 1, Page(s):597 - 605, April 2000.

[55] Pierantoni, L.; Massaro, A.; Rozzi, T.; " Accurate modeling of TE/TM propagation and losses of integrated optical polarizer," *Microwave IEEE Transactions on Theory and Techniques*, Volume 53, Issue 6, Part 1, Page(s):1856 - 1862, June 2005.

[56] Schmidt, R.; Russer, P.; " Modeling of cascaded coplanar waveguide discontinuities by the mode-matching approach", *IEEE Transactions on Microwave Theory and Techniques*, Volume 43, Issue 12, Part 2, Page(s):2910 - 2917, Dec. 1995.

[57] Lorenz, P.; Russer, P.; " Hybrid Transmission Line Matrix (TLM) and multipole expansion method for time-domain modeling of radiating structures", 2004 I*EEE MTT Microwave Symposium Digest*, Volume 2, 6-11, Page(s):1037 - 1040, Vol. 2, June 2004.

[58] D. Lukashevich, B. Broido, P. Russer, " Using of transmission line matrix method and mode matching approach for simulation of MMICs ," 2003 *IEEE MTT-S International Microwave Symposium*, 8-13, pp. 993 -996, Vol. 2, June 2003.

[59] F. Coccetti, P. Russer, "Application of System Identification to Time-Domain Modeling of Electromagnetic Structures," in "Fields, Networks, Methods, and Systems in Modern Electrodynamics", Ed.: P. Russer and M. Mongiardo, Springer, Berlin, pp. 143-156, 2004.

[60] L. Menezes and W. Hoefer, " Modeling of general constituve relationships in SCN TLM", *IEEE Trans. Microwave Theory Techn.*, 44(6), pp 854-861, July 1996.

[61] P. Russer, P. So, and W. Hoefer, " Modeling on nonlinear active regions in TLM ", *IEEE Microwave and Guided-Wave Letters*,1(1):pp 10-13, 1991.

[62] P. P. M. So and W. J. R. Hoefer, " Time domain TLM modeling of metamaterials with negative refractive index ", 2004 *Int. Microwave Symposium Digest*, Fort Worth, pages 1179-1182, June 2004.

[63] P. Naylor, C. Christopoulos and P. B. Johns, " Coupling between electromagnetic fields and wires using transmission-line modelling ", Proc. IEE, Part A, 134(8), pp 679-686 , 1987.

[64] C. Christopoulos and P. Naylor, " Coupling between electromagnetic field and multiconconductor transmission systems using TLM", *Int. J. Numer. Model.*, 1, pp 7-17, 1988.

[65] A. P. Duffy, *Coupling of Electromagnetic Waves into Wires- Experiments and Simulations*, PhD thesis, University of Nottigham, UK, 1993

[66] A. Wlodarczyk and D. P. Johns, "New wire interface for graded 3-D TLM", *Electron. Lett.*, 28(8), pp 728-729, 1992

[67] A. Wlodarczyk, V. Trenkic, R. Scaramuza, C. Christopoulos, " integrated Solution for Modeling of Multiconductors in TLM ", *IEEE Trans. Theory Tech.*, Vol. 46(12), pp. 2431-2437, 1998

[68] J. A. Porti, J. A. Morente, M. Khalladi and A. Gallego, " Loaded-wire node for TLM method ", *Electron. Lett.*, 28(20), pp 1910-1911, 1992

[69] J. A. Morente, J. A. Porti, G. Gimenez and A. Gallego, " Loaded-wire node for TLM method ", *Electron. Lett.*, 29(2), pp 182-184, 1993

[70] J. A. Morente, J.A. Porti, and M. Khalladi, " Absorbing boundary conditions for the TLM method ". *IEEE Trans. Microwave Theory Techn.*, 40(11), pp 2095-2098, November 1992.

[71] K. Mei, " On the integral Equation of Thin Wire Antennas ", *IEEE Trans. Antennas Propagation*, AP-13(3), pp. 374-378, 1965

[72] S. Yee, " Numerical solution of initial boundary value problems involving Maxwell's equations in isotropic media ", *IEEE Trans. Antenna Propagat.*, Vol.14, pp. 302-307, May 1966.

[73] X. M. Zhang and J. F. Lee, " Application of the AWE method with the 3D-TVFEM to model spectral responses of passive microwave components ", *IEEE Trans. Microwave Theory Techn.*, vol. 46, pp 1735-1741, November 1998.

[74] S. Hein, " Finite-difference time-domain approximation of Maxwell's equations with nonorthogonal condensed TLM mesh ", *Int. J. Num. Mod.*, 7:179-188, 1994.

[75] S. Hein, " Consistent finite-difference modeling of Maxwell's equations with lossy symmetrical condensed TLM node ", *Int. J. Num. Mod.*, 7, pp-179-188,1994.

[76] P. Russer, P.So, and W. Hoefer, " Modeling on nonlinear active regions in TLM ", *IEEE Microwave and Guided-Wave Letters*, 1(1):pp 10-13, 1991.

[77] J. Dubard and D. Pompei, " Simulation of Berenger's perfectly matched layer with a modified TLM node ", *IEEE Trans. Antennas and Propagation*, 144(3), pp-205-207, March 1997.

[78] N. Pena and M.M. Ney. " Absorbing-boundary conditions using perfectly matched-layer (PML) technique for three-dimensional TLM simulations ", *IEEE Trans. Microwave Theory Techn.*, Vo. 10, pp-1749-1755, October 1997.

[79] W. Dressel, *Subgridding in the TLM method*, PhD thesis, Technische Universitt Mnchen, 2005.

[80] J. Herring and C. Christopoulos, " Solving electromagnetic problems using multiple grid transmission line modelling method ", *IEEE Trans. Antennas and Propagation*, 42(12), pp:1654-1658, Dec. 1994.

[81] B. Isele and P. Russer," Improved skin effect model in TLM", COMPUMAG,1993.

[82] J. P. J. Davies and D. B. Duncan, " Averaging techniques for time marching scheme for retarded potential integral equation " 1995, preprint

[83] A. Sadigh, A. Ercument, " Treating the instabilities in marching-on-in-time method from a different perspective ", *IEEE Trans. Ant. Prop.*, vol. 41, pp. 1695-1702, December 1993

[84] W. B. Wang, *Transient electromagnetic field*, Xi an Jiaotong University Press, 1991

[85] M. Krumpholz, *Über die Grundlagen der TLM-Methode.* PHD thesis, Technische Universität München, 1994

[86] P. Russer. *The transmission Line Matrix Method*, chapter Applied Computational Electromagnetics, pages 243-269. NATO ASI. Springer, Cambridge, Massachusetts, London, England, 2000.

[87] Z. Chen, M. Ney, and W. J. R. Hoefer. " Absorbing and Connecting Boundary Conditions for the TLM Method ", *IEEE Trans. Microwave Theory Techn.*, 41(11), pp-2016-2024, November 1993.

[88] J. Rebel, T. Mangold, and P.Russer. " On the Practical Use of Layered Absorbers for the simulation of Planar Microwave Circuits using the SCN-TLM Method ", In 16th Anual Review of *Progress in Applied Computational Electromagnetics Digest*, Monterey, March 2000.